Univerzita Karlova v Praze
Matematicko-fyzikální fakulta

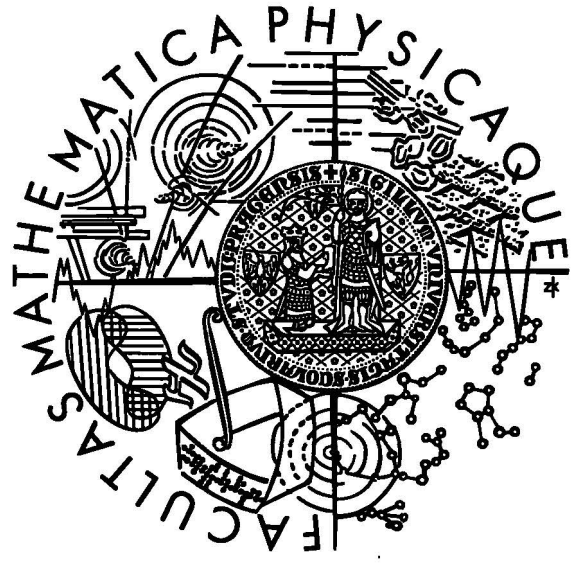

DISERTAČNÍ PRÁCE

Zdenka Kuntová

Povrchová difúze adsorbovaných atomů v nerovnovážných podmínkách

FZÚ AV ČR - Oddělení tenkých vrstev
Vedoucí diplomové práce:
doc. RNDr. Zdeňek Chvoj DrSc

Studijní program:
F3 - Fyzika kondenzovaných látek a materiálový výzkum

Poděkovaní

Me díky patří zejména mému školiteli doc Zdeňku Chvojovi za trpělivost s kterou sledoval mé nekonečné vychytávání chyb v simulacích, i za pečlivé přečtení a připomínkování mé práce. Stejnou míru trpelivosti projevil i prof. M.C. Tringides a v neposlední řade patří můj dík oběma pánům nadřízeným z Oddělení tenkých vrstev FZÚ AV ČR - RNDr Janovi Kočkovi a RNDr. Vladimírovi Chábovi za jejich citlivé šéfování i přiblížení vybraných experimentálních technik.
Na závěr bych ještě poděkovala obecně všem členům rodiny, kolegům i přátelům kteří mi po dobu studia poskytovali zázemí, rady i rozptýlení.

Acknowledgements

This work was supported by the Grant Agency of Academy of Sciences of the Czech Republic (Grant no. IAA 1010207), Grant Agency of the Czech Republic no. 202/98/K002 and Grant FRVŠ 1840/2004, The research work at the Institute of Physics is supported by Institutional Research Plan No. AV0Z10100521

Prohlašuji, že jsem svou diplomovou práci napsala samostatně a výhradně s použitím citovaných pramenů. Souhlasím se zapůjčováním práce.
V Praze dne 18.9.2006
Zdenka Kuntová

Contents

Abstrakt

Název práce: Povrchová difúze adsorbovanch atomů v nerovnovážných podmínkách
Autor: Zdenka Kuntová
Ústav: FZÚ AV ČR - Oddělení tenkých vrstev
Vedoucí diplomové práce: doc RNDr. Zdeňek Chvoj DrSc
e-mail vedoucího: chvoj@fzu.cz
Abstrakt: Tato publikace je věnovaňa studiu kinetiky adsorbovanch atomů v systému Ag/Ag(111) a Pb/Si(111). V případě difuse jediného atomu na periodockém povrchu je možné získat potřebné výsledky analyticky. V Kapitole 1 budou pomocí "Master equation" rekonstruovnávy obrázky z STM experimentu. V dalších kapitolách jsou studovány modely popisující rozpad a růst ostrůvků Ag/Ag(111) a Pb/Si(111) a k určení vývoje systému v čase bylo použito simulacích Monte Carlo. Rozvoj experimentálních technik, zejména STM s atomarním rozlišením, umožnuje v poslední dobe měření systémů o malých rozměrech. Pro neperiodocké uspořádání o vysokém počtu částic (500 atomu) zpravidla vylučuje přesnější analytický výpočet. A je také otázka zda takto malé systémy mohou být popsány v rámci makroskopických termodynamických modelů, či zda musí být pro ně navržen detailnější kinetický model. S pomocí MC jsme zjistili řadu rozdílu mezi výsledky kinetického modelu a TD aproximace. V poslední části je navržen mikroskopický model částečně popisující samoorganizaci ostrůvků Pb/Si(111) (existenci specifické výšky ostrůvku pro dané pokrytí a teplotu) i neobvyklý růst ve dvopjvrstvách. Tyto výsledky jsou srovnány s STM experimenty a dvají dobrou shodu.
Klíčová slova: Monte Carlo, samoorganizace, difúze, růst

Abstract

Title: Surface diffusion of adsorbed atoms in non-equilibrium conditions
Author: Zdenka Kuntová
Department: FZÚ AV ČR - Oddělení tenkých vrstev
Supervisor: doc RNDr. Zdeňek Chvoj DrSc
Supervisor's e-mail: chvoj@fzu.cz
Abstract: This publication refers to a study of kinetics of adsorbed atoms in systems Ag/Ag(111) and Pb/Si(111). In cases of single atom diffusion on a periodical surface we can obtain the result analytically. The Master equation will be applied to the reconstruction of STM pictures in Chapter 1. In the next chapters the kinetic models are studied describing decay and growth of Ag/Ag(111) and Pb/Si(111) islands and the Monte Carlo simulation was used to determine the evolution over time of the system. The progress in experimental techniques in the last decade, namely STM with atomic resolution, allows for the measurement of nanosize systems. More accurate calculations are impossible for non-periodical ordering with a high number of particles (500 atoms). With this also arises the question if these systems can be described in terms of microscopic thermodynamic models, or whether a more detail kinetic model must be used. We found out many difference between the kinetic model and TD approximation using the Monte Carlo simulation. In the last part a microscopic model is designed describing the self-organization of Pb/Si(111) islands (this means the existence of preferred island height at a given temperature and coverage) as well as the unusual double-layer growth. The results are compared with the STM experiment and are in agreement with them.
Keywords: Monte Carlo, selforganization, diffusion, growth

Introduction

The tempestuous development of new technologies, especially in information science, brings new challenges for basic research. In the forefront of research are studies of systems and their properties on the nanoscale, i.e. systems with a characteristic dimension less than 100nm. On this mesoscopic scale we meet with new problems. On one hand these systems are too small for rigorous application of the concepts of thermodynamic and statistical physics concepts. On the other hand they are too large for first principle calculations. Also the understanding of the formation and stability of nanostructures is an open question. In statistical physics and thermodynamics, processes are described by mean values of characteristics and controlled by averaged processes. These concepts are well established on the macro scale. However, on the mesoscopic scale we encounter different behaviors of these processes. The most probable or fastest processes can play the decisive role, atoms in a special positions can play an important role, nanostructures are formed at non-equilibrium conditions and they are in a metastable state.

All the parts of this thesis try to analyze different STM experiments studying nano-size objects. In the case of Pb/Si(111) at a low coverage an STM with atomic resolution was realized by the group of RNDr. Vladimŕ Chab in FZÚ AV ČR at low coverages of Pb. In this part we reconstructed the patterns which arise due to the quick diffusion of Pb inside the unit cell and it is based on the Monte Carlo simulation of Pavel Jelinek. The analytical calculation validates and specifies the result from the Monte Carlo simulation and can show the results without the influence of the statistics. The results of MC and analytical calculations was practically identical, but in applying these of the free parameters, the analytical method was allowed to us determine the parameters with higher precision (Chapter 2).

The other parts of this thesis arise from the cooperation of the group of my supervisor Zdenek Chvoj with the experimental group of prof. M. C. Tringides from Ames Laboratory at Iowa State University. At first, we tried to analyze the experiments of prof. Morgenstein which conflicted with previous experiments which had partly been done by the Tringides group. In this part we tested if this difference between the experiments could be caused by the use of the thermodynamical Gibbs-Thompson approximation on the ensemble of atoms which is too small to be described by macroscopical values. The conclusions of the experiments, methods and results are in Chapter 1.

The last two chapters of this thesis are dedicated to an analysis of the newest experiments of the group from the Ames laboratory with the deposition of Pb island on the Si(111)-(7x7) surface. At higher coverage, Tringides's group observed quite unusual behavior - they observed the self-organization of nano-island at given temperatures and coverages, the growth from the perimeter towards the center of the island with the typical ring-shape, and at least the existence of preferred heights and, with this phenomena, together with double-layer growth. In this work are presented the microscopical models with new surface potentials which can partly illuminate some of the mentioned problems. The Monte Carlo is used as the intermediary between the simple kinetic model and the results of the experiment.

The Monte Carlo simulation is used as a way to simulate the evolution of the system which

is described by a kinetic model too complicated for analytical calculation. In the kinetic model the averages variables (i.e. bond energy per unit length, density) are substituted for by several elemental processes (jump). Due to this substitution the model is more precise, but the analytical solution is even more remote. The Monte Carlo in the algorithm used in this work simulate in each step the movement of one atom in the system. Each movement is "random" which means that it is necessary to choose the most probable jump in each MC step. But on average at long-time interval each jump is represent by its probability which is given as parameter of the Monte Carlo simulation. This probabilities (of frequencies) of the mentioned elemental processes must be either determined from other calculation (ab-initio, Molecular Dynamics) or are free parameters of the model. Nevertheless the more accuracy the kinetics model gave for some small systems gives different results in thermodynamic approximation which will be shown in Chapter 1. All these simulations are in agreement with the experiment and also allow us to study details which can not be measured.

Chapter 1

Are thermodynamic concepts valid on a nanoscale?

The evolution over time of nanostructures can reveal information about the microscopic mechanisms and energetic barriers which control nanostructure stability. As the nanostructures become smaller in size, the discreteness in their structure implies a large variation in their shape, with different types of atoms at the boundary, and that, in turn, changes the effective controlling barrier [1]. The ratio of the number of atoms with a lower coordination (which are the ones which detach more easily) to the ones with a higher coordination increases as the structure size decreases. The measured macroscopic time of the island decay can be used as a probe to identify the controlling microscopic detachment barriers and changes in the barrier distribution with a reduced nanostructure size.

Many important processes which involve collective changes of the nanostructure (i.e. nanostructure coarsening, nanostructure decay , etc.) are built from individual atomistic events i.e. the detachment of single atoms. For example in sintering processes, an initial size distribution of catalytic particles coarsens in time to larger sizes which degrades the catalytic function of the particle [2]. It is still not clear how single atom detachment determines the overall time in sintering. Since the catalytic particle size distribution changes, it is important to know the dependence of the detachment rate to size. The need to know the connection between single atom detachment rate and the evolution time of the composite structure is also evident from the diffusion of the adatom or vacancy clusters [3]. Although the cluster diffuses as a collective entity with a well-defined diffusion coefficient D and the relation D vs N (the cluster size) obeys simple scaling, it is essential to understand the origin of these universal results in terms of single atom events. This is related to the previous question i.e. how the single atom detachment rate depends on cluster size. One expects that for nanostructure sizes above some minimum size a thermodynamic description of the evolution [4] by means of an average detachment rate (in terms of a uniform chemical potential across the perimeter) is applicable. However, as the nanostructure decreases in size the atoms at the few sites of lower coordination become a larger fraction of the barrier distribution and have a larger proportionate contribution to the evolution. The presence of different types of binding sites (i.e. corner atoms, straight step atoms, kink atoms etc.) and the larger role of fluctuations for smaller systems imply that it is not possible to use a single curvature dependent value for the chemical potential to describe the adatom energy cost along the nanostructure perimeter.

To better understand the processes on the mezoscopic scale, we explored the non-equilibrium processes of nano-island decay with realistic Monte Carlo simulations, which cover non-equilibrium conditions and aspects of nanoscale. We will study the failure of the thermodynamic analysis for the decay of sufficiently small island sizes. These results have general

implications as to whether the physics applicable on the macroscopic scale can be safely extrapolated to the nanoscale, and more specifically, whether they are relevant to island-within-island STM experiments monitoring the decay of a small island (adatom or vacancy) located at the center of a larger vacancy island [10].

1.1 Overview of experiments of Ag/Ag(111)

Over the last ten years, several experiments have been realized with the purpose to determine the Ehrlich-Schwöbel barrier (E_s) and ratio ($\frac{\nu_s}{\nu_t}$) of attempt frequencies for jump on the terrace and jumps across the edge. These experiments were realized at different temperatures and analyzed by different methods using the theory of nucleation [5] and the thermodynamic Gibbs-Thompson approximation [10]. The results obtained by these analysis were different. The possible explanation of this problem is the existence of size limits for the use of thermodynamic approximation.

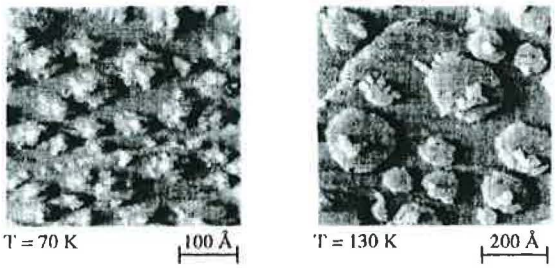

Figure 1.1: STM pictures of measurement of nucleation on the islands top [5]. The left picture was taken at 70K, the second one at 130K.

1.1.1 Nucleation in the second layer of Ag(111) at $T < 150K$

In experiment [5] the population of the islands Ag which nucleate on the top of another island Ag(111) with radius R during the deposition with flux θ was studied. The probability of the nucleation $\Omega(T, R, \theta, p_{i->t}, i)$ is derived from the concentration of atoms on the island top using the theory of the nucleation [6]. i is the size of the critical cluster and $p_{i->t}$ is the probability that an atom on the welt will jump across the edge on the lower layer. The density of the atom on the island top is proportional to the probability of falling down from the island. This probability is the product of probability that an atom on the welt of the island will fall down: $p_{i->t} = \frac{\nu_s}{\nu_t} \exp(-E_s/k_B T)$ multiply by the probability that the atom will reach the welt of the island with radius R: $p(R)$.
The more precise shape of $\Omega(T, R, \theta, p_{i->t}, i)$ was published in [6, 7] as it depends on R, T and $p_{i->t}$. The measured dependency of $\Omega(T, R, \theta, p_{i->t}, i)$ on R at different temperatures is in Fig(1.2). The temperature dependency allows to separate $\frac{\nu_s}{\nu_t}$ and E_s in temperature dependcy $p_{i->t}$ with results $E_s = (0.12 \pm 0.015)eV$ and $\frac{\nu_s}{\nu_t} = 10^{2\pm1}$. The value of E_s agree with previous experiments [8] $E_s = (0.15 \pm 0.02)eV$ as well as with both further RHEED measurement of homoepitaxial growth [9]. The first experiment published in [9] is practically

identical with [5], the second experiment observes the nucleation in the second layer at a different deposition rate θ. Both results give $\frac{\nu_s}{\nu_t} >> 1$ ($\frac{\nu_s}{\nu_t} = 10^{2\pm0.3}$) and E_s $0.5eV$. All these experiments were done at $T < 150K$.

Nevertheless there exists the experiment [10] realized at RT which predicts a similar value

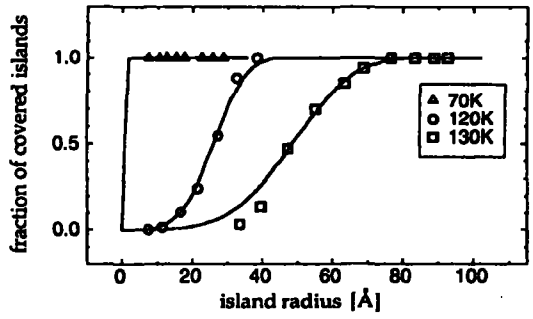

Figure 1.2: Result of experiment [5]: Quantitative probability of the nucleation probability for Ag on 2D Ag islands on Ag(111). The fraction of covered island is shown as a function of the island radius and deposition temperature (flux $\theta = 1.1^{-3}ML/s$) which correspond to probability of the nucleation $\Omega(T, R, \theta, p_{i->t}, i)$.

for E_s but which gives $\frac{\nu_s}{\nu_t} \simeq 1$. This experiment will be discussed in more detail in the next section, as simulation of this experiment is the theme of this whole chapter.

1.1.2 Decay of island within vacancy at RT

In experiment [10] the decay of Ag island on Ag(111) surface surrounded by the vacancy island was measured (see Fig(1.3)). This ordering was prepared by bombarding by Ag atoms at low temperature. On the begin of the experiment they increases the temperature thus the system start from the non-equilibrium shape. In this experiment two configuration was measured - in the first the Ag island in the center of the big vacancy was placed, in the second configuration the vacancy island was made in the center of the big vacancy (see Fig(1.3) and Fig(1.4)). From a comparison with the decay of vacancy and adatom islands at the same condition, the Ehrlich-Schwöbel barrier E_s and ratio of prefactors $\frac{\nu_s}{\nu_t} \simeq 1$ were determined.

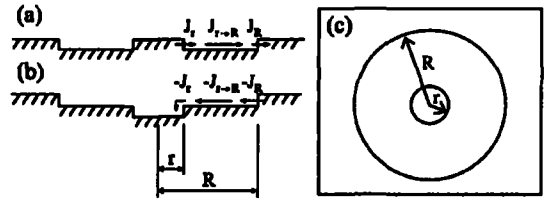

Figure 1.3: Adopted from [10]: Schematic view of a theoretically modeled geometry with diffusion flux: (a) adatom island and (b) vacancy island both surrounded by an ascealing step; (c) top view of (a) and (b).

These conclusions are based on the the analyze describes the decay of big adatom island [11] and combines a steady state hypothesis and Gibs-Thompson approximation. But it is

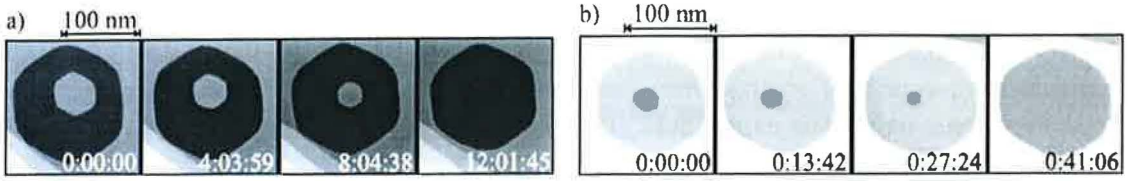

Figure 1.4: Adopted from [10]. STM images of decaying islands of monoatomic height on Ag(111): (a) adatom island at 300K. R=73nm, U_t=-1.91V, I_t=0.09nA. (b) vacancy island at 360K, R=51nm, U_t=-2V, I_t=0.1nA.

unclear if the steady-state model is a reasonable approximation for small systems with quick diffusion on the terrace like Ag/Ag(111). The velocity of diffusion on an fcc(111) surface can be so quick in comparison with the velocity of detachment from the edges of the island that the macroscopical values (like density and gradient of the density of atoms on the terrace with one single atom) make no sense. In the next parts we examine the use of the Monte Carlo (MC) simulation to compare the result from the steady-state model with the result of the microscopic model.

Analyzes of the experiment [10] using steady-state approximation

In work [10] the steady-state approximation was used because the changes of the radius of the central island are slow during decay. It was also considered that the distribution of atoms between the edges of central the island and the big surrounding vacancy is constant and it has the equilibrium distribution of this density in radius $\rho_{eq}(r')$. The atomic density of atoms in quasi-equilibrium near the island edge with a curvature $1/r'$ is described by the Gibbs-Thompson relation: $\rho_{eq}(r') = \rho_\infty \exp(\gamma'/k_b T n r')$, where ρ_∞ is the atomic density in front of a straight segment, n is the atomic density of one monolayer, γ' is line tension, T temperature and k_B is the Boltzmann factor. Within the steady-state region a differential equation:

$$\frac{d(\pi r^2)}{dt} = \beta(T)\left(\exp\left(\frac{\gamma'}{kTnr}\right) - \exp\left(\frac{\gamma'}{kTnR}\right)\right)\left(\frac{a}{r\frac{\nu_s}{\nu_t}\exp\left(\frac{-E_s}{kT}\right)} + \ln\left(\frac{R}{r}\right) + \frac{a}{R}\right)^{-1} \quad (1.1)$$

was derived in [10] for a time derivation of the area of the central island (which has a nearly circular shape with the radius r and is deponed in the center of a vacancy with radius R). Value $\beta(T)$ is the probability of detachment of the atom from the edge and is suggested in the shape $\beta(T) = \beta_o \exp\left(\frac{-E_e}{kT}\right)$. All the other parameters are temperature independent and meaning: E_e is the activation energy for detaching from the edge, β_o is the attempt frequency for detaching from the edge , $\frac{\nu_s}{\nu_t}$ is the ratio of the prefactor for a jump on the terrace and the prefactor for a jump across the edge, E_s is the Ehrlich-Schwöbel barrier and a is the lattice constant of silver. The numerical solution of this equation was used as a function which was fitted to experimental data. Parameters $\{E_e, E_s, \frac{\nu_s}{\nu_t}, \beta_o, \gamma'\}$ were used as free parameters of the fitting. The solution of the equation (1.1) with parameters taken from [10] is outlined in (Fig(1.5)).

The gradient of density drives the decay of the central vacancy island. This is the main problem of this analysis, because for a quick terrace diffusion, the terrace is usually empty or there are only a few atoms and the definition of the gradient of density is problematic. It

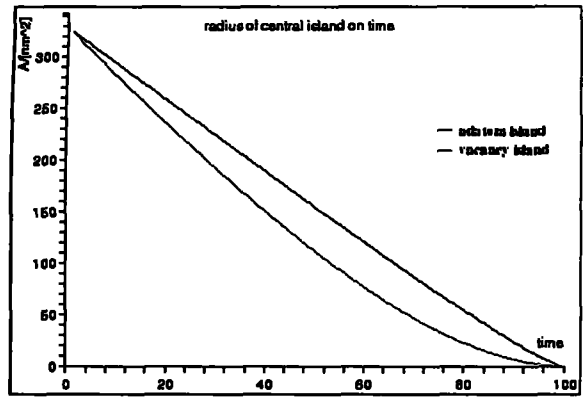

Figure 1.5: The decay law for the adatom and vacancy island was obtained as a numerical solution of (1.1) with parameters taken from [10]

will also be shown that the density sensitively depends on the shape of the big surrounding island, which can hardly be including in the model. In [12] the microscopical model was proposed in which the velocity of detachment was driven by the number of less coordinated atoms on the edge. In [12] the rough presumption of the ratio of prefactor $\frac{\nu_s}{\nu_t} \simeq 30$ was also published. This value is close to the experimental value for T¡150K, the value E_s was supposed $0.13eV$ which is value from all previous experiments. A more precise analysis of the published microscopical model is the main aim of this MC simulation.

1.2 Model of the nano-islands decay

We try to simulate the decay of central vacancy island as well as the relaxation of the big vacancy. The size of the big vacancy island was R 70nm in the experiment [10]. In the simulation we need two layers of atoms (for vacancy island decay) and the simulated area is 3R. The computer time is proportional to the number of atoms which can move (in kinetic Monte Carlo (kMC) algorithm which was used), thus we must reduce the size of the big vacancy island because of the computer time. Thus in Our MC we use R 70atoms and the results of the simulation was correcter to size effect which was also obtained from MC with different R.
The interaction of Ag is long-rang thus there exist lot of possible steps of Ag atoms on the Ag(111) surface, but in our Monte Carlo simulation we sorted the steps to several classes (19) which we suppose to can be approximately described by single barrier. The sorting of different steps into this classes and assigning of the energy barrier for steps from each class construct of the kinetic model which describe simulated system.

1.2.1 Quantities characterizing the decay processes in Monte Carlo

In the microscopical model [12] the decay law is given by the velocity of detachment $E(r)$ from the border with curvature r and by the probabilities of diffusion between the central island and the border of the big surrounding vacancy. The decay law was derived in the

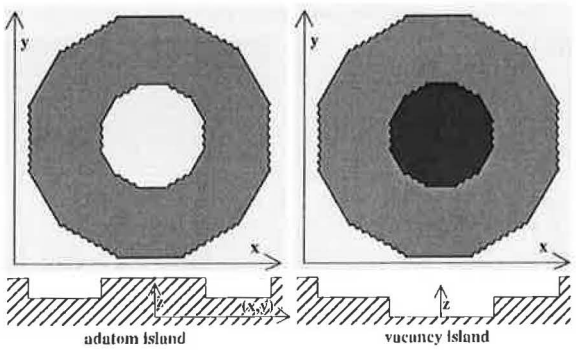

Figure 1.6: The schematic picture of the simulated area - vacancy and adatom islands which are deponed in the center of big vacancy island. The radius of the central island in MC is r=$20a_o$ and the radius of the big vacancy island is R=$70a_o$, where a_o is a lattice constant.

following form:

$$\frac{dA}{dt} = a(2\pi R)s(E(-R) - E(r))/\ln(\frac{R}{r}) \tag{1.2}$$

where s is the probability of gluing to the island if the particle is on the island border- for adatom island it is $s = 1$ and for vacancy island it is $s = \frac{\nu_s}{\nu_t}\exp(-E_s/k_bT)$, where R and r are the radii of the big surrounding island and the central island respectively.
In [10] $E(-R)$ and $E(r)$ was proportional only to binging energy $\gamma(R)$ where the radius R is a macroscopical (average) value and the microscopic structure of the edges do not play any role. In our model we do not assume anything about the velocities of detachments $E(-R)$ and $E(r)$. Both these values can be measured from the Monte Carlo simulation. As an implementation of MC, the kinetic Monte Carlo in Bortz-Kalos-Lebowitz algorithm [13] within a lattice gas model was chosen.
The silver atoms have a complicated, long-distance interaction and therefore the barriers for atom diffusion depend not only on the configuration of atoms in neighboring positions but also on the configuration of atoms in the remote vicinity. These also influence the diffusion barrier. Accordingly, in real case the number of variant energy barriers will be immoderate by height. In our model the number of barriers which describe the diffusion on the Ag(111) surface was reduced. We divided the different steps with commonly different barriers into 19 groups, in which all variant jumps were modeled only by one of these barriers. All jumps to more coordinated position ($n_f \rightarrow n_i; n_f > n_i$ in Fig(1.7)) are denoted as the same, where n_i is the number of the nearest neighbor in the initial position and n_f is the number of the nearest neighbor in the final position. For the opposite case of jumps to less coordinated positions, one group is made up of jumps with the same number in the initial and final positions (without influencing the actual configuration). In MC the jumps from bottom layer to higher layer are disabled because the probability is very low. The descent from upper layer is realized either by jumps across the border of the upper layer - this possibility is characterized by the Ehrlich-Schwöbel barrier - or it can fall to a hole which is erased after a move of an atom in its neighborhood in the lower layer. This step has a zero barrier.
In generaly, there exist two types of jumps on fcc(111) surfaces which has the same configuration of atoms in initial and final positions. These steps differ only in the position of the atoms in the lower layer. They are usually marked as step A and step B (see Fig(1.7)).
In general, both steps A and B have diverse barriers. Diffusion barriers for system Ag/Ag(111) were calculated in [14] by the semi-empirical Embedded-Atom-Method [16] and by molecular

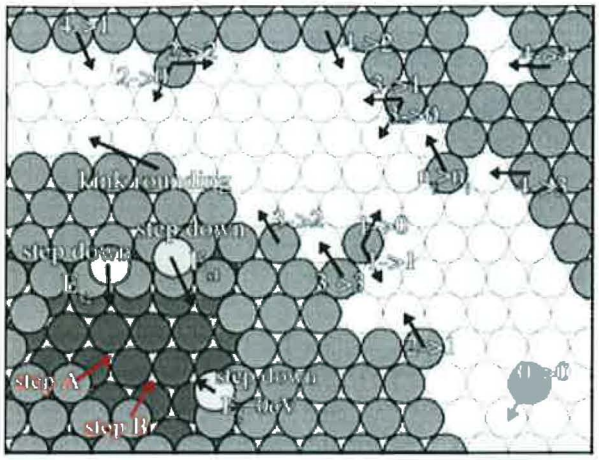

Figure 1.7: Available steps included into MC simulation.

type of process	ref[14] [eV] step A	ref[14] [eV] step B	ref[15] [eV] step A	ref[15] [eV] step B	used in MC [eV]
$0 \rightarrow 0$	0.061		0.067		0.061
$1 \rightarrow 0$	——	——	0.315		0.315
$1 \rightarrow 1$	——	——	0.077	0.132	0.077
$1 \rightarrow n_f > 1$	——	——			0.290
$2 \rightarrow 0$	0.758	0.691	——	——	0.520
$2 \rightarrow 1$	——	——	0.257	0.317	0.317
$2 \rightarrow 2$	0.294	0.338	0.221	0.296	0.300
$2 \rightarrow n_f > 2$	——	——			0.290
$3 \rightarrow 0$	——	——	——	——	0.650
$3 \rightarrow 1$	——	——	0.423	0.478	0.478
$3 \rightarrow 2KR$	0.579	0.582	——	——	0.582
$3 \rightarrow 2$	0.471	0.540			0.540
$3 \rightarrow 3$	——	——	0.387	0.457	0.382
$3 \rightarrow n_f > 3$	——	——			0.290
$3 \rightarrow 1$	0.571	0.527	——	——	0.780
$3 \rightarrow 2$	——	——	——	——	0.580
$3 \rightarrow 3$	——	——	——	——	0.400
$3 \rightarrow 4$	——	——	——	——	0.550
$3 \rightarrow n_f > 4$	——	——	——	——	0.290
descent down	0.130		0.240		variable

Table 1.1: Set of barriers A and B calculated by two different methods in eV. In the first column the barriers were calculated by the Embedded-Atom-Method [14]. The second column contains barriers as calculated by molecular dynamics [15]. The third column contains barriers, which were used in the MC simulation.

dynamics (MD) [15]. Both methods of calculation reveal quite a significant difference between step A and B, but for individual steps they do not predict the same values (compare row 2 and 3 in Tab(1.1). It was determined from observation of equilibrium shapes by STM [17] that the barrier for steps A and B on Ag/Ag(111) are nearly equal - the difference between them is less than 5%. In the MC simulation we used a set of barriers in which step A is equivalent to step B. Our choice of barriers combines values obtained from MD [15] and semi empirical calculation [14] (third row in Tab(1.1).
The probability of a jump from j-th to i-th position is given by the standard Arrhenius expression $p_{ij} = \nu_{ij} \exp(-E_{ij}/k_B T)$, where E_{ij} are the barriers mentioned above. For the prefactor ν_{ij}, two values are supposed: $\nu_{ij} = \nu_t$ for a jump on the terrace in the same layer and $\nu_{ij} = \nu_s$ for a jump across the edge from the upper to the lower layer. One of the aims of this work is to determine the ratio of ν_s/ν_t. In our MC we use a time unit (τ_u) in which the average time for a jump on the terrace at RT is 1, thus for attempt frequency with this time unit we obtain $\nu_t = \exp(\frac{0.061e}{k_b T}) \simeq 1179\tau_u^{-1}$, where e is the charge of the electron.

1.2.2 Slecting a set of barriers

The success of the MC model depend on the suitable dividing of an enormous number of possible jumps of atoms on the surface into several classes. Jumps in the same class are described by one barrier. The barriers are usually taken from some ab-initio or MD calculation, but calculation of the barrier is quite sensitive in used method of calculation and is unclear how much it describes real Ag/Ag(111) system. This MC simulation was based on the set of barriers calculated in [14]. Nevertheless in this set of barriers there are huge differences between the set steps A and B. If we used this set of barriers we obtained a "triangular" shape of big surrounding vacancy which is typical for vacancies on Pt(111), but which is wrong for Ag(111). The result of this MC is in Fig(1.8) (a) and the decay law is in (b). Also the experimental work predict that the difference between steps A and B would be smaller than 5%. For this reason we modified the original set of barrier and used the same value for

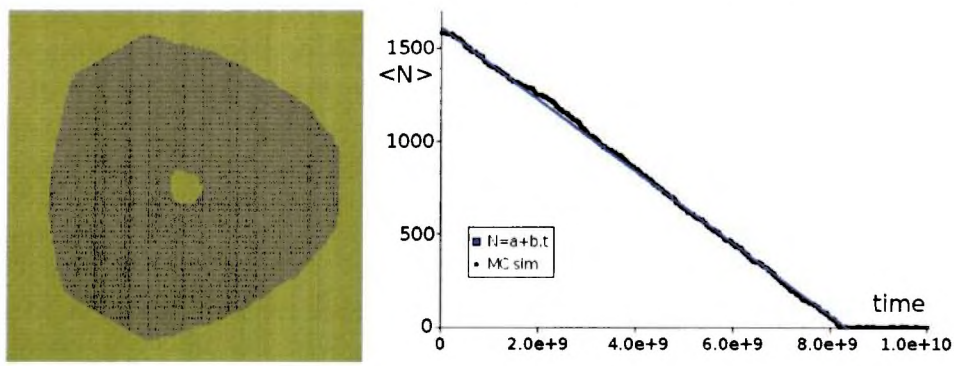

(a) (b)

Figure 1.8: (a) The quasi-equilibrium shape from MC with barriers from [14]. (b) The dependency of the number of atoms in the central adatom island over time (decay law).

both steps A and B. The result is shown in figure 1.9. The quasi-equilibrium shape here is a regular hexagon with kinked sides. This shape is closer to the equilibrium one but from

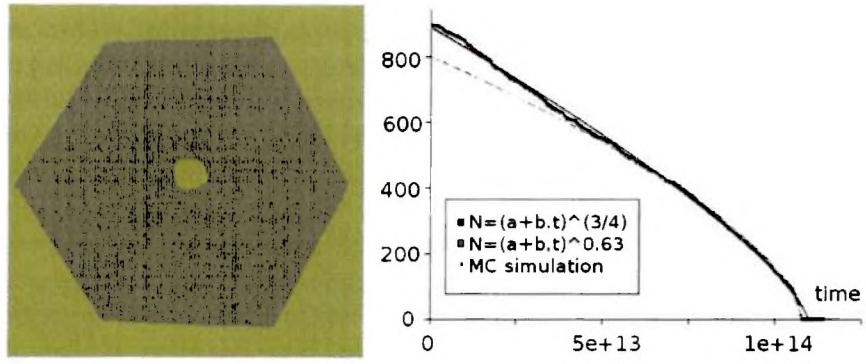

(a) (b)

Figure 1.9: (a) The quasi-equilibrium shape from MC with barriers from [14] but with barriers for steps A equal to barrier for steps B. (b) The dependency of the number of atoms in the central adatom island over time (decay law) for this set of barrier.

[17] it is known that the length of the straight segments is approximately 1/2 of the kinked. The rough shape of the big vacancy island can be seen also from Fig(1.4). For this reason we modified the barrier for kinked and straight segments to prefer the straight segments. In the final set of barriers we used the modified of barriers from [12] and [15] to obtain agreement with experiment. This set of barrier is written in Tab(1.1.

1.2.3 Results and discussion of MC simulation of adatom and vacancy decay at RT

Within the model described above we try to simulate the system which was measured in work [10]. In the simulation of the vacancy decay there is one free parameter- the effective Ehrlich-Schwöbel barrier E_s^{eff}, which drives the falling down from the terrace to the central vacancy island. The frequency factor is generally different for a jump on the terrace (ν_t) and for a jump across the step (ν_s). In the equation (1.1) it was considered that the probability that some atom would fall to the central vacancy island is:

$$p_{terrace \to vacancy} = \frac{\nu_s}{\nu_t} \exp(\frac{-E_s}{k_B T}) = \exp(\frac{-E_s^{eff}}{k_B T}) \tag{1.3}$$

which is also the definition of the effective Ehrlich-Schwöbel barrier E_s^{eff}.
For the adatom island it is $\nu_t = \nu_s$ and $E_s = 0$ because the atoms move in only one layer and no barrier joined with a jump across the edge is present. For the vacancy island the atoms from the terrace must jump across the edge and generally there exist nonzero Ehrlich-Schwöbel barrier E_s and a different ratio of prefactors $\frac{\nu_t}{\nu_s}$ for a jump across the edge. The equation (1.1) imply that the decay of vacancy island with E_s^{eff}=0 give the same result as the simulation of adatom decay. This result we try to confirm in MC simulation using our microscopic model.

Adatom island decay
This part of the story is the most important - in the work [3] was realized the simulation of adatom island Xe/Pt(111). The mobility of this island depended only on the average number of bonds of atoms on the edge to the cluster, because only these atoms can move along the

edge of the island or detach from the island easily. In [10] a classical schema is usedin which the detach velocity depends on the curvature which changes continuously during evaporation. Two examples of the decay law obtained in MC are shown on the picture Fig(1.10). In our MC we plot the number of atoms N in the cluster which is proportional to the area A of this island. For fcc we can write: $A = N\frac{\sqrt{3}}{2}a_0^2$. Because both A and N differ only in the multiplication constant we can confuse A and N only by a change of the parameters in the equations for time derivations. In MC we will use N because it is easier to obtain.

To this decay law was fitted the linear dependency and also the dependency obtained from

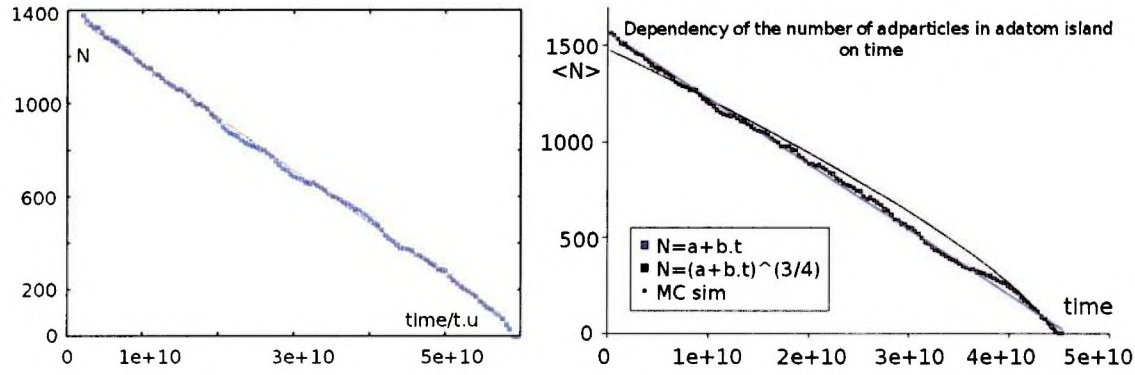

Figure 1.10: The decay laws for two different MC simulations of adatom island decay. The fitted curve is linear on the main part of the dependency. At the end of the simulation the average shape of the island changes and consequently the velocity of detachment is change.

the [10]. In this work the published shape of the decay law is in Fig(1.11)(a). In Fig(1.11)(b) are decay laws which were also measured by the group of Prof. Morgernstein but have not yet been published. Both sets of these experiments were interpreted by the semi-classical Gibs-Thompson approximation. Nevertheless these analysis give a different ratio of prefactors. Especially from the new pictures it can be seen that there could exist two parts. The

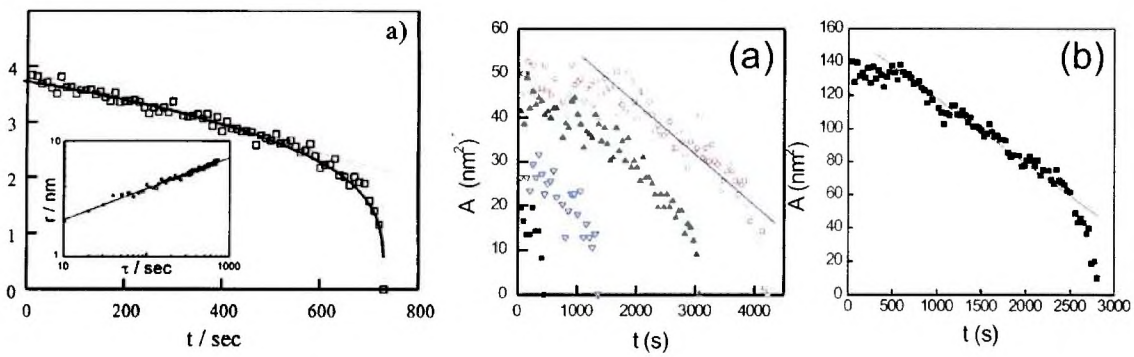

Figure 1.11: The decay law of the adatom island within the big vacancy island. The radius of the big vacancy was R=70nm. The picture on the left (a) was published in [10], the next pictures (b,c) were measured by the same group as the first one but have not been published yet.

first of these can be fitted by the linear dependency, while the second part of dependency can be fitted by the curve $(a + bt)^{3/4}$.

In MC we start with the shape of a regular dodecagon which is not the correct equilibrium shape at RT and with an empty terrace at the beginning of the simulation. This initial condition is close to the experimental one, because the "island within an island" is made by bombardment by Pb atoms at a low temperature. The simulation start by heating up the RT. It means that the shape and the number of atoms on the terrace are also not in equilibrium at RT at the beginning of the experiment.
During the simulation we also check the average number of the bonds of atoms on the edge to the central adatom cluster (γ_c) and on the edge of the big surrounding vacancy (γ_v). This value corresponds with the shape of the island. The shape of the islands changes during the simulation. It quickly switches from the original shape to the equilibrium at the beginning of the simulation. Then it slowly change and after the central adatom island is nearly evaporated, the shape (γ_c) quickly changes to prefer the less coordinated atoms (see Fig(1.12)(a) and Fig(1.15)). This is in agreement with the previous simulation [3] and also with the STM experiment of Prof. Morgenstein [18].
The average velocity of detaching from the edge is reciprocally proportional to the number of

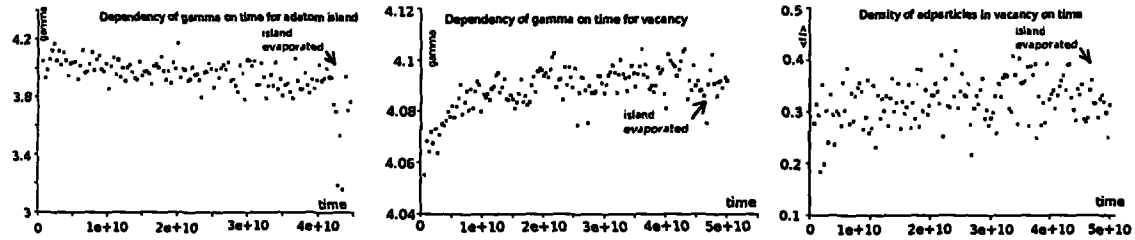

(a) (b) (c)

Figure 1.12: (a) The average number of bonds between an atom on the border of the central adatom island and the island (γ_c). (b) The average number of bonds between an atom on the border of the central adatom island and the island (γ_v). (c) The average number of atoms on the terrace.

bonds to the edge. In Fig(1.13) is the normalized difference of the velocity of detachment from the edge of the central adatom island and the velocity of detachment from the big vacancy island. This value, which is the right part of the equation (1.2) determines the derivation of the "decay law" (N(t)). In the first part the derivation is practically constant (see Fig(1.13)) and it does not change until the end of the decay. Only on the end of the dacay for radius of central island $r < 10$ the derivation changes to more curvatures (see Fig(1.13)). It mean that the average number of bonds (or parameter γ) is not constant during the simulation- this change can be caused by increases of rate of number of atoms with two or three bond. This effect for small atoms was described on work [3] for Xe cluster Pt(111).
The average density of atoms on the terrace is practically constant in case of the decay of the adatom island: $\rho_{ad} \simeq 0.2 atoms$ where $\rho_{ad} = \sum_{\Delta t} N_{terrace} \Delta t / \sum_{\Delta t} \Delta t$ is the the actual number of atoms in the time interval Δt on the terrace ($N_{terrace}$) averaged over time.

Vacancy island decay

We can observe a more complicated situation during the simulation of the decay of the vacancy island where we can recognize the relation between the density of the atoms on the surface and between the shape of the big vacancy island. This dependency shows that the changes in shape is not realized by a periphery diffusion but also the detachment and joining of atoms to/from the edge is important. This dependency is in conflict with the simply de-

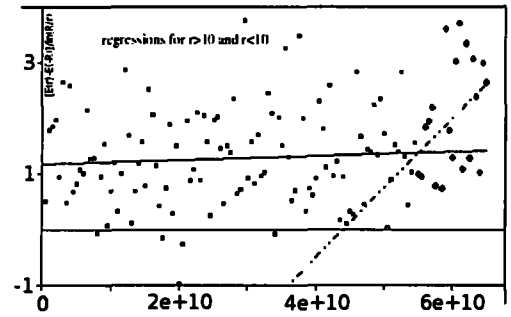

Figure 1.13: The dependency of the first time derivation of N $\frac{dN}{dt}$ over time. This is equal to the right-hand of the equation (1.2): the difference of velocities of detachment from the central adatom island minus the velocity of detachment from the big vacancy and normalized in size- $\frac{E(-R)-E(r)}{ln(\frac{R}{r})}$. The dark point mark the points where the radius of the central adatom island was smaller than $10a_0$.

pendency of the velocity of decay in the semi-classical model. In the Gibs-Thompson model the velocity of detachment is proportional only to the curvature (1/R) and this number is nearly constant during the experiment and also during the simulation.
At the beginning of the simulation, the majority of atoms on the terrace reach the central vacancy island and fall inside. The number of atoms is then smaller than in the case without the vacancy and for this reason the shape of the big vacancy island differs slightly from cases with a central adatom or a vacancy island respectively. The atoms from the terrace slowly fill the vacancy, their size decreases and, with the decrease in size, also the probability that the same atoms will fall into the vacancy. The density of atoms on the terrace starts increasing and continues after the central vacancy is filled (red arrows in Fig(1.14)). With the changes of the density of atoms correspond also the changes of the shape of the big vacancy island. It can be seen directly from the pictures from the MC simulation (Fig(1.15) (c)) and also from the chart Fig(1.14) (b) which shows the average number of bonds of atoms on the edge to the other atoms in the same layer. Especially the part after the central vacancy disappears is interesting because the increase of the density of atoms on the terrace can be caused only by changes in the shape of the big vacancy island.
This effect is stronger for smaller E_s^{eff} and less distinct for a bigger barrier, nevertheless for 0.23eV it is still notable.

The cooperation of result for adatom island and vacancy island with $E_s^{eff} = 0$ is important. It was discussed at the beginnig of this caption that the solution of equation (1.1) for both cases gives the same result. The results of MC simulation are in Fig(1.16) From the adatom island decay was obtained the decay law with a linear dependency ($q = 1$) (Fig(1.10)) and only at the end the exponent changes to $q = 3/4$. The average number of atoms $\overline{n}$ on the terrace is practically constant for the adatom island (Fig(1.12)(c)) while for the vacancy, the decay decreases because in this case the atoms can evaporate only from the edge of the big vacancy island (see Fig(1.16.b)). In case of the vacancy island, the density increases after the size of the central vacancy island starts to be small, while with the adatom island it is practically constant for the whole simulation.
The average number of bonds of atom on the edge of the big vacancy island is also constant for adatom island (Fig(1.12)(b)). But the shape of the big surrounding vacancy (and γ_v), in case of central vacancy decay, changes quite a lot (see Fig(1.16.c)) because of the changing

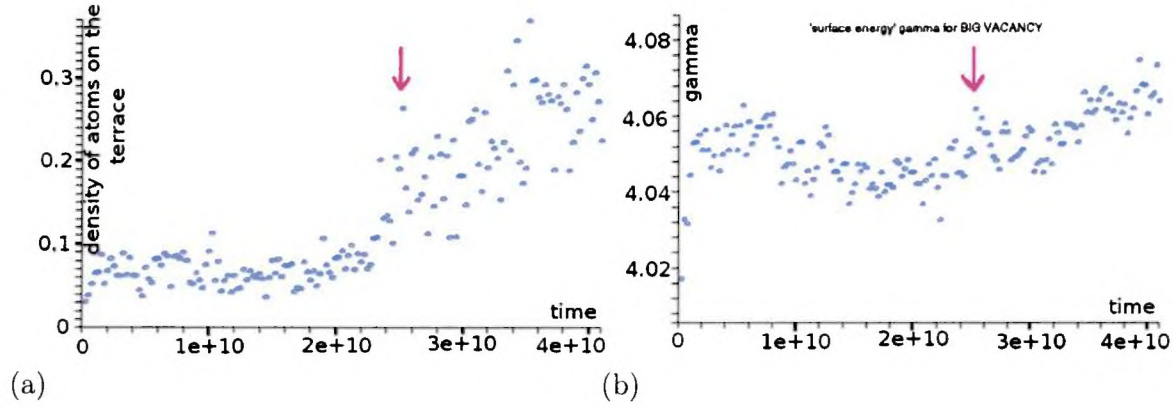

(a) (b)

Figure 1.14: The results of the simulation of the vacancy island at T=300K and $E_s^{eff} = 0.23eV$. (a) The average number of atoms on the terrace per unit time ($\overline{n}$). (b) the average number of bonds of the atoms on the edge of the big vacancy island (γ_v).

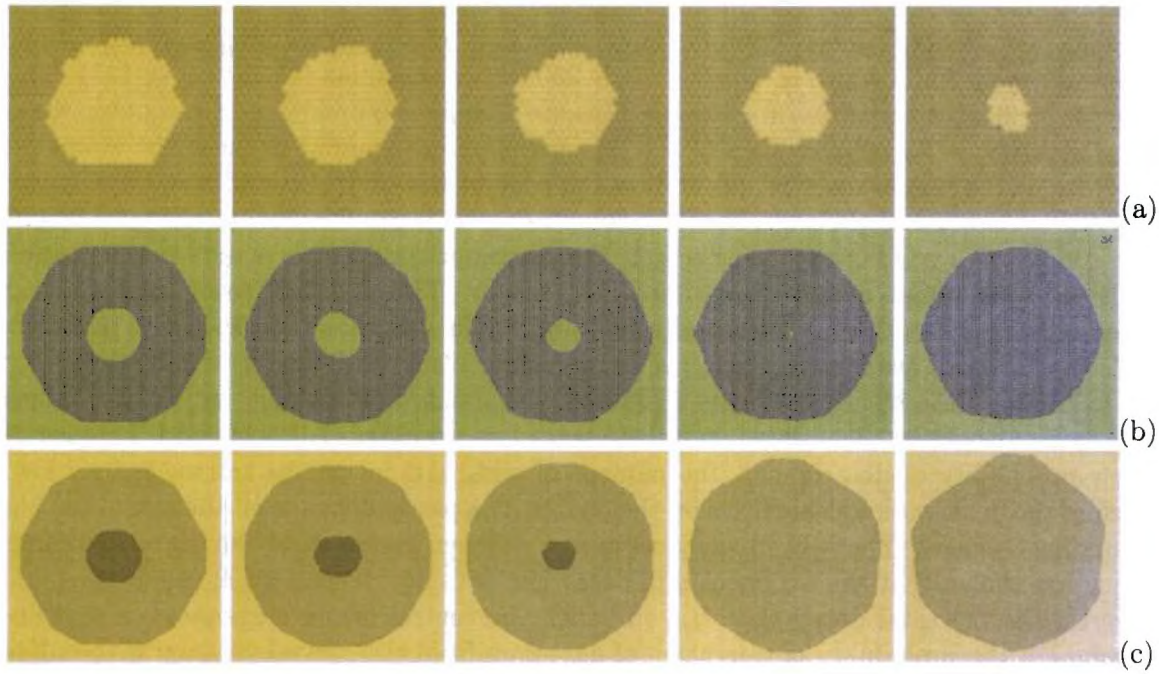

Figure 1.15: (a) The detail of the central adatom island during simulation. The changes in the shape of the big vacancy island during the decay of the adatom island (b) or the vacancy island with $E_s^{eff} = 0.23eV$ (c) respectively.

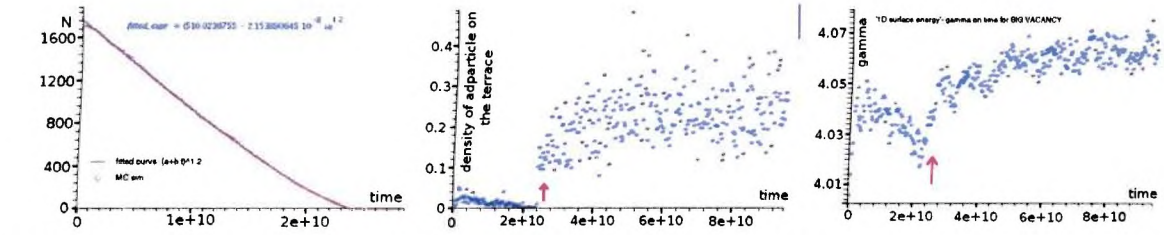

(a) (b) (c)

Figure 1.16: The results of the simulation of vacancy island at T=300K and $E_s^{eff} = 0eV$. (a) The decay law in the shape $N = (a+bt)^q$(b) The average number of atoms on the terrace per unit time $(\overline{n})$. (c) the average number of bonds of the atoms on the edge of the big vacancy island γ_v.

of the density of atoms on the island. The difference is caused by the mentioned sensitive dependency of the shape of the big vacancy island on the density of atoms on the terrace $\overline{n}$. Also the expection that the line tension γ' in equation (1.1) is equal for both the adatom and the vacancy decay is problematic, because the average number of bonds γ_v of the big surrounding vacancy and γ_c for the central adatom island are too different and inconstant.

1.2.4 Size dependency in the MC simulation

The STM experiment [10] was done for quite large sizes of the surrounding vacancy - their radius was nearly 70nm which is approximately 250 lattice constants ($250a_0$) of Ag(111). The size of the central island was 7nm ($20a_0$). Because of high requirements of computer time, we ran simulations for smaller sizes of the big surrounding vacancy. Because the atoms on the border of the big vacancy island and on the edge of the central island has, on average, nearly the same bond to the edge, then the computer time is proportional to the total length of the edges. As a consequence of this fact, the computer time for the simulation increases quickly with the radius of the big surrounding vacancy. This was the reason why we used smaller diameters for the big surrounding vacancy than was measured in the experiment [10]. The velocity of evaporation from the borders depends on the sizes of islands, thus if we want to compare the results from the STM and MC simulation, we must adjust the values to the same diameters. The diffusion on the terrace is very fast (0.061eV) and, because of the low probability of detachment, the number of add-particles on the terrace is very low. Therefore the density of add-particles on the terrace also partly depends on the size of the big surrounding vacancy. The MC simulations with a different radius R of the big surrounding vacancy has shown that the exponent q in decay law does not depend on R (see Fig(1.17)).

Nevertheless the total decay time t_{tot}, in which the central island evaporates, is size dependent. For the probability of migration of any atom from the central vacancy with radius r to the edge of the big vacancy R we can state: $p(r \rightarrow R) = \frac{2c\pi}{\ln(R)}$, the probability of migration from the big vacancy to the center one is $p(R \rightarrow r) = \frac{2c\pi}{\ln(r)}$, where c is the normalization constant. If we suppose that the average energy per unit length of the big vacancy γ will be constant, we can state that the velocity of evaporation from the central adatom island decreases with R: $E(r) \sim const - \frac{1}{\ln(R)}$, and for the central vacancy, increases with R: $E(-r) \sim const + \frac{1}{\ln(R)}$. The total times of evaporation of the central island are proportional to the velocity of evaporation:

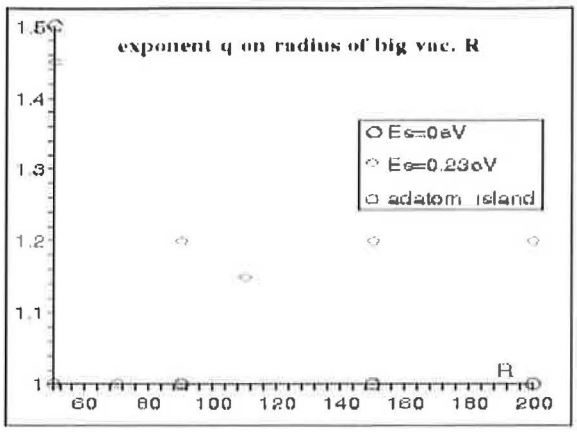

Figure 1.17: Dependency of exponent q in the decay law on the radius of the big surrounding vacancy for the adatom and the vacancy island (with E_s=0eV and $E_s = 0.23eV$)

$$t_{tot}(r) \sim \frac{1}{const \pm \frac{1}{ln(R)}} \tag{1.4}$$

where + is for the adatom and - for the vacancy island. From (1.4) we obtain a decreasing dependency for an adatom island and an increasing dependency for a vacancy island. But the MC simulation gives a decreasing dependency of t_{tot} for both the adatom and vacancy island.

The reason for this is probably the different shape of the edge of the big vacancy island. In

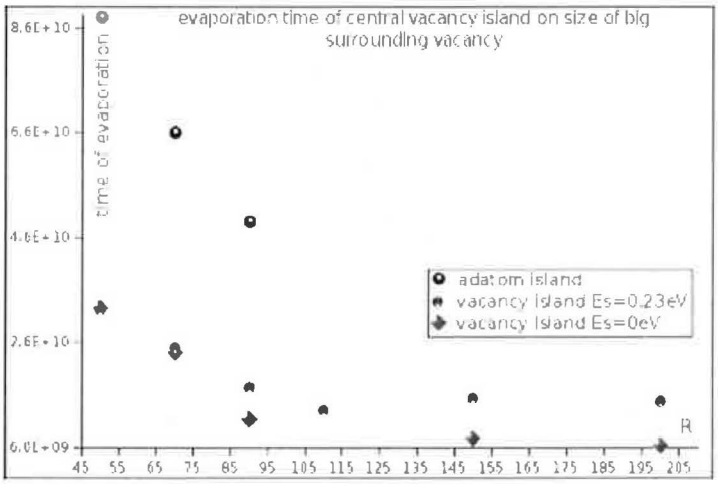

Figure 1.18: Dependency of decay times on the radius of the big surrounding vacancy for the adatom and the vacancy island (with E_s=0eV and $E_s = 0.23eV$).

the next part will be shown that the velocity of detachment from the edge of the big vacancy island $E(-R)$ very much depends on its shape. It also implies that the average energy per unit length γ_v is not constant and (1.4) is not valid.

To estimate the size effect in MC simulations, we compare the exponent q in the decay law and the decay times τ for different radii R of the big surrounding vacancy. The MC was

realized for R from 50 to 200 lattice constant (a_0) for the adatom island and for the vacancy at two values of the Ehrlich-Schwöbel barrier: E_s=0eV and E_s=0.23eV. The total times for evaporation t_{tot} of these islands are drawn in Fig(1.18). From the MC simulation for total time to evaporation we obtained a dependency which is nearly constant for $R > R_{min}$ and reciprocally proportional to R in the interval $R < R_{min}$. This picture holds true for both the adatom and the vacancy island. It shows that the energy for detachment from the edge γ_v is also a function of R. The $R_{min} \sim 60a_0$ for a vacancy island and $R_{min} \sim 90a_0$ for an adatom island. For determining the Ehrlich-Schwöbel barrier it is important to know the ratio of the decay times for the vacancy and adatom islands at different temperatures and for $R = 70a_0$ which is the radius used in the MC simulation. It is possible to obtain it from experimental results after correcting the size effect. We can approximately assume that the decay time is constant in R for the vacancy island and the decay time of the adatom island can be substituted by $t_{tot}^{R=70a_0} \doteq 1.2t_{tot}^{R=200a_0}$.

1.3 Temperature dependency

In this work we do not realize our complete goal. The construction of the Arrhenius plot and dividing of ratio of the prefactors and the Ehrlich-Schwöbel barrier is too expensive in computer time. From the simulation at RT we state that E_s^{eff} is higher than 0.35eV. But still the decay time of the vacancy island with $E_s^{eff} = 0.35eV$ is not 18 times longer than the decay time of the adatom island. We can predict that the right value is 0.38eV which implies either $\nu_t/\nu_s << 1$ if we consider the well-known value of the Ehrlich-Schwöbel barrier for Ag $E_s = 0.13eV$ or some big value E_s. This result is in conflict with both previous experiments where ν_t/ν_s 1 [10] or $\nu_t/\nu_s >> 1$ [5]. It was unfortunate that the construction of the Arrhenius plot could not be done precisely because of the huge demand on computer time. This is the theme of Appendix A, but for completeness we bring out the result (with a margin error) of obtained from the Arrhenius plot: $\nu_t/\nu_s = (0.005 \pm 0.06)$ and $E_s = (0.25 \pm 0.33)eV$ which can be rewritten as $\nu_t/\nu_s << 1$ and $E_s < 0.58eV$.

1.4 Conclusion

The inconsistent results for the ratio of prefactor and E_s barrier at RT show that our barriers do not work in all aspects of simulation of Ag/Ag(111). Nevertheless the simulation of the decay of the adatom and vacancy island at RT show that the system which we simulated has a richer behavior than can be described by the semi-classical model. The velocity of detachment from the big vacancy island depends sensitively on the shape of the big vacancy island, which is backwardly dependent on the density of atoms on the terrace. For this reason we also obtain different dependencies of decay time t_{tot} on the radius of the bid vacancy island. As strong influence on the size dependency is the structure of the edge and the simple macroscopic presumption gives the opposite dependency in size than the MC simulation.
From the different results of the MC simulation of the decay of adatom island and the vacancy island with $E_s^{eff} = 0$, we can derive that some of the parameters of equation(1.1), which are suppose to be constant change during the simulation. It was shown that one inconstant parameter is line tension γ' $\gamma_{v(c)}$, which depends sensitively on the microscopic structure of the vacancy edge.
Last, the decay law of the adatom island is not a simple curve with dependency with the

constant exponent. The derivation of this curve changes with the shape of the central adatom island. In the first experiments [10] the measured dependency conformed to the function (1.1), nevertheless the scattering of the experimental points is quite wide and the five free parameters in this dependency allows this equation to fit a large amount of experimental dependencies. With this data can also be conformed the linear dependency (for the first 2/3 of the time) and the last part must be fitted by a curve with exponent higher than 1. This corresponds with changes in the velocity of detachment from the edge (Fig(1.13)) which is equal to the derivation of the decay law (dN(t)/dT). At the beginning this velocity of detachment is practically constant and it increases at the end of the decay (where $r < 10$). The next experiments of the Morgerstein group (see Fig(1.11)) provide the decay law with a smaller scatter and the difference in both parts of the curve is stronger than in previously (published) experiments.
Nevertheless it is unclear how much this effect can influence the analysis of the Morgenstein experiment. The partial results from the temperature dependency are not demonstrative. But the results from RT show that not all can be described by microscopical values. The great problem that not clear is how much our barriers are valid for Ag/Ag(111). All presented results only show that the usage of G-T in analysis of nano-experiments is not evident and we must carefully weigh if a particular system and sizes of nano-structures allow the for use of microscopical techniques.

Chapter 2

Single atom diffusion of Pb on a Si(111)-7x7 surface

Diffusion on a semiconductor surface is a complex problem set by a strong potential corrugation resulting in multiple energy barriers that determine the jumping rate of a particle. Because of the fast particle movement on a limited area the commonly accepted criteria for surface diffusion is not fulfilled. Typical examples are observed in STM experiments on the Si(111)-7x7 surface. Ag, Sn or Pb adsorbates exhibit localised movement of single atoms in a half of the Si(111)-7x7 unit cell with rare jumps among these adjacent structural units. In a simplified approach, the lattice gas model is applied to get a diffusion coefficient from the experiment where half of the Si(111)-7x7 is taken as a single adsorption position for a subsequent jump on the surface.

This approach is too simplified and so it has to be revised. The determination of dynamics of a Pb atom inside a unit cell of the Si(111)-7x7 surface was stimulated by the fact that diffusion has been approximated only by one effective diffusion barrier for a jump between adjacent halves of the cells in most of the experiments. The omission of the movement of a particle in a half of the Si(111)-7x7 unit cell automatically leads to the supposition that a jump between adjacent halves of unit cells occurs from any position in the half-that is close to a miracle at the size of the Si(111)-7x7 unit cell. The energy barrier between "initial" and "final" halves is not the only factor that defines the probability of a jump between the halves of adjacent cells. The diffusion path and the probability of occurrence in each seat on the diffuse path that Pb passes in an initial half are equally important. The STM experiments at low coverage clearly demonstrate preferential occupation of a so-called unfaulted half of the Si(111)-7x7 unit cell. The mechanistic interpretation of data using the lattice gas model shows the presence of an asymmetric barrier between faulted and unfaulted halves, however, temperature studies prove a different diffusion path in the halves as well.
For the understanding of well-established experimental parameters of diffusion on the Si(111)-7x7 surface, we need to determine the dynamics of an adatom inside the unit cell. One method applicable to this aim is the Monte Carlo simulation that was used for an adjustment to the experiment of ab initio calculated diffusion barriers [20]. The other much more flexible possibility is an analytical calculation using the master equation for time evolution of occurrence of a Pb atom at different adsorption positions in the Si(111)-7x7 unit cell. In this paper we present the application of the master equation in order to describe the tracer diffusion in as limited an area as the Si(111)-7x7 unit cell. The results demonstrate the possibility of the use of this method for describing different diffusion paths in faulted and unfaulted halves, comparable with the results of the Monte Carlo simulation and possessing identical assump-

tions and limitations. However, the analytical formula for the evaluation of mean values of diffusion parameters is much more comfortable and rapid.

2.1 The experiment and the Monte Carlo simulation

The pattern observed after the deposition of Pb atoms on the Si(111)-7x7 surface by STM microscopy is explained by the rapid frequency of jumps of a single Pb atom inside one half of the 7x7 unit cell at RT [21]. Single atom diffusion has not been observed, only jumps of this fuzzy object between adjacent halves of the 7x7 unit cell was pictured with STM. The jump rate between these halves is very low, therefore an atom moves inside a particular half for a long period. The STM of a Pb atom inside a half of the cell reflects the mean time that an atom resides in particular positions during scanning. We considered the theoretical simulation of this diffusion in the limited area as the main goal of this work. Diffusion barriers in the initial stage were taken from calculations using the extended Hückel approximation [19]. The absorption sites that are used in this paper are taken directly from the STM experiment and were confirmed by the kinetic Monte Carlo simulation as well (for detail see [20]).
The STM images fig(2.2) show that the probability of finding a Pb atom in any adsorption position is equal inside the unfaulted half. On the other hand, the probability of finding a Pb atom in the centre is higher in the faulted half. Performing the MC simulation of Pb atom diffusion in the 7x7 unit cell with barriers calculated by Hückel approximation [19], we obtain an identical probability distribution of Pb atom in both halves, in contradiction to the STM experiment. Therefore, in [20], another set of diffusion barriers fitting the STM experiment at low temperature (50 K) has been proposed. The list of both sets of diffusion barriers is shown in Tab(2.1). In this work we report the results of the analytically calculated parameters for tracer diffusion of a Pb atom inside the 7x7 cell. Consequently, the effective energy barrier and difference in binding energy between neighbour halves of an unit cell on the 7x7 surface was estimated. The diffusion parameters obtained from the analytical calculation, the experiment and the MC simulation were compared.

2.2 Theory and results

Our calculations use a lattice gas model [27], i.e. the Pb atom can occupy only nine positions in each half of the unit cell, and the times for jumps between these positions are considered to be zero. We use the same adsorption sites as in [20, 21]. Thus, we can recognize three equivalent types of positions: sites A, B in the faulted half (A', B' in the unfaulted half) mark the positions on top of the adatoms and R (R' in the unfaulted half) marks the position on top of the restatom. All these positions with paths of permissible jumps are shown in Fig. 1. Their geometry is the same in both halves of the unit cell as is well known from the DAS model [19].
We shall study the diffusion on a 2D surface with translation symmetry of the unit cell. The probability of the occurrence of a single Pb atom in adsorption places on the surface is given in general by the master equation:

$$\frac{\partial \overrightarrow{p}(t)}{\partial \overrightarrow{t}} = -W.\overrightarrow{p}(t) \tag{2.1}$$

where vector $\overrightarrow{p(t)}$ contains the probabilities of occurrence in each place on whole surfaces and W is the infinity transfer matrix between these places. The number of columns and rows of W

Barriers from:		Hückel approximation [19]	MC sim. [20]	Analytic calculation	Error of fitting
Unfaulted half (inter-half barriers)	E_{AR} [eV]	0.7	0.09	0.086	9.6e-05
	E_{RA} [eV]	0.16	0.07	0.072	7.3e-06
	E_{BR} [eV]	0.62	0.16	0.162	6.9e-06
	E_{RB} [eV]	0.33	0.09	0.0877	7.3e-06
	E_{AB} [eV]	2.15	0.75	0.5914	0.76
	E_{BA} [eV]	1.92	0.8	0.586	0.78
Faulted half (inter-half barriers)	$E_{A'R'}$ [eV]	0.66	0.14	0.1414	1.2e-04
	$E_{R'A'}$ [eV]	0.21	0.1	0.0988	1.2e-04
	$E_{B'R'}$ [eV]	0.61	0.14	0.1393	9.8e-05
	$E_{R'B'}$ [eV]	0.4	0.1	0.101	9.9e-05
	$E_{A'B'}$ [eV]	2.15	0.8	0.63	0.77
	$E_{B'A'}$ [eV]	1.92	0.8	0.72	0.78
Intra-halves barriers	$E_{A'A}$ [eV]	1.45	0.6	0.6030	7.0e-08
	$E_{B'B}$ [eV]	1.51	0.55	0.5736	1.2e-04
	$E_{AA'}$ [eV]	1.64	0.65	0.5547	1.1e-04
	$E_{BB'}$ [eV]	1.69	0.65	0.6095	1.7e-04

Table 2.1: The energetic diffusion barriers for acceptable jumps between two neighbouring places on Si(111)-7x7 surface. In the first column are the diffusion barriers from the Hückel approximation [19], in the second are barriers from the MC simulation [20]. The third and fourth are the result of fitting the analytical results on the same experimental data as in [20]- we obtain nearly the same set of energies.

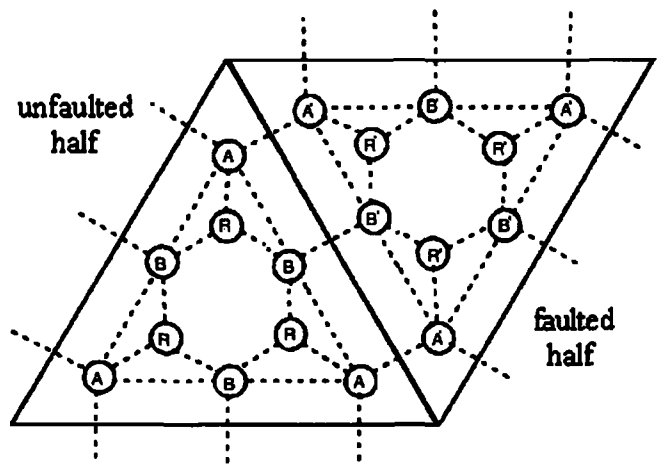

Figure 2.1: The Si(111)-7x7 unit cell with considered adsorption places. The geometry of faulted (dashed) and unfaulted (undashed) is the same, the potential surface in both halves differs because of the diverse configuration of the lower layer.

rows of W is equal to the number of adsorption places. We are interested only in the stationary solution of the master Eq. (1), which does not depend on the initial position of the adatom. This solution also corresponds with the STM picture. The effect of different initial conditions disappears in the limit of long time: $p_i \equiv p_i^{eq} \equiv \lim_{t\to\infty} p_i(t)$ Because of translation symmetry on the surface there will be the same distribution of probability of occurrence in different places inside each unit cell. There also exists symmetry inside the unit cell: from 18 adsorption places only six of them have independent values of probability of occurrence. Thus using the translation symmetry and the symmetry of unit cell, the infinity matrix can be reduced into a matrix with only 6 x 6 components:

$$W = \begin{pmatrix} p_{A\rightarrow} & p_{RA} & 2p_{BA} & 2p_{A'A} & 0 & 0 \\ p_{AR} & p_{R\rightarrow} & 2p_{BR} & 0 & 0 & 0 \\ 2p_{AB} & 2p_{RB} & p_{B\rightarrow} & 0 & 0 & p_{B'B} \\ 2p_{AA'} & 0 & 0 & p_{A'\rightarrow} & p_{R'A} & 2p_{B'A'} \\ 0 & 0 & 0 & p_{A'R'} & pR' \rightarrow & 2p_{B'R'} \\ 0 & 0 & p_{BB'} & 2p_{A'B'} & 2p_{R'B'} & p_{B'\rightarrow} \end{pmatrix} \tag{2.2}$$

The sub-matrix $\{W_{ij}\}_{i,j=1}^{3}$ describes the diffusion inside the unfaulted half of the unit cell and the sub-matrix $\{W_{ij}\}_{i,j=4}^{6}$ the diffusion inside the faulted half. Items $W_{14}; W_{41}; W_{36}$ and W_{63} describe inter-halves jumps. Due to the symmetry the number of components in vector $\vec{p}(t)$ in (1) will also to be reduced to six different values:

$$\vec{p}(t) = (p_A(t), p_R(t), p_B(t), p_{A'}(t), p_{R'}(t), p_{B'}(t)) \tag{2.3}$$

Each of these components is the time density of probability of the presence of a Pb atom in the appropriate site (for example A for the first component, R for the second etc.) at time t. The total probability of the localization of Pb in the unit cell is normalized, $\sum_{i=1}^{6} p_i(t) = 1$. W_{ij} is the probability of a jump from ith to jth types of positions, $i, j \in \{A, R, B, A', R', B'\}$. W_{ii} presents the probability of the escape of ith position: $W_{ii} = p_{i\rightarrow} = -\sum_{i,i\neq j} W_{ij}$. The W_{ij} component of the matrix can be obtained as a product of the probability p_{ij} for a single jump from ith to jth position, multiplied by the number of neighboring places of jth type. The probability of a single jump between i and j positions depends on the size of the energetic diffusion energy barrier by Arrhenius shape $p_{ij} = \nu \exp(\frac{E_{ij}}{k_B T})$. The frequency μ inside the cell determined from the calculation of phonon spectrum [25, 26] as well as from experiment [20, 24] is $10^{12-13} s^{-1}$. In our analytical calculation we used the value $\nu = 10^{12} s^{-1}$. The stationary values p_i that we obtain as a solution of master equation 2.1 are in Tab(2.2) and they are displayed in Fig(2.2) for both sets of barriers.

2.2.1 Intra-halves diffusion

The frequency of jumps observed at 50 K is given mainly by the frequency of jump inside the halves. Jumps between the halves of the unit cell were not observed during the STM measurement. In the next calculation of the frequency of jumps at 50K, the jumps across the boundary of different halves of the cell are allowed, but their probability is small because of the high diffusion barrier between the places from t neighbour halves.

The characteristic value describing intra-half diffusion is the mean value of the time, that a Pb atom spends in ith position and is proportional to the probability of occurrence p_i. The mean frequency of jumps between neighbouring positions is given as a product of the probability of occurrence p_i in ith position multiplied by the inverse time for escaping from

	T = 50K		T = 300K	
	Hückel [a]	MC [b]	Hückel [a]	MC [b]
p_A	1	9.22e-06	0.9993	0.115
p_R	4.16e-55	8.92e-08	8.63e-10	0.053
p_B	6.66e-26	0.999991	6.36e-05	0.795
$p_{A'}$	7.34e-20	8.50e-11	6.47e-04	0.0167
$p_{R'}$	3.53e-65	7.96e-15	1.81e-11	0.0036
$p_{B'}$	4.97e-44	8.50e-11	6.06e-08	0.0167

[a] Barriers from [19]
[b] Barriers proposed in [20]

Table 2.2: The density probability of the occupation for six expectant types of adsorption positions of Pb in faulted and unfaulted (dashed) halves of Si(111)-7x7 unit cell.

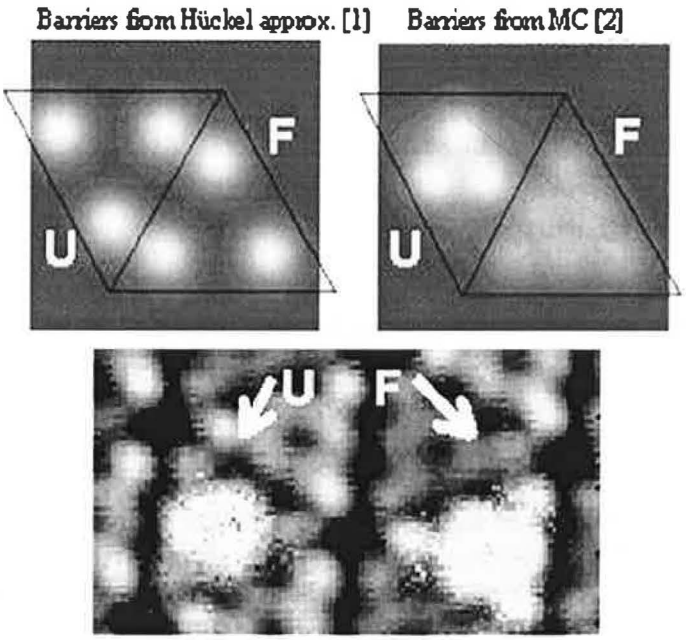

Figure 2.2: The reconstruction of STM images from analytic calculation at 300 K of density probability of appearance in different positions (based on two sets of energies taken from [19] (figure a) and [20] (figure b)). The probabilities of occurrence in different positions are fuzzed by normal distribution around the adsorption seat. The integral sum of probabilities is still one in each of the halves. The analytical results are compared with STM. We obtain the same picture also for T=50K. The particular values for probabilities of occurrence at different temperatures are shown in Tab(2.2).

this position:

$$\Gamma = \sum_{i=1}^{6} \frac{p_i}{\tau_{i\rightarrow}} \tag{2.4}$$

In equilibrium the mean value of time for the escape from the ith position: $\tau_{i\rightarrow} = 1/W_{ii}$ can be also derived from the energetic barriers. The value of the frequency of jumps calculated from the master equation, determined by the MC simulations and extracted from the experiment, are shown in Tab(2.3).
The numbers in Tab(2.3) show that the frequency of jumps calculated (resp. simulated) using the result of theoretical works [19] is much lower than values observed by STM at 50 and 70 K [20].
For thermally activated motion the average frequency of jumps should follow an exponential dependence on temperature

$$\Gamma = \nu_d \exp\left(-\frac{E_d}{k_b T}\right) \tag{2.5}$$

where E_d and ν_d is an effective diffusion barrier and the frequency factor for motion inside the halves of the unit cell. For the interval of temperatures between 320 and 370 K the parameters of Eq. (2.4) for both sets of energies were obtained from temperature dependency (2.4) with the following results: $E_d^{Huc} = 0.7eV, E_d^{MC} = 0.14eV$. The high value of activation energy for diffusion inside the halves of the unit cell taken from Hückel approximation corresponds to the low frequency of jumps, which was discussed above. The value 0.7 eV is too high for the diffusion inside the halves of unit cell because the barrier for diffusion between the halves, which was measured at the same temperature interval, is $E_{eff} = (0.64 \pm 0.07)eV$ [21] and $E_{eff} = (0.56 \pm 0.07)eV$ [22]. The value calculated from MC barriers 0.14 eV describes well the high frequency of jumps, as was measured in [20].

2.2.2 Inter-half diffusion

The temperature dependence of frequency Γ_{UF} for jumps between cells (or equivalently halves of unit cells) has the same shape as the Eq. (2.4), only the mean value of activation energy and the frequency factor are different:

$$\Gamma_{UF} = \nu_{eff} \exp\left(-\frac{E_{eff}}{k_B T}\right) \tag{2.6}$$

This quantity was determined from experiment [21, 22, 23]. The other way of determining the frequency Γ_{UF} is from the dynamics of a single Pb atom on the surface. In our model it can be described as the product of frequency p_{ij} of jumps across the border between two places from faulted and unfaulted halves multiplied by probability p_i of occurrence at the initial position and summed over all appropriate jumps:

$$\Gamma_{UF} = 3(p_A 2p_{AA'} + p_{A'} 2p_{A'A} + p_B p_{BB'} + p_{B'} p_{B'B}) \tag{2.7}$$

The relations (2.6) and (2.7) allow us to determine the effective barriers and the attempt jump frequency for diffusion between the halves of the unit cell from Arrhenius plot (Tab(2.4)). Different depths of minimum potential energy curve for single Pb migration in unfaulted and faulted halves of cells were also mentioned in the experiment [20, 21, 22]. The difference in binding energies can be estimated in equilibrium from ratio of the number of single atoms in the unfaulted and faulted half [20, 22] or, if the condition of detailed balance is executed, from the ratio of the frequency of jumps from the unfaulted to the faulted half and the

	T=50 K		T=71 K	
	Hückel app. [19] (^{a})	MC sim. (^{b})	Hückel app. [19] (^{a})	MC sim. (^{b})
$\Gamma_{calc}[s^{-1}]^a$	6.41E-59	0.0162	4.54E-38	253.6
$\Gamma_{MC}[s^{-1}]^b$	1.11E-70	0.0116	8.26E-38	233
$\Gamma_{exp}[s^{-1}]^c$	0.011		0.05	

[a] Barriers taken from [19].
[b] Barriers proposed in [20].
[c] Results of [20].

Table 2.3: Comparison of the frequencies of a single Pb atom jumps obtained from the experiment, analytic calculation and the MC simulation using the two set of barriers (barriers determined by Hückel approximation [19] (^{a}) and barriers proposed in [20] (^{b})).

inverse processes [21]. In the first case, according to Boltzmann thermodynamics, it yields the following expression:

$$R(T) = \frac{n_U}{n_F} = \frac{\sum_{i \in unfaultedcell} p_i}{\sum_{i \in faultedcell} p_i} \simeq \exp\left(\frac{\Delta E}{k_B T}\right) \tag{2.8}$$

In comparison with the theory and the experimental results, we obtain the energy difference between the binding energies of single Pb at the unfaulted and faulted halves (Tab(2.5)).

2.3 Discussion

The results of the MC simulation [20] were based on the adsorption sites determined by the extended Hückel theory [19]. In our calculation, we extended these first findings [20] by determining other characteristics (effective diffusion barriers E_d for intra-half, E_{eff} for inter-halves diffusion and the difference ΔE in binding energy of Pb atom in the faulted and unfaulted halves) of diffusion of Pb on Si(111)-7×7 surface using the energetic diffusion barriers from Hückel theory[19] and barriers proposed in MC simulation [20]. The extended Hückel calculation can describe well the adsorption positions. But their diffusion barriers are less precise and cannot be used in the computation of the dynamics of Pb adatom at Si(111)-7×7 surface. It follows that the frequency of jumps inside one half of the unit cell Γ_{Huc} and between the halves Γ_{UF} are too small in comparison with the experimental results (see Tab(2.3 and Tab(2.4).

Also the STM image simulation of Pb single atom inside the unit cell, calculated from barriers obtained from Hückel calculations, is not consistent with the STM experiments at 300 K (see Fig. 2a and c). We can see that there is no difference between patterns in faulted and unfaulted halves in the Fig. 2a, and the maximum intensity is placed above the corner adatoms. However, in Fig. 2c one can see an equal intensity in the faulted halves and a sharp maximum in the centre of the unfaulted half.
Based on these reasons a second set of barriers was established in [20] to reproduce the experimental findings.
Using these barriers, we found a value $E_{eff}^{MC} = 0.654eV$ for an effective intra-halves diffusion barrier, which is in agreement with the experimental values $(0.64 \pm 0.07)eV$ [21] and

E_{eff}^{Huc}	E_{eff}^{MC}	E_{eff}^{expa}	E_{eff}^{expb}	$\nu_{eff}^{Huc}[s^{-1}]$	$\nu MC_{eff}[s^{-1}]$	$\nu_{eff}^{exp}[s^{-1}]^a$
1.64 eV	0.654 eV	$(0.64 \pm 0.07)eV$	$(0.56 \pm 0.07)eV$	1.1×10^{13}	1.6×10^{13}	$10^{(6\pm1)}$

[a] Experimental result [21].
[b] Experimental result [22].

Table 2.4: The effective diffusion barrier and the effective frequency of attempts to jump between cells at 320370 K. Subscripts ^{Huc} and ^{MC} have differing values based on energies from Hückel theory [19] (^{MC}), and on the barriers proposed in the MC simulation [20] (^{Huc}). Superscripts ^{a} and ^{b} mark the experimental results accepted from Refs. [21, 22].

ΔE^{Huc}	ΔE^{MC}	ΔE^{expa}	ΔE^{expb}
190 meV	93 meV	$(27 \pm 9)meV$	$(42 \pm 11)meV$

[a] Experimental result [22]
[b] Experimental result [23]

Table 2.5: The energy difference between the binding energies of single Pb at the unfaulted and faulted halves at 320370 K. Subscripts ^{Huc} and ^{MC} have differing values based on energies from Hückel theory [19] ^{Huc}, and on the barriers proposed in the MC simulation [20] ^{MC}. Superscripts ^{a} and ^{b} mark the experimental results accepted from Refs. [22, 23].

$(0.56 \pm 0.07)eV$ [22]. But the prefactor $\nu_{eff}^{exp} = 10^6 s^{-1}$ is around 10^7 times higher than the calculated value $\nu_e^{MC} ff \sim \nu_{eff}^{Huc} \sim 10^{13} s^{-1}$. The frequency of attempts to jump inside the halves determined from calculation of the phonon spectrum [25, 26] as well as from experiment [20, 24] is $10^{12-13} s^{-1}$. It is conceivable that the frequency of jumps between two halves is 10^7 times smaller than inside one half.
Both sets of diffusion barriers [19, 20] are characterized by the difference in the binding energies ΔE of Pb adatom in the faulted and unfaulted halves of the Si(111)-7×7 unit cell. This is a well-known fact from experiments [21, 22, 23]. The unfaulted halves are always preferred in both cases. The difference ΔE^{Huc} in binding energies between both halves equals 190 meV according to the Hückel theory i.e. nearly 7 times higher than experimental results. ΔE^{MC} is equal to 93 meV, it use barriers taken from MC simulation [20]. For comparison, the experimental values are $\Delta E^{exp} = (42 \pm 11)meV$ [23], $\Delta E^{exp} = (27 \pm 9)meV$ [22].
The fitting of diffusion barriers in MC simulation was done at the temperature T=50 K. Due to the low temperature and to the finite time for simulation, the inter-halves barriers $E_{AA'}, E_{BB'}, E_{A'A}, E_{B'B}$ have a large statistic error. Thus the R (and ΔE^{MC}, which is derived from the temperature dependence of R) calculated with these energy barriers also has this statistical error.
From our calculation, we obtain a more precise formula for ratio R, thus we can still specify the values $E_{AA'}, E_{BB'}, E_{A'A}, E_{B'B}$. When we minimized the differences between the calculated and experimental values of R and Γ, we found the same values for all barriers except for the four inter-halve barriers $E_{AA'}$, $E_{BB'}$, $E_{A'A}$, $E_{B'B}$ (see columns in Tab(2.1). With these four new energies we acquire $E_{eff}^{\prime MC} = 0.594eV$ and $\Delta E^{\prime MC} = 20.4meV$.

2.4 Conclusion

We calculated effective diffusion barriers E_d for intra-half, E_{eff} for inter-halves diffusion and the difference ΔE in the binding energy of Pb atom in the faulted and unfaulted halves from the dynamic of Pb atom on the Si(111)7×7 surface using the analytical approach. We found values, which are in excellent accordance with available experimental data. Also based on the adsorption positions taken from the extended Hückel approximation work, we were able to reproduce the STM picture in both halves of a unit cell at room temperature.

Chapter 3

The growth Pb islands on Si(111) - Self-assembling processes on Pb/Si(111)

The Si(111) is a well studied surface for which the structure of the surface is known. After adding a trace amount of some metal the surface reconstruction can be completely different and the position of atoms of the surface alloy is problematic. Some of these metals are also Pb and the changes in reconstruction in one special event of system Pb/Si(111)-(7x7) was discussed in Chapter 2. The next two chapters of this thesis the growth of the Pb island's on Si(111) will be disscussed - namely the self-assembling processes at variables coverage and temperature (in this chapter) and the kinetic model of nucleation and growth in height (in the next chapter). In this chapter we try to reconstruct the phase diagram in which the island's height at equilibrium is given by temperature and coverage. Nevertheless in the next paragraph the knowledge about system Pb/Si(111) at different coverages and temperatures will be briefly compiled.

3.1 Ordered phases of Pb/Si(111)

Chemically, Pb does not react with bulk Si and they are mutually insoluble [28, 29, 30]. On the other hand on an Si surface, ordered Pb phases are formed depending on the coverage, temperature and annealing history. DFT calculations have shown that the Pb-Si bond is aproximatelly 15% longer than the Si–Si bond. For example for coverage 1/6ML, the so-called mosaic phase (γ–$\sqrt{3} \times \sqrt{3}$R30°) was experimentally observed [31, 32] and the DFT calculations [33] give a length of the Pb-Si bond of 2.82Åand a length of Si–Si of 2.44Å. Pb adatoms are, in this system, moved upwards with respect to Si adatoms and Si atoms in the substrate under Si adatoms are pushed down. The difference in the adatoms height was found to be 0.87Å.
As the coverage increases, the Si atoms sitting at the the T4 (see Fig(2.1) in Chapter 2) site are gradually replaced by Pb atoms [34]. At coverage between 1/6 and 1/3 above room temperature, a phase coexistence was found between $\sqrt{3} \times \sqrt{3}$R30° also known as β-phase and the 1×1 phase. As the temperature is lowed below room temperature both the $\sqrt{3} \times \sqrt{3}$R30° and 1×1 transform into a 3×3 phase and $\sqrt{3} \times \sqrt{7}$ respectively [35, 36, 37]. The exact nature of the transformation of the $\sqrt{3} \times \sqrt{3}$R30° into the 3×3 phase is still a matter of intense scientific debate. Several physical processes, such as the charge density waves [38],

the influence of the point defects [39], the electron mediated adatom-adatom interaction [40] or the recently proposed stabilization role of the surface soft phonon [41] have been proposed as the driving force for this phase transition. At coverage 2/3 Lay et all [30] observed a stable phase with an ordered structure $\sqrt{3} \times \sqrt{3}$R30° with two Pb atoms adsorbed at T4 sites but since then, no other group reported this phase at this coverage. Five stable configurations were found in DFT calculations [33]: T4–T4, T1–T1, H3–H3, T1–B and T4–H3. These configurations are labelled by positions of Pb atoms within a unit cell; B means adatom in bridge position. In the case of T4– H3 configuration both Pb adatoms are placed off–site. All configurations use two Pb atoms in a $\sqrt{3} \times \sqrt{3}$R30° cell. At a coverage of 1 ML alteenating domains composed of $\sqrt{3} \times \sqrt{3}$R30° unit cells are observed. STM experiments observed alternation domains of trimers with quasi-1 × 1 regions in between [42]. The trimers are composed of three Pb atoms at T1 sites displaced either towards H3 or T4 sites.
Ordered structures exist also for coverage between 1 and 4/3 ML [43, 35, 33, 44]. The reconstruction in the interval 1.2-1.3ML was found to be highly dependent in coverage with a "devil's staircase" phase diagram [45]. The microscopic model of this quick changes between different reconstructions in not fully clear.
At higher coverages the ordered reconstructions of the surface are replaced by an amorpheous wetting-layer which is approximately 1 layer thick and is present at coverage lower than 3.5ML at 130K or 1.5ML at 270K (see Fig(3.2)). Above this value of coverage the nucleation of separated Pb islands start. These Pb islands have a lot of unique characteristics which are put down to quantum effects. The next two chapters are dedicated to the domain of system Pb/Si where the nucleation and growth of Pb islands is observed.

3.2 Experimental overview

The observation of Pb islands with preferred heights [46] was first observed on systems Pb/Cu(111) [47] and later also for Pb/Si [48],[49],[49],[51]. In these experiments only certain heights of islands were observed. It is considered that the existence of preferred heights joins with the quantum character of the total energy of Pb islands. At low temperatures (1K-4K) another quantum effect can also be observed: the superconductivity of nanomer-size of Pb islands was studied [51] on islands with ranges from 80 to 300 nm in diameter and 7,9,11 and 13 monolayers in thickness. At a temperature as low as in this experiment the wetting layer formed on Si surface has a thickness of 3ML and the Pb islands grow above this WL.

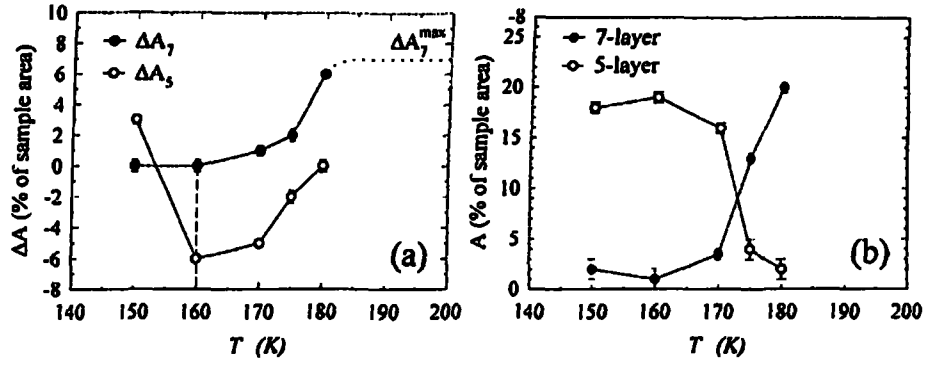

Figure 3.1: The population of 5 and 7 layer height islands after adding of 0.5ML at different temperatures. Picture and description are taken over from [50]. (a) Change in island area vs. T_G of 5- (o) and 7-layer islands (•) after depositing an additional 0.5 ML of Pb. The dotted line shows the saturation value ΔA_7^{max}. The vertical dashed line marks the onset of seven-layer island nucleation. (b) Island area vs. temperature T of 5-(o) and 7-layer islands (•) from the initial Pb deposition.

The developing of the island population over time was studied in work [50]. In the picture Fig(3.1) is the population of 5layer and 7layer height islands. At the critical temperature T_c, the 5 layer islands change to 7layer height islands. Above the critical temperature $T_c \simeq 180K$ 7-layer tall islands dominate, under this temperature 5 layer height islands dominates. In this experiment 0.5ML was added in a second deposition at different temperatures - they determined if Pb atoms occupy rather 5th layer or 7th layer height island or if they form a new 2 and 3 layer height island. At the lower temperature $T < 175K$ the initial distribution does not change. For temperatures between 175K and 180K, each additional 0.5ML implies the growth in height of 5 layer height island - on the chart the population of 5 layer islands decreases for the benefit of 7-layer islands.
The height of Pb/Si islands which are preferred at a given coverage and temperature is unambiguously determined by the phase diagram Fig(3.2). This phase diagram was published in [49] and was measured by two types of experiment: at a constant coverage and increases in temperature ($120K < T < 250K$) and at a constant temperature and increases in coverage ($\theta < 7$).
The STM picture taken in the mentioned experiment [49] at coverage $\Theta = 3ML$ and temperature $T = 192K$ close to the critical temperature $T_c \simeq 180K$ is in Fig(3.3). On the histogram Fig(3.3.b) are the numbers of atoms with "stable" heights 5 (peak 6.7) and unstable heights 2 (peak 3.8), 4 (peak 5.7). In our work we number layers from the wetting-layer (WL) - it mean that a 5-layer island has 6 layers of Pb above the Si(111) surface. On Fig(3.3) are the

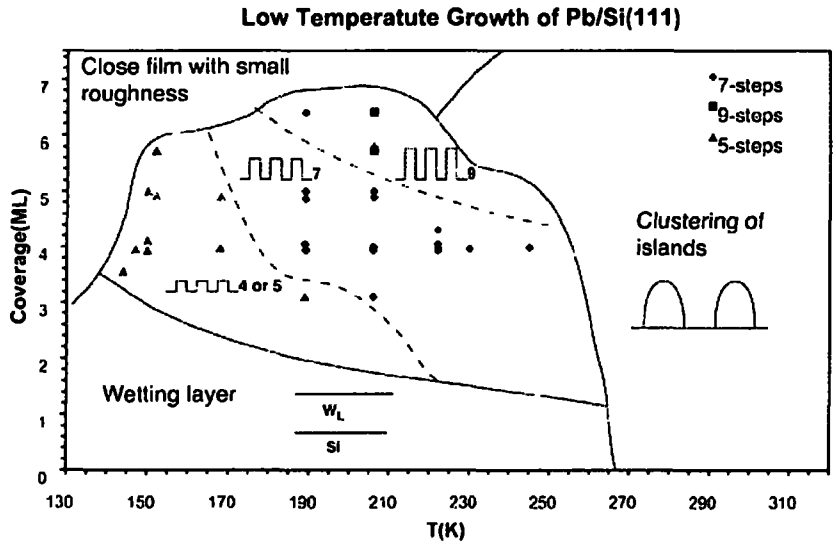

Figure 3.2: The dependency of island height on the coverage and temperature taken from [49]. The points in the chart were obtained at constant coverages and increasing temperatures as well as at a constant temperatures and increasing coverage.

layers numbered from Si. The STM pictures from this experiment is in Fig(3.4) - in the first pictures the nucleation of new small islands is quite common, at a higher temperature the small island's slowly decay and the other 5 and 7 layer height island grow. above 175K the small 2,3 layer height island disappear and the 5layer islands change to 7-layer islands.

3.3 Ab-initio calculation and Quantum Size Effect (QSE)

In the population of the islands which are observed at different temperatures and coverages at equilibrium, not all heights are represented with the same probability. There exist heights which are strongly preferred. At a higher velocity of vaporation of Pb on Si the population with different heights was measured, but only odd heights was measured in the experiment [46].

The stability of islands with preferred heights is interpreted as the result of quantum size effect (QSE). The calculation of the energy of freestanding Pb slab [52] was done for a thickness from 1ML up to 25ML, the maximum difference in energy per 1x1 unit cell between the following layers was 0.08eV 1,3,5 above the wetting layer were calculated as superstable.

With the increasing height the difference between stable and unstable layers decreases. The chart of surface energy per 1x1 unit cell which was published in [52] is shown in Fig(3.5). The energy of an unit cell of Pb (Pb/Si) was calculated by a different ab-initio method [53, 52]. In [53] the surface energy per unit cell with Si slab was also calculated. The comparison between the results for a freestanding slab and a Pb/Si slab which was published in [53] is in Fig(3.6)

Nevertheless the connection between the energy of the Pb slab and some surprising details of experiment is not clear and due to the size of the system the whole island can not be exactly calculated. In this and next chapter Monte Carlo was used to find a possible explanation for

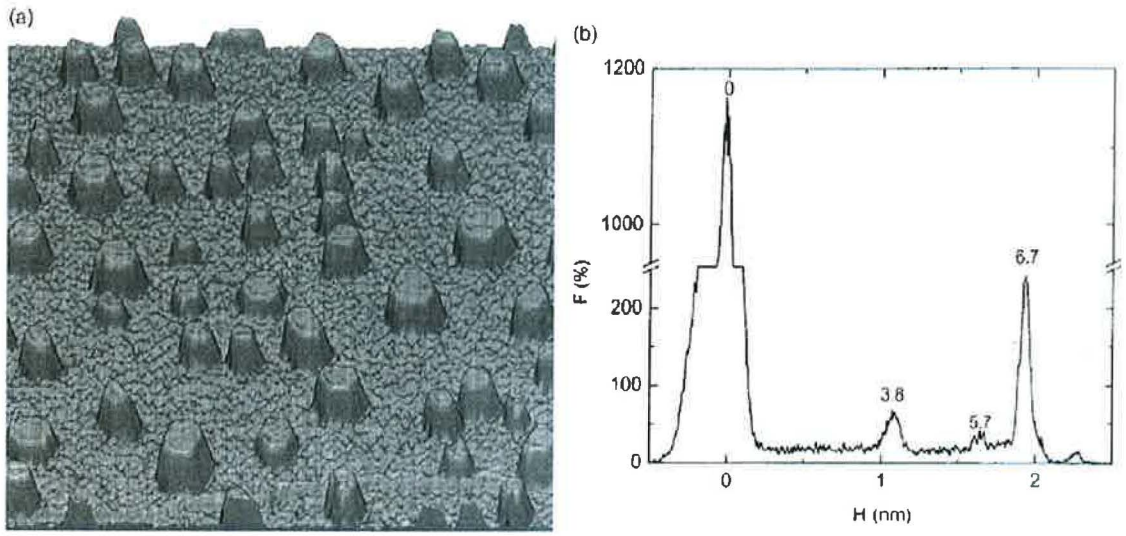

Figure 3.3: The STM pictures of the distribution of Pb/Si(111) islands. Taken from [49]. (a) An STM image obtained after the deposition of 3ML of Pb at 192K showing the uniform height islands with flat tops and stepped edges. The scale is 200x200 nm^2. (b) A height histogram showing the preferred heights in the previous image. Island heights of 6.7-step also seen with some "wrong" heights at 5.7-step. The average island size is 12nm and the average island separation is 30nm, consistent with the diffraction results.

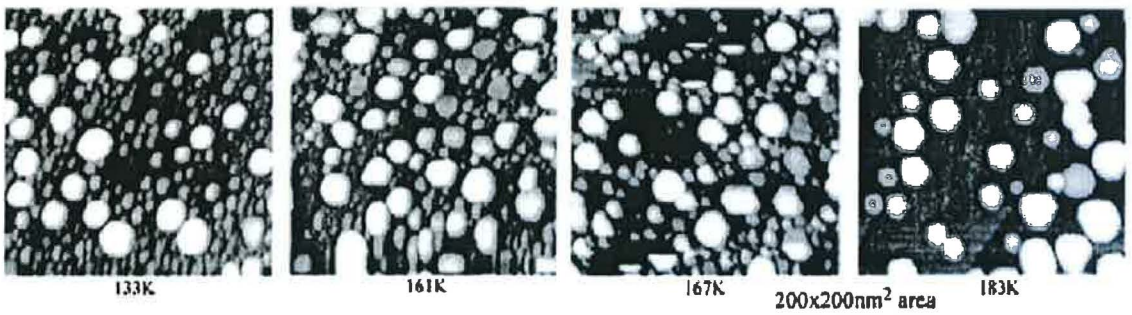

Figure 3.4: The STM pictures and caption taken from [50]. STM images at four annealing temperatures. The brightest islands are seven-layers high. At 133 K small two- and three-layer islands have nucleated. By 161 K some five-layer islands have formed. By 180 K small islands have vanished, leaving predominately seven-layer islands.

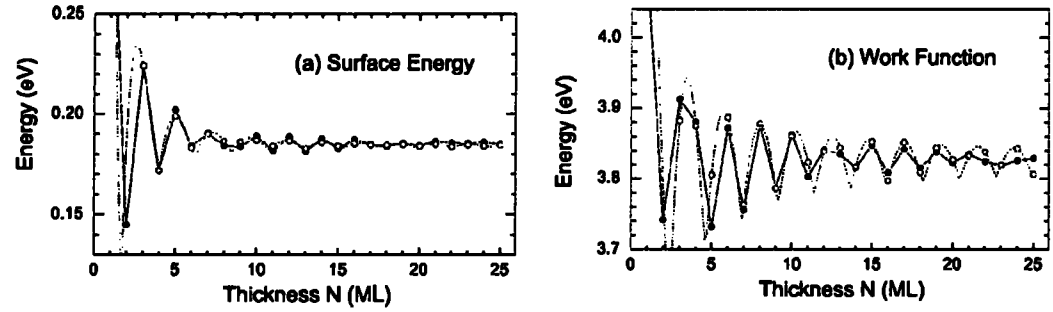

Figure 3.5: The results of ab-initio calculation and the captions adopted from [52]. (a) Surface energy per 1×1 unit cell and (b) work function of Pb(111) thin films as a function of thickness. The calculated results (solid circles) are obtained using the generalized gradient approximation as the theoretical lattice constant with layer spacing fully relaxed. The open circles and dashed lines represent the fitted values for surface energy and work function respectively.

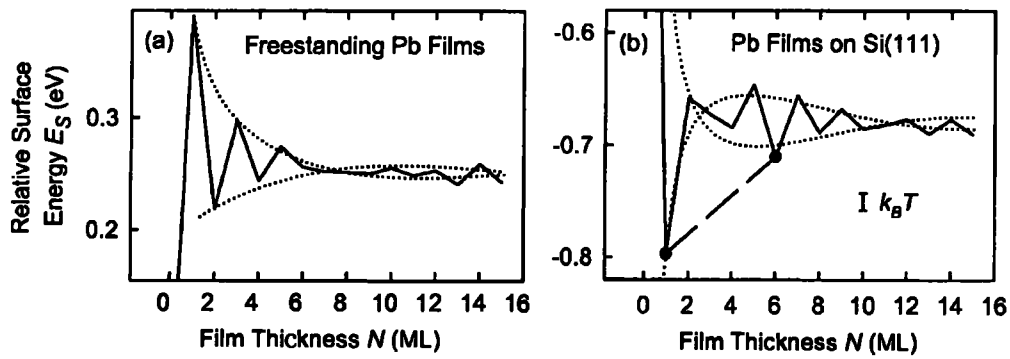

Figure 3.6: The results of ab-initio calculation and the captions adopted from [53]. The wetting layer (WL) is here marked as 0 layer. (a) Calculated relative surface energy per surface atom for freestanding Pb films as a function of layer thickness N. (b) The same for Pb films on Si. The dotted curves represent envelope functions for the quantum oscillations.

the phase diagram, the formation of double layer will be analyzed in the next chapter.

3.4 A theoretical model

In this model the growth of the ensemble of islands will be studied. The growth is driven by only two currents: the first is proportional to the probability of a jump of some atom from WL on the island's side and the second one to the probability of a jump from the side on the island's top. The first probability depends on the perimeter of the island's base and the density of atoms on WL. The second probability is a function of the density of atoms on the islands sides, thus both probabilities depend on the proportion of the islands. In this model we try to explain the observed switching in the mode of growth and the phase diagram by a simple model in which the growth is driven by different probabilities for a jump from WL on the sides of the islands with different sizes. Within this hypothesis the observed phase diagram is only a result of statistically driven diffusion of Pb atoms from WL on the sides

and from the sides on the island's top.

3.4.1 Definitions of values of the model

We begin with a system of N islands. The main characteristics of the system are the radius of the islands, denoted as $r_j = j$, and height $h_i = 2i + 1$. The fact that only odd heights are counted reflects the measured QSE. In the experiment with long relaxation times only stable heights were observed. For islands under 10 layers hight odd layers are stable, for higher islands it is not so clear, because the ab-initio calculation predicts that 10 are also stable and odd-height islands after that. Nevertheless we want to simulate the growth for island maximally 9 layers hight, thus the odd numbers describe the stable heights well.
Each island is determined by the point (i, j). m_{ij} is the number of islands of type (i, j). The boundary condition has the form: $\sum_{i,j} m_{ij} = N$.The shape of the Pb/Si(111) island is known from many experiments [49, 50, 51] and for smaler coverage it is roughly a prism with a hexagonal base and top. For a larger coverage, the islands start to be irregular (see Fig(4.1)). Label the volume of double-layer of atoms on the top of island (i, j) as S_{ij}, P_{ij} the volume of one-layer shell of island (i, j). S_{ij}, P_{ij} are calculated by the number of atoms position, which fill the relevant volume. So $S_{ij} = 6j(j+1)+2$, $P_{ij} = 6j(2i+1)$. The diffusion on the surface is considered infinitely quick, so the growth of the islands does not depend on the distances between the islands. Following this assumption, the matrix $M = m_{i,j}$ fully determine the state of our ensemble of islands on the surface.

3.4.2 Process of the growth of the islands

The growth is, in this model, simulated at a constant temperature and increasing coverage. The deposition rate is constant and the atoms are considered to fall only on the wetting layer. The current of the deposited atoms on the island's top is negligent. All the processes on the surface are of only two types: either the atom jumps from WL on the islands shell with a probability π_1 or a jump from the shell on the island's top with a probability π_2. The probabilities $\pi_{1(2)}$ mean the probability of each event per unit time. Backwards jumps are included in the probabilities - the probability of these jumps is dictated by the average increase of the number of atoms on the shell/top per time unit and per unit length of the island perimeter. As the system of islands accrue new atoms per time unit $\pi_1 Q$, Q is the total length of the islands perimeters. The perimeter of one island (i, j) is $Q_{ij} = 6j$, so $Q = 6\sum_{i,j} j m_{ij}$
Due to the quick diffusion on the WL, the probability π_1 is only given by the deposition rate, thus this value is independent of temperature T.
The probability π_2 is temperature dependent and we suppose it in the Arrhenius form $\pi_2 = \nu \exp(-E/k_B T)$, where ν is frequency factor, E the energy barrier for the jump of the atom, k_B the Boltzmann constant. The meaning of values used in the model are written in Fig(3.4.2).

The scenario of the growth proposed in our model is the following. Atoms attach to islands with the frequency $\pi_1 Q$. Either they stay on the shell or they jump to the top of the island with the probability π_2. We will distinguish three results of the atom jump:

1. After a jump from WL on the island's shell the new atom completes the shell of one of the islands and the following changes are detected

$$\{j \to j+1; m_{ij} \to m_{ij} - 1; m_{i(j+1)} \to m_{i(j+1)} + 1\} \tag{3.1}$$

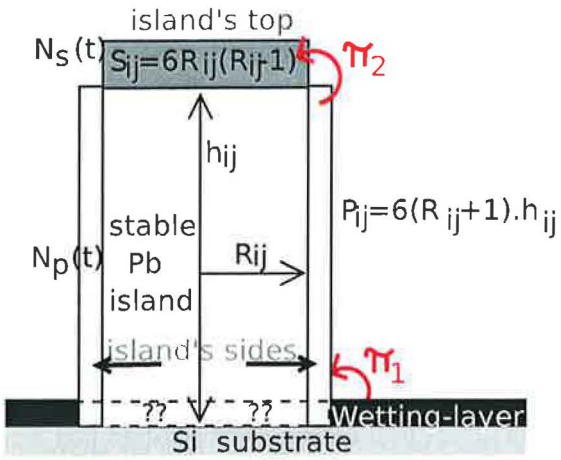

Figure 3.7: The meaning of values used in the analytic model. In the picture is an island (i, j) with the height $h_{ij} = 2i + 1$, radius $R - ij = j$ and $N_p(t), N_s(t)$ are the actual numbers of atoms on the island's side or top respectively. The sizes of the islands determine the number of atoms on a side: $P_{ij} = 6(R_{ij} + 1)h_{ij}$ and the number of atoms on the double-layer on the island's top: $S_{ij} = 3R_{ij}(R_{ij} - 1)$. π_1 is the temperature independent probability of a jump from WL to the island's side and π_2 is the probability of a jump from the island's side to the top.

2. After a jump from the shell to the island's top the new atom completes a new double-layer on the top of the island and the following changes are detected

$$\{i \to i + 1; m_{ij} \to m_{ij} - 1; m_{(i+1)j} \to m_{(i+1)j} + 1\} \tag{3.2}$$

3. m_{ij} are not changed.

During the processes 1. or 2. two elements of matrix M are changed. Both cases represent the jump of an atom on the shell/top which has exactly one empty site which the new atom fills. Then we obtain a new matrix. From the total number of atoms on an incomplete shell $(N_p(t))$ or the top double-layer $(N_s(t))$ we subtract S_{ij} or P_{ij} atoms. All processes are stochastic processes. It should be Markoff's discrete process in an open system.

3.4.3 Transition probabilities

In our stochastic model the development of the population of the islands (represented by the matrix M of the island's population) is given by the probabilities that after the jump of an atom (neither from WL on the shell or from the shell to the top) some shell or top is filled. Since the transition of atoms between the islands is suppressed, we observe the evolution of the islands of each group (i, j) separately. (i, j) mark all islands with radius $2i + 1$ and radius j. This means that, we determine the mode of growth for each (i, j) group of islands independently of the rest of the groups. The distribution of atoms on the islands which do not belong to the (i, j) group is not important. Our system is represented by $N_p^{ij}(t)$ atoms on the incomplete shells and $N_s^{ij}(t)$ atoms on the incomplete top double-layers of all m_{ij} islands (i, j). We suppose that all configurations of atoms on the tops and shells are equivalent. The

number of all possible distributions of atoms on the incomplete top layers is

$$ {}^{t}C_s^{ij} = \begin{pmatrix} S_{ij}m_{ij} \\ N_s^{ij}(t) \end{pmatrix} \tag{3.3} $$

The number of all possible distributions of atoms on the incomplete shells are

$$ {}^{t}C_p^{ij} = \begin{pmatrix} P_{ij}m_{ij} \\ N_p(t)^{ij} \end{pmatrix} \tag{3.4} $$

The total number of all configurations of all atoms on the incomplete surface of the islands (i,j) is

$$ {}^{t}C_t^{ij} = \begin{pmatrix} S_{ij}m_{ij} \\ N_s^{ij}(t) \end{pmatrix} \begin{pmatrix} P_{ij}m_{ij} \\ N_p^{ij}(t) \end{pmatrix} \tag{3.5} $$

We shall determine the probability of the event, that after the attachment of one atom on the shells or tops, the matrix M changes following the process 1. or 2. First we describe the growth in area - process 1. This process turns up, when at time t at least one island of type (i,j) exists, on which is $(P_{ij}-1)$ atoms on the shell. By attachment of one atom this shell is filled and the radius is changed from j to $j+1$. At time t there are $N_p^{ij}(t)$ atoms on the incomplete islands. Because no island has a filled shell up to this time, these $N_p^{ij}(t)$ atoms are distributed to $P-N$ sites. The total number of such configurations is

$$ C_p^{ij}(t) = \begin{pmatrix} (P_{ij}-1)m_{ij} \\ N_p^{ij}(t) \end{pmatrix} \tag{3.6} $$

We shall ask how many configurations result in "almost" filled 1,2, 3, ... islands of (i,j) type. Now we must know the exact number of "almost" filled islands, since we will calculate with the probability that one deposited atom strikes one "almost" filled island. Denote P_n^{ij} the number of configurations that exactly n islands are "almost" filled. The probability that an atom strikes the island if exactly n of islands are "almost" filled is

$$ p_n = n\frac{Q_{ij}}{Q}\pi_1 Q = \frac{jn}{\sum_{i,j} jm_{ij}}\pi_1 \tag{3.7} $$

We calculate the probability that exactly n island of (i,j) type is "almost" filled - P_n^{ij} by the following procedure. We choose n islands (i,j) with $(P_{ij}-1)$ atoms on the shell. The other islands will occupy at most $(P_{ij}-2)$ atoms. Together the configurations

$$ P_n^{ij} = \begin{pmatrix} m_{ij} \\ n \end{pmatrix} \cdot \begin{pmatrix} (P_{ij}-2)(m_{ij}-n) \\ N_p^{ij}(t) - n(P_{ij}-1) \end{pmatrix} \tag{3.8} $$

If we multiply these numbers of configurations by the probability that one atom strikes the appropriate island, we obtain the total probability of the change of radius $j \to j+1$

$$ P_{j,j+1} = \frac{p_1}{C_p^{ij}(t)} \sum_{k=1}^{n} k P_k^{ij} \tag{3.9} $$

We can also introduce similar values for the growth in height $i \to i+1$. In time t $N_s^{ij}(t)$ atoms are in the system on the incomplete top surface of islands, which are all filled at most by $S_{ij}-1$ atoms. Together the configuration is

$$ C_s^{ij}(t) = \begin{pmatrix} (S_{ij}-1)m_{ij} \\ N_s^{ij}(t) \end{pmatrix} \tag{3.10} $$

Only the atoms in the distance of one lattice constant from the top edge of the island can jump on the top side from the shell. It means that the probability of the jump of one atom from the shell to the top of one island (i,j) per time unit is proportional to the density of atoms and length of the ring close to the top edge of the island

$$s_1 = \pi_2 \frac{N_p^{ij} Q_{ij}}{P_{ij} m_{ij}} \tag{3.11}$$

The probability that this event is realized at one from n islands is

$$s_n = n s_1 \tag{3.12}$$

The number of configurations, that exactly n islands of (i,j) type have "almost" filled the top surface is S_n^{ij}. We calculate this number of configurations by the following procedure:

$$S_n^{ij} = \begin{pmatrix} m_{ij} \\ n \end{pmatrix} \begin{pmatrix} (S_{ij}-2)(m_{ij}-n) \\ N_s^{ij}(t) - n(S_{ij}-1) \end{pmatrix} \tag{3.13}$$

If we multiply these numbers of configurations by the probability that we strike with one atom the appropriate island and divide this number by the number of all possible configurations, we get the total probability of the change $i \rightarrow i+1$.

$$S_{i,i+1} = \frac{s_1}{C_s^{ij}(t)} \sum_{k=1} k S_k^{ij} \tag{3.14}$$

3.4.4 Analysis of the model

The equations (3.9,3.14) give the probability of the transitions of elements in matrix M. Let the function $f(M|t)$ represent the distribution function of matrix M at time t. The changes of matrix M distribution can be expressed by the Master equation:

$$\begin{aligned} &f(...,m_{ij},...|t+\mathrm{d}t) - f(...,m_{ij},..|t) = \\ &\mathrm{d}t[S_{i-1,j} f(...,m_{(i-1)j}+1, m_{ij}-1,...|t) + P_{(j-1)j} f(...,m_{i(j-1)}+1, m_{ij}-1,...|t) \\ &-S_{i(i+1)} f(...,m_{ij}, m_{(i+1)j}-1,..|t) - P_{j(j+1)} f(...,m_{ij}, m_{ij+1}-1,...|t)] \end{aligned} \tag{3.15}$$

with the condition that

$$\sum_{(i,j)} m_{ij} = N \tag{3.16}$$

Using these probabilities of the time derivation of average values of components of matrix M, we can derive from the master equation for the development of distribution function of matrix M. The result is:

$$\frac{\partial \overline{m}_{ij}(t)}{\partial t} = \overline{S}_{(i-1)i} \overline{m}_{(i-1)j} (\overline{m}_{ij}+1) + \overline{P}_{(j-1)j} \overline{m}_{i(j-1)} (\overline{m}_{ij}+1) - (\overline{S}_{i(i+1)} + \overline{P}_{j(j+1)}) \overline{m^2}_{ij} \tag{3.17}$$

where: $S_{i(i+1)} = \overline{S}_{i(i+1)} m_{ij}$, $P_{j(j+1)} = \overline{P}_{j(j+1)} m_{ij}$
To determine which mode of growth is preferred, in area or in height, we calculate the ratio of corresponding probabilities:

$$B = \frac{\overline{P}_{j,j+1}(t)}{\overline{S}_{i,i+1}(t)} \tag{3.18}$$

If $B > 1$, preferentially islands grow in area, in the case $B < 1$, islands grow preferentially in height. If $B \sim 1$, both modes are possible. Now we can evaluate $\ln B$ as a function of S_{ij}, P_{ij}, as a function of the rate π_1, π_2 and time dependent values $N_p^{ij}(t)$, $N_s^{ij}(t)$.

Suppose that at time $t = 0$ the system of (i, j) islands is $N_{tot}^{ij}(0)$ atoms which are randomly distributed on the incomplete shell or incomplete top surface of islands from (i, j) group - $N_p^{ij}(0)$, $N_s^{ij}(0)$. The initial conditions have the form:

$$N_p^{ij}(0) + N_s^{ij}(0) = N_{tot}^{ij}(0) \tag{3.19}$$

$$\frac{N_p^{ij}(0)}{N_s^{ij}(0)} = \frac{P_{ij}}{S_{ij}} \tag{3.20}$$

During the time interval dt in the (i, j) system, $m_{ij}Q_{ij}\pi_1 \mathrm{d}t$ atoms accrue in the shell sites. During the time interval dt $\mathrm{d}N_s^{ij}(t)$ atoms jump to the top surface:

$$\mathrm{d}N_s^{ij}(t) = N_p^{ij}(t)\pi_2 \frac{Q_{ij}}{P_{ij}} \mathrm{d}t \tag{3.21}$$

If we suppose that during this time interval matrix M did not chang, we obtain the differential equation:

$$\frac{\mathrm{d}N_p^{ij}(t)}{\mathrm{d}t} = m_{ij}Q_{ij}\pi_1 - N_p^{ij}(t)\pi_2 \frac{Q_{ij}}{P_{ij}} \tag{3.22}$$

The solution of this equation with boundary conditions (3.19, 3.20).

$$N_p^{ij}(t) = \exp(-\frac{Q_{ij}}{P_{ij}}\pi_2 t)\left[\frac{m_{ij}P_{ij}\pi_1}{\pi_2}(\exp(\frac{Q_{ij}}{P_{ij}}\pi_2 t) - 1) + N_p^{ij}(0)\right] \tag{3.23}$$

On the top surface of the islands we have atoms:

$$\begin{aligned} N_s^{ij}(t) &= N_{tot}^{ij}(t) - N_p^{ij}(t) = tm_{ij}Q_{ij}\pi_1 + N_{tot}^{ij}(0) - \\ &\exp(-\frac{Q_{ij}}{P_{ij}}\pi_2 t)\left[\frac{m_{ij}P_{ij}\pi_1}{\pi_2}(\exp(\frac{Q_{ij}}{P_{ij}}\pi_2 t) - 1) + N_p^{ij}(0)\right] \end{aligned} \tag{3.24}$$

From the approximated analytical relations of the dependence of $\ln(B)$ on the rate (π_1/π_2) we can determine the critical value of the parameter π_{2crit}. This value means that for the fixed deposition rate π_1 (for simplicity we choose $\pi_1 = 1$) exists such a value of π_2, that for higher values the growth is in height, below π_{2crit} the growth is in area. This critical π_{2crit} depends on the height i and radius j of the islands. These dependencies are demonstrated in Fig(3.8), Fig(3.9) in a particular case. The qualitative dependencies do not change with i and j. This is an important result. From Fig(3.8), Fig(3.9) we can conclude that if we start from the higher value of π_2 then it is a critical value, the growth is in height. Since the parameter π_2 depends on temperature, at a constant temperature the value π_2 is also constant. But by increasing i, this value remains above π_{2crit} and the growth is henceforth in height. For lower values we have a similar situation. If we start with $\pi_2 < \pi_{2crit}$, growth is in area and so π_2 remains below its critical value and growth is henceforth in area.

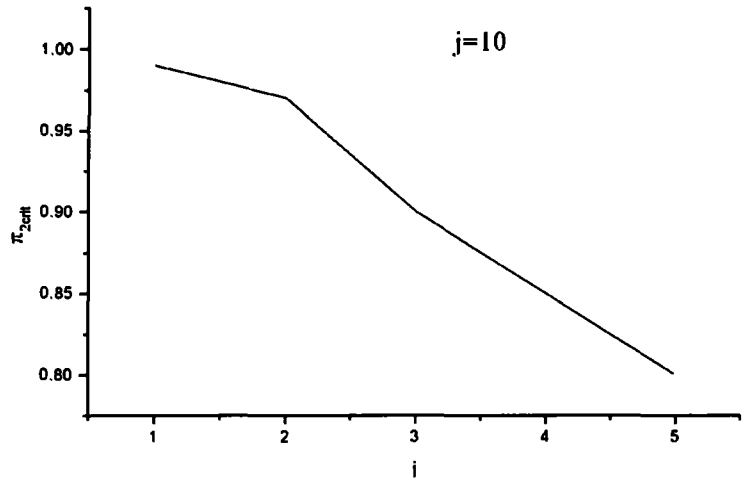

Figure 3.8: Dependence of the critical value π_{2crit} on the high i of the island.

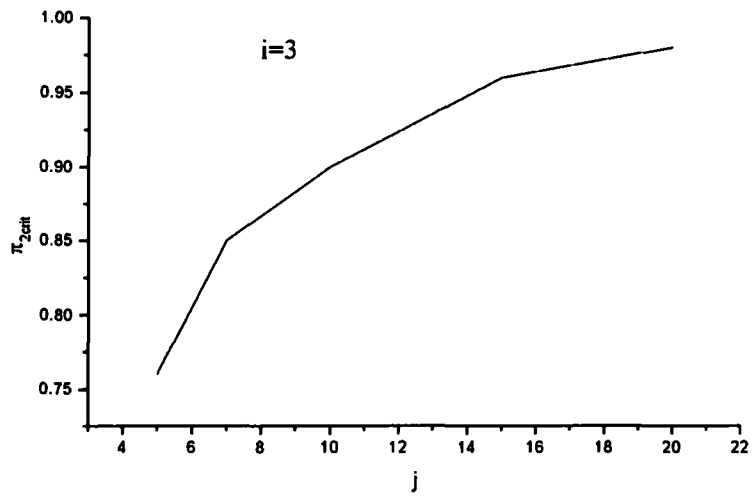

Figure 3.9: Dependence of the critical value π_{2crit} on radius j of the island.

3.5 The solution of the theoretical model using the Monte Carlo simulation

The idea of this model is the hypothesis that the existence of preferred heights is not driven by changes in barriers (here represented by the probabilities π_1 and π_2), but rather by the collective growth of the assembly of islands- mainly by different currents on islands with different diameters. In the previous part a soft dependency of the probabilities of growth on the radius and heights was derived (see (3.27)). Consequently the growth of the island in radius or height is more likely for islands with smaller diameters. It is unclear if this influence is sufficient for the creation of islands with uniform sizes at a given temperature and coverage. The answer to this can be given by the MC simulation.

3.5.1 Monte Carlo simulations of the island's ensemble

Since the analytical solution of the Master equation is difficult, we use the Monte Carlo simulations to investigate features of our model of growth of Pb nano-islands on an Si(111) surface. The development of the island's population is simulated in steps in which some of the components of matrix M is changed. This master equation for the development of the matrix of population M can be described in MC by the equation for components of matrix M: (3.15)

$$\Delta m_{ij} = S_{(i-1)i} m_{(i-1)j} + P_{(j-1)j} m_{i(j-1)} - (S_{i(i+1)} + P_{j(j+1)}) m_{ij} \tag{3.25}$$

The expressions (3.14,3.9) contain the sum in probability of the existence of exactly one, two etc. islands with exactly one empty place on the top/shell. This value is difficult to evaluate, but in most cases it can be approximated by the probability that minimally one island is "almost filled". The probability that more than two islands are "almost filled" is much less likely than that minimally one is "already filled" for small values of this probability. We can rewrite the expressions (3.14,3.9) in this form:

$$S_{i(i+1)} \simeq s_{ij} S_1^{ij} = s_{ij} \begin{pmatrix} (S_{ij}-2)(m_{ij}-1) \\ N_s^{ij} - S_{ij} + 1 \end{pmatrix} : \begin{pmatrix} S \\ N_t \end{pmatrix}; \quad s_{ij} = s_1 = N_p^{ij} \pi_2 \frac{Q_{ij}}{P_{ij} m_{ij}} \tag{3.26}$$

$$P_{i(i+1)} \simeq p_{ij} P_1^{ij} = p_{ij} \begin{pmatrix} (P_{ij}-2)(m_{ij}-1) \\ N_p^{ij} - P_{ij} + 1 \end{pmatrix} : \begin{pmatrix} P \\ N_t \end{pmatrix}; \quad p_{ij} = p_1 = \pi_1 j \tag{3.27}$$

These expressions determine the probabilities of the change of the configuration on the simulated surface (height or radius of some island). The main part of the MC simulation can be described by this loop:

1. We choose one of two events - a particle jumps from the wetting layer on the island's side (with probability p_{ij}) or a particle jumps from some side to the island's top (s_{ij}).
2. For each side/top (it depends on the type of jump which we choose in the previous step) we ask if it was completed by the addition of the atom. The probability that the island (i,j) has a filled side is $S_{i(i+1)}$, and the probability that it has a filled top is $P_{i(i+1)}$.
3. If one side P_{ij} or top of island S_{ij} is filled, we change the relevant component of the matrix of islands population M, $m_{ij} \rightarrow m_{ij} - 1$ and $m_{(i+1)j} \rightarrow m_{(i+1)j} + 1$, $N_p^{ij} \rightarrow N_p^{ij} + 1 - P_{ij}$ for a filled top or $m_{i(j+1)} \rightarrow m_{i(j+1)} + 1$, $N_s^{ij} \rightarrow N_s^{ij} + 1 - S_{ij}$ for a filled side of the island (i,j). If no side or top has been filled, we only increase N_s or N_t by 1.
4. Return to 1.

3.5.2 Results of the MC simulation

For the growth of islands the ratio of probabilities $\frac{\pi_1}{\pi_2}$ plays the decisive role, whether the islands will grow in area or in height. The modes of growth are characterized by the changes $\mathrm{d}S$ of the total area of the island's top: $S_{tot}(\pi_1/\pi_2) = \sum_{(i,j)} m_{ij} S_{ij}$ and the changes $\mathrm{d}h$ of the total height of all the islands $h_{tot}(\pi_1/\pi_2) = \sum_{(i,j)} h_i m_{ij}$. Both values are normalized by the maximal value.
Fig(3.10) shows the dependence of $\mathrm{d}S$ and $\mathrm{d}h$ on the ratio of probabilities π_1/π_2. The sharp switching of modes of growth in area or in height respectively is evident at a ratio close to 1. Since only the probability π_2 is temperature dependent, while the probability π_1 is given by experimental conditions (flux rate), we can interpret the x-axes also in temperature units. To evaluate of temperature range, we use the experimental value of the barrier for the jumps of atoms from the island shell to the top surface E_s=0.32eV which was established in [50]. The frequency factor can be determined from information that the switching between modes of growth is realized at 180K thus:

$$(\frac{\pi_1}{\pi_2})_{cr} = \nu \exp(-E_s/k_B T) \tag{3.28}$$

From MC the critical ratio was established as $(\frac{\pi_1}{\pi_2})_{cr} \simeq 1$, accordingly the frequency factor is approximately $\nu = 10^{12}\ s^{-}1$.

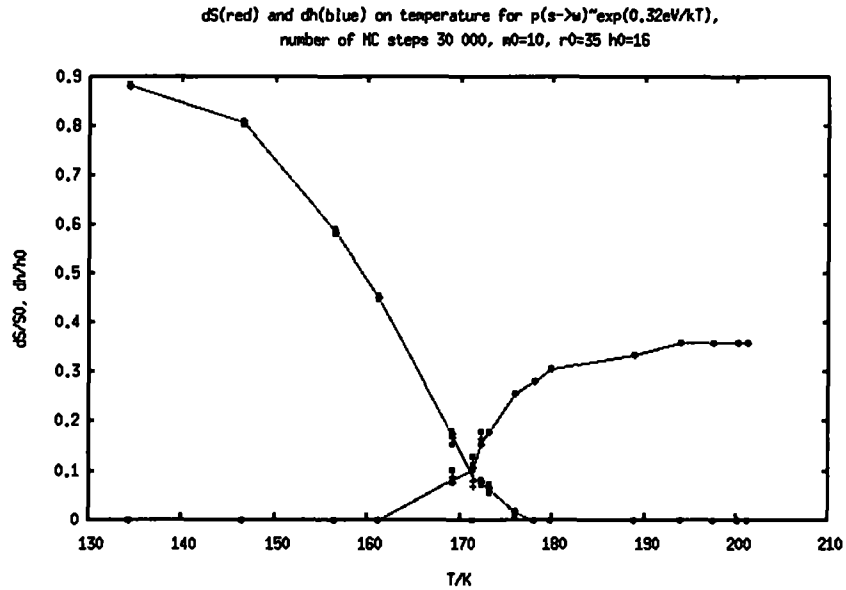

Figure 3.10: Changes in the total area or height of islands during growth as a function of the ratio of probabilities π_1 and π_2.

These results qualitatively describe the experimental observation of the switching of growth modes, published in [50]. In the y-axis the average difference in height is much higher than in the experiment. The reason for this is that in our simple model at a constant temperature we obtain either growth in height or on the sides. On the other hand in the experiment it was observed that after growth in height there was a big interval in coverage where the island grows on the sides.
It can be seen also from the analytical model (see Fig(3.8),Fig(3.9)) - the dependency of critical values $(\frac{\pi_2}{\pi_1})^c_{anal}$ on the radius and height is practically constant. The dependency of

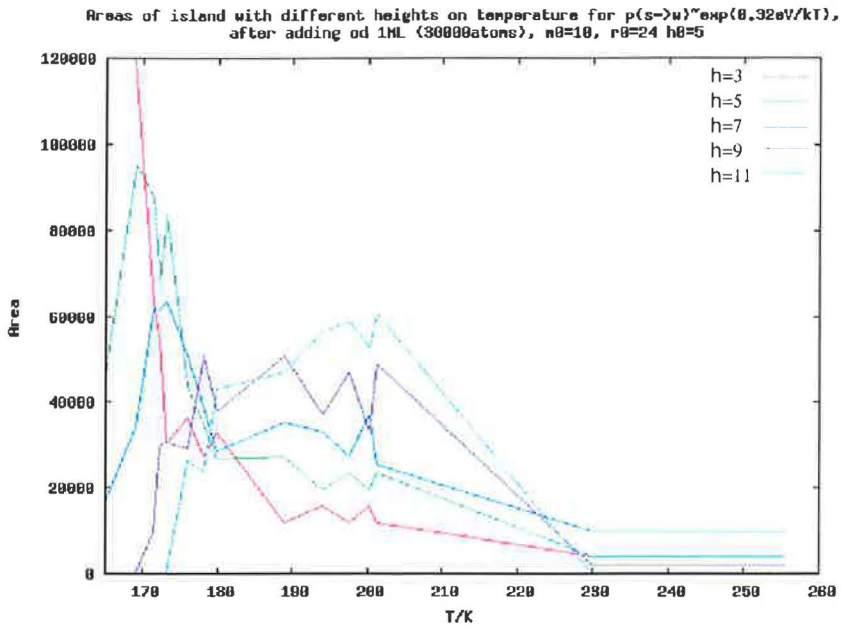

Figure 3.11: The dependency of area of islands with certain heights on the temperature after the addition of 3ML. Different colors mark different islands sizes.

area S_{ij} of the different island's heights h_i on temperature is in Fig(3.11). From the picture Fig(3.11) it is clear that this model demonstrates the sharp switching between modes in which islands grow in height or radius respectively. Nevertheless the population of an island is not uniform - there does not exist characteristic heights at any given T and Θ. In Fig(3.12) the average matrix is m_{ij} which is the average number of islands with radius $R_{ij} = j$ and $h_{ij} = 2i + 1$. In the analytical part as well as in MC simulation we obtain the growth in radius for parameter pi_2 smaller than some critical value $\pi_2 < \pi_2^c$. For above-critical value we obtain growth in the height.
In the experiment we observe another situation. Let us begin with a distribution of atoms where $i = 2, \quad j = 15$. At low temperatures, growth is in area. But above a critical temperature around 175K, the islands start to grow in height. This corresponds to the above critical value of parameter π_2. Nevertheless now the simulation diverges from the experiment where after the growth in height is completed at $i = 3$, growth continues in area. This cannot be explained by the constant value of parameter π_2 and we need the dependency in height i and radius j in a more precise model.

3.5.3 Monte Carlo simulation including the stress and QSE

In the previous model the uniform island's heights was suppose to be the result of random growth of the ensemble of islands. But the results of this model are not in agreement with the experimental results. It seems that the ratio of probabilities $\frac{\pi_2(T)}{\pi_1}$ must be a function of the height and radius of the island. The dependency on height provides an abortion of the growth in height. If the growth in height shall continue after adding a certain amount of Pb again, then the ratio $\frac{\pi_2(T)}{\pi_1}$ must also depend on the island's radius. This theory is due to the new model of growth where the uniform height is not a result of the behavior of the ensemble but it is an issue of the dependency of the ratio of probabilities $\frac{\pi_2(T)}{\pi_1}$ on the size of

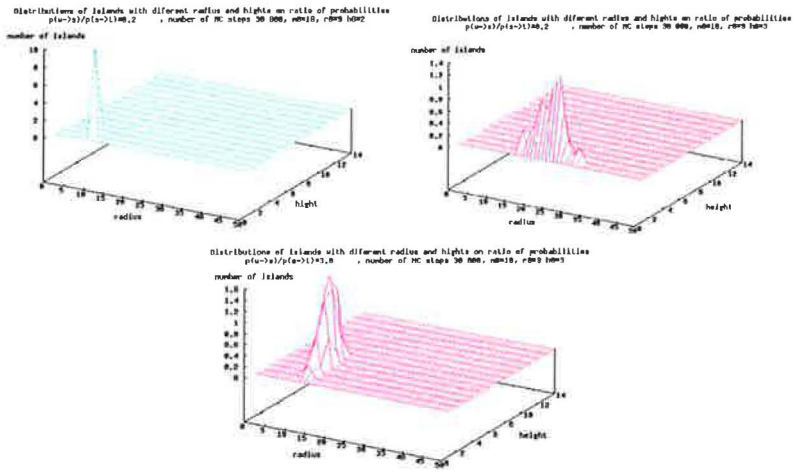

Figure 3.12: Matrix m_{ij} where $R_{ij} = j$ and $h_{ij} = 2i + 1$. On the left is the initial shape of m_{ij} - all islands had the same height and radius 3,10 on the beginning. The second pictures is for $\frac{\pi_2}{\pi_1} = 0.2$ and show the island's distribution after adding 30000atoms (1.5ML). In the third picture is a case where $\frac{\pi_2}{\pi_1} = 3.0$.

the island.

Details of the simulation

The statistic in the ensemble of islands is not important in the new model, because the growth of one island now drives the dependency $(\frac{\pi_2}{\pi_1})(T, r, h)$ and not the difference in currents to/on islands with different sizes. Thus now we can simulate only one single island with the radius r and height h. This new MC model is much simpler than the previous one because now we simulate only one single Pb island. The algorithm of the main MC loop is reduced to:

1. We choose one of two events - a particle jumps from the wetting layer on the island's side (with the probability $p_1 = 6r\pi_1$) or a particle jumps from some side to the island's top ($p_2 = 6r\frac{N_s}{6rh}\pi_2$).

2. If we move an atom from the side to the top we control if $N_t = 6r(r + 1)$ (the island's top is filled). If it is valid we change $h \rightarrow h + 1, N_t \rightarrow 0, \frac{pi_2(T)}{pi_1}$.

3. If we add an atom on the side we control if $N_s = 6(r + 1)(2h + 1)$ (the island's shell is filled). If it is valid we change $r \rightarrow r + 1, N_s \rightarrow 0, \frac{pi_2(T)}{pi_1}$.

4. If no side or top has been filled we only increase N_s or N_t by 1.

5. Return to 1.

The simulation is stopped after the addition of a defined amount of lead atoms. In [54] the experiment was done between a coverage of 3ML to 6.5ML. The distance between islands was approximately 10 atomic units. This means that after the addition of 1ML, the increase of atoms on one island is 2.10^4 atoms. In a previous MC simulation, a model with constant parameters in height and radius was used. The phase diagram was suppose to be a result of the growth of the islands ensemble, nevertheless this model was shown to be too simple to

describe the experiment [49]. In the new model we suppose the dependency of the ratio of probabilities π_2/π_1 in temperature, height and radius. The dependency in temperature is the same as in the previous model, the dependency in height is derived from the quantum size effect. The dependency in radius rootage in stress is caused by a different lattice constant of Si and Pb. Without the dependency in radius, the phase diagram can not be reconstructed. The reason is the same as in the previous case: the problem that growth in height never stops above a critical ratio of probabilities $\pi_2/\pi_1 > (\pi_2/\pi_1)^c$ is corrected by the dependency in height-after some time the high is so height that $\pi_2(h_0 + \Delta h)/\pi_1 < (\pi_2/\pi_1)^c$ and the growth in height is stopped. Nevertheless in the experiment the area where islands growth in height alternated with areas where for 2ML islands growth in radius. This means that after island growth to height $\pi_2(h, r_0)/\pi_1 < (\pi_2/\pi_1)^c$, it grew in radius again. But if we increase the coverage more (by 1ML) the islands start growth in height again. It mean that after island growth in radius by approximately $\Delta r = 20$ the ratio of probabilities changed: $\pi_2(h, r_0 + \delta r)/\pi_1 > (\pi_2/\pi_1)^c$.
The dependency of the ratio of probabilities on temperature, radius and height is shown by the following shape:

$$\frac{\pi_2}{\pi_1} = \underbrace{\pi_0 \exp(\frac{\Delta E}{k_b T})}_{a} \underbrace{\exp\left(\alpha\left(1 - \frac{T_c}{T}\right)\frac{\ln(1+\beta(r-r_0))}{1+\beta(r-r_0)}\right)}_{b} \underbrace{\exp\left(-(h-h_0)\left(\frac{\gamma}{T}\right)\right)}_{c} \tag{3.29}$$

The first term is identical with (3.28). It describes the difference in temperature dependencies of π_1 and π_2 which we show by the Arrhenius shape.
The second term b describe the influence of the stress on the diffusion and barriers. We assume that the growth of Pb/Si running in the so-called Stranski-Krastanov growth mode [55], which describes the heteroepitaxy growth. In this systems the driving force for the self-assembling mechanism is the strain inside the deposited film, which is caused by the different lattice constants as well as different crystalic structures. In a low coverage smaller than a certain critical coverage $\theta_c(T)$, Pb on the Si(111) surface creates the amorphous wetting layer. By increasing coverage, the elastic energy of the wetting layer increases and the adhesion between the Si substrate and the Pb ad-layer decreases. At some point close to coverage $\theta_c(T)$ the nucleation in the next layer starts. The uniform size distribution of the islands is the main advantage of the strain induced islands origin.
The stress in WL drives the migration of atoms from WL on the island's sides in further vaporation at $\theta > \theta_c(T)$. In the easiest growth models only the influence of lateral binding energy $E_{isl}(r)$ on the radius in this shape is consider [55, 56]:

$$E_{isl}(r) \simeq \frac{1}{r} ln(r) \tag{3.30}$$

The dependency in r source in the different structures and lattice constants of Si and Pb - this means that the shape of (3.30) depends on the materials and also it depends on the temperature due to different temperature distensibility. We introduce new coefficients β, r_o, α_1. Coefficient β describes material characteristics and is determined by the difference in lattice constants. r_o is the reference radius - in our simulation it is the beginning of the simulation. The temperature dependent term $\alpha(1 - T_c/T)$ is derived from the most simple assumption that the temperature dependency of the stress induced barrier E_{stress} which we assume takes the form:

$$E_{stress} = (E_0 + \alpha_1 T)\left(\frac{\ln(1+\beta(r-r_0))}{1+\beta(r-r_0)}\right) \tag{3.31}$$

where E_0 is reference energy and α_1 is the coefficient in linear dependency which is caused by the difference in temperature distensibility. The stress term b in the equation for probability π_2/π_1 has a standard Arrhenius form:

$$\exp\left(\frac{E_{stress}}{k_BT}\right) = \exp\left(\frac{E_0 + \alpha_1 T}{k_BT}\frac{\ln(1+\beta(r-r_0))}{1+\beta(r-r_0)}\right) = \tag{3.32}$$

$$= \exp\left(\alpha\left(1-\frac{T_c}{T}\right)\frac{\ln(1+\beta(r-r_0))}{1+\beta(r-r_0)}\right) \tag{3.33}$$

where now $\alpha = \alpha_1/k_B$ and $T_c = -E_0 k_B/\alpha_1$.
In [56] is presumed also the dependency of $E_{isl}(r)$ also in height. In [52] the total energy for one unit cell slab decreases with the thickness of the of slab (see Fig(3.5) and Fig(3.6)). In equation (3.29) is added this last term (c) in the Arrhenius shape $\exp(-E_{height}/k_BT)$, where the parameter E_{height} is approximated by a simple linear dependency. The term in the ratio of probabilities π_2/π_1 can be than rewritten as:

$$\exp\left(-\frac{E_{height}}{k_BT}\right) = \exp\left(-\frac{\gamma(h-h_0)}{T}\right) \tag{3.34}$$

where $\gamma = E_{height}/k_B$.
The parameters in equation (3.29) were fitted to obtain the phase diagram and the values are written in table 3.5.3. The resulting phase diagram is shown in figure 3.13. The green line is the border between the area with an occurrence of 5 and 7 layer tall islands, the red one is area between 7 and 9 layer tall islands.

π_0	α	β	γ	T_c	ΔE
$0.85s^{-1}$	21	$0.01m^{-1}$	$50K$	$180K$	$0.001eV$

Table 3.1: The barriers in dependency (3.29) and the parameters used in the MC simulation

3.6 Conclusions

The presented model of Pb island growth on an Si(111) surface is based on the assumption that the changes of the modes of growth (in area or in height) are determined by the ratio of the probabilities of atoms entering the system π_1 divided by the probability for jumping from the shell to the top of island's surface π_2. If $\frac{\pi_2}{\pi_1}$ is too low, atoms stay on the site of islands and growth in area dominates. If $\frac{\pi_2}{\pi_1}$ is sufficiently high then the flux from the WL to the top is slow enough that the atoms can leave the sides of the island and jump to the top of the island. The number of atoms on the shell slowly increases to a certain density in which the incoming and outcoming flux is equal, but the shell is never filled. In this case the growth in height is dominant.
In the simplest model only π_2 depends on temperature and the critical temperature at which we observe switching of growth modes exists. In this way the first simplest model is roughly able to explain the interesting temperature dependent switching in the mode of the growth of Pb islands (see Fig(3.10)). Nevertheless this switching is really sharp which means that at temperatures $T > T_c$ islands grow only in height and in temperatures $T < T_c$ they grow only on the sides. This is in conflict with the experiment where after island growth in height, the growth continues on the sides until a certain point where the island can grow in height again.

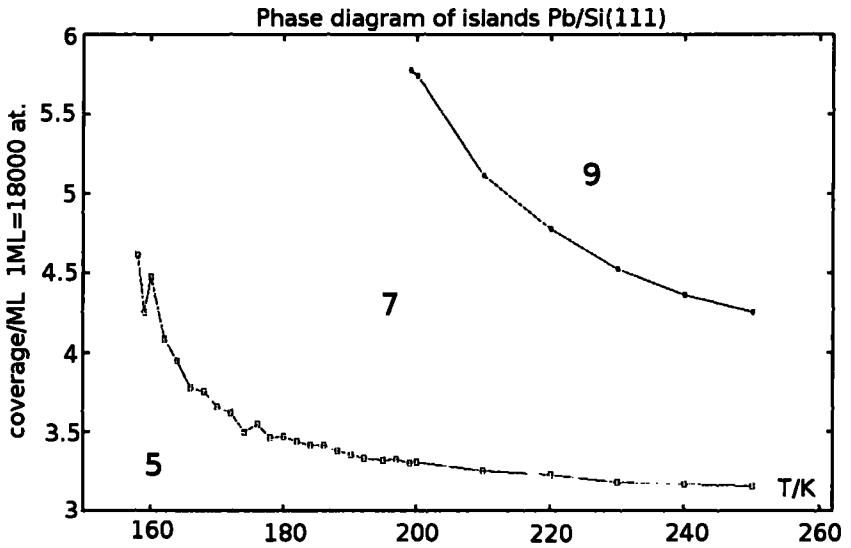

Figure 3.13: The result of MC of one island. Each point is the average value from 9 MC simulations. The green line is the border between an area with the occurrence of 5-layer or 7-layer high islands. The red line is between areas with 7-layer and 9-layer high islands. For the determination of the coverage in ML the proportions measured in [49] were used (see Fig(3.3)). From this value we determine $1ML \simeq 7000$ atoms per average area for one island (the total area divided by the number of islands).

For this reason we need the dependency of π_2/π_1 in height but also in radius. At the beginning of the deposition the island grows in radius, so $\frac{\pi_2}{\pi_1}$ must be bigger than the critical value $\left(\frac{\pi_2}{\pi_1}\right)^c$. At some point the island grows in height which implies that $\frac{\pi_2}{\pi_1} < \left(\frac{\pi_2}{\pi_1}\right)^c$ and after this point the growth in radius continues. The model with these attributes can be constructed with the assumption that the flux from WL to the base of the island depends on stress and the flux from the side to the top depends, due to QSE, on the height of the island. The shape of the function $\left(\frac{\pi_2}{\pi_1}\right)(r, h, T)$ was derived in shape 3.29 and the constant was the value written in Tab(3.5.3). The phase diagram is in accordance with the experimentally founded phase diagram [49].
Even thought this model seems to be successful in the interpretation of experiments published in [49], it is still a simple model which can still be refined. One insufficiency is the absence of the backward fluxes, from the top surface to the shell and out of the system. Incorporation of these fluxes enables us to study the changes of the distribution of the island as a function of temperature under a fixed coverage (along the x-axis in phase diagram - Fig(3.13)). The extension of the model by the nucleation processes on the wetting layer brings us closer to the real processes during the growth of Pb islands on an Si(111) surface.

Chapter 4

Kinetics of Pb/Si(111) at coverages higher than 3ML

The system Pb/Si(111) system has been studied recently by different groups under different conditions. There are still open questions about adsorption positions of single atoms on the surface at different reconstructions, the reasons for quick fluctuations of the border between different reconstructions (with different coverage), phase transformations of the Pb/Si surface which amazingly quickly change with coverage (the devil staircase) and the coverage of some reconstructions is also uncertain, etc. At higher coverage (approximately above 1ML), different reconstruction changed into an approximately 1 layer thick amorphous wetting layer (WL) which is present for coverage under 3.5ML at 130K or 1.5ML at 270K. Above this value of coverage the nucleation of Pb islands on the wetting layer is observed. These Pb islands have lots of unique characteristics and due to the complexity of the system, which does not allow calculations of this system by the ab-initio method, lots of experiments are not fully enlightened. This chapter is dedicated to kinetics of the growth of new layer of Pb islands on Si(111) surface.

4.0.1 Experimental overview

The growth of Pb islands on Si(111) has some unusual characteristics. Such as the existing

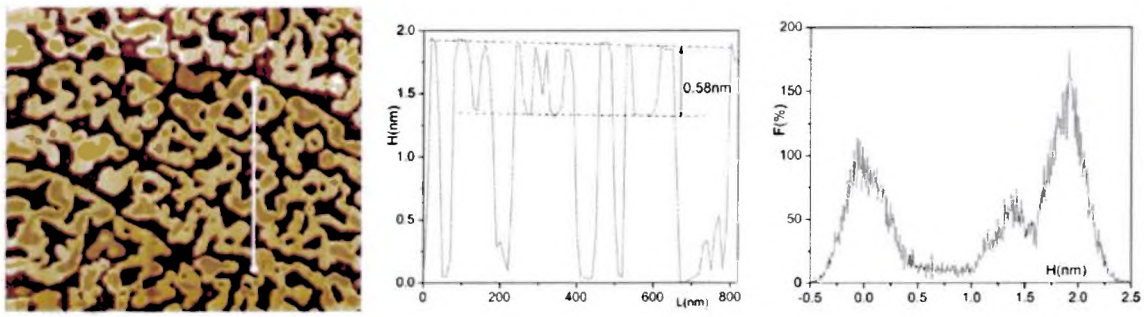

Figure 4.1: (a) An STM picture of the Pb/Si surface after the deposition of 5ML of Pb on a blank Si(111) surface. The darkest areas correspond with lower places, the brightest areas are the highest. On the top of irregular islands can be seen the lighter rings on the edge. On the chart in the middle picture (b) is the height of Pb surface along the line drawn in the STM image (a). Also from this diagram it can be seen that the height of the island is higher on the border. In the right picture is a percentage representation of heights along this line. This experiment was done in Ames laboratory by the group of Myron Hupalo.

of preferred heights of the island at specific temperatures and coverage (stable layer). On the other hand there exist heights which appear only temporally after deposition (unstable layers) [46]. During the non-equilibrium growth unstable islands are also present [49]. The reason for the existence of preferred heights is probably due to the quantum-size effect (QSE). Also the growth of new "island tops" proceeds in an unusual manner. The difference between two stable heights is an odd number, so during the growth of the island, a new double-layer must grow up. In practically all experimental conditions, the growth is not layer-by-layer. From STM measurement it can be seen that the growth starts on the perimeter of the island and the ring with a stable height is formed on the perimeter of the island (see Fig(4.1), Fig(4.2), Fig(4.3)). Then the center of this island is slowly filled. This type of growth was observed in experiment at 200K [49] but this work was focusen on QSE growth and the anomaly way in formation of new layer was not detailed disscused. More detailed was the formation of new layer studied in [57, 59] at 180K and quite a quick deposition as well, as at RT where the growth was started by triggering the island top [60, 61].

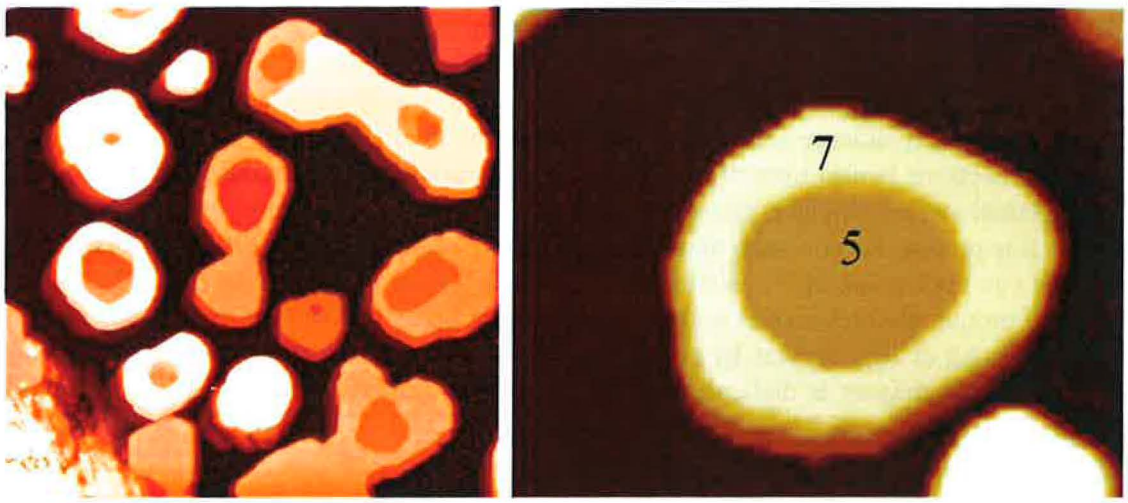

Figure 4.2: The detailed STM picture of a Pb islans on Si(111) surface after the deposition of 5ML of Pb on a blank Si(111) surface (measured by Myron Hupalo).

The thickness of this ring depends on the conditions of the experiment. At higher temperatures and constant coverage, the atoms nucleate on the top of the ring which quickly grows in height and the center of the island stays empty [59] (see picture Fig(4.2)). Nevertheless the growth here was triggered by STM scanning at height voltage. In a second similar experiment [61] also at a constant coverage and RT, the growth did not start until the edge of the top of the island was disturbed by a height voltage of the STM tip. The growth in one layer was than observed by STM at a smaller voltage. The nucleation of a second layer started again after triggering by the STM tip. During the deposition many island heights are observed (with different counts), but after relaxation some of them disappear [54].

4.0.2 Ab-initio calculation and Quantum Size Effect (QSE)

The difference between a stable and unstable height of the island was found during most of experiments at different conditions [54, 50, 60, 61] and is considered to be connected to quantum size effect in which the stability of the height depends at least on the height of the

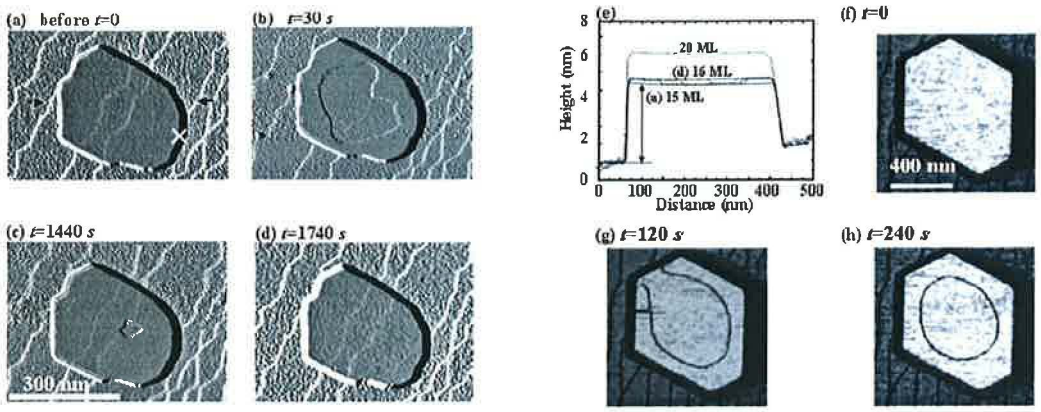

Figure 4.3: The STM picture of the Pb/Si surface after growth which is triggered by the tip with voltage U=-3V. This picture is adopted from [61]: An example illustrating precise control over the thickness of a Pb mesa with single-layer precision. (a) shows the STM image of the mesa prior to the triggering pulse. (b) A new layer with an annular shape was triggered by positioning the tip at the edge of the mesa [white cross in (a)] at a tip voltage of $V_y = 3V$ and a tunnel current of $I_t = 1.5nA$ for 30s. (c) Without the tip assistance, a new layer grows until the layer is completed as in (d). The profiles marked as 15 and 16 ML in (e) correspond to the line profiles in between the arrows indicated in (a). (e) shows, in addition, a line profile (marked as 20 ML) across the mesa (image not shown here) obtained after repeating the manipulation process five times such that exactly 5 ML were added on top of this mesa. (f)(h) show a case where, after triggering, an incomplete annular shaped edge island was observed on top of a mesa. However, the edge island quickly formed a closed annular shape within 2 min.

island [52, 53, 57]. By a different ab-initio calculation the oscillating dependency of energy of the Pb slab on its thickness was obtained. For less thick layers, the minimum is quite deep and results in the same thickness of stable slabs as the height of the stable island from the experiments.
Nevertheless the ab-initio calculation of the island (no infinity slab) is a difficult goal and the calculation of diffusion barriers on the Pb island is practically unrealizable.
Pb atoms have a quite complicated non-additive interaction thus the Molecular Dynamics simulation of this system is also problematic. For this reason we set the simple modeling surface potential of Pb/Si(111) which can describe the mentioned experiments. In this microscopic model we propose that differences in modes of growth can be caused by different backward currents of free particles from the top of the island to the wetting layer (WL) with different heights. These barriers were also calculated by ab-initio methods [59]. They obtain a small barrier for falling from the top of the island for unstable layers (6th, 8th) and a big barrier for stable heights. The indication that this could also be true is the experiment at a lower temperature (180K) where the growth is double-layer or layer-by-layer dependent on the deposition rate [57]. The diffusion on the wetting-layer is very quick (in [57] the double-layer islands top was formed in less than 2min after the deposition of 0.5ML of Pb) and also the diffusion on the top of the island is supposed to be quick (0.05eV-0.01eV [59]).

4.1 Kinetic Model

With this information we set the potential which can qualitatively describe double-layer growth, ring formation and nolinearity over time of island growth. The proposal of the shape of the potential which was used in the MC simulations is in Fig(4.4) and the values and meaning of the barriers are written in Tab(4.1). The most important barrier there is the deep energy hole on the perimeter of the island E_b (bound strong to the perimeter). Due to this barrier, the density of atoms is higher in the ring on the perimeter than on the terrace and the nucleation starts there.

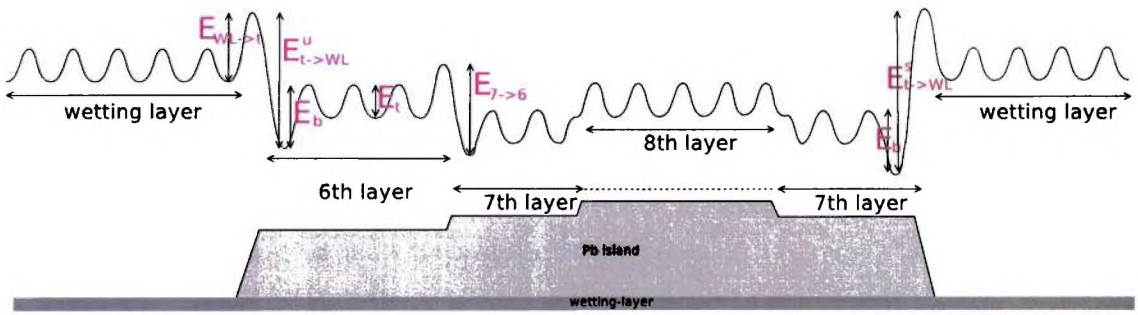

Figure 4.4: The surface potential proposed in our kinetic model. The description of the different barriers is in Tab(4.1)

E_b	0.17	- jump from the ring of the island toward center
E_t	0.05	- diffusion on terrace
$E_{8\to7}$	0	- jump from 8^{th} to 7^{th} layer
$E^{stable}_{t\to WL}$	0.32	- hopping from a stable layer of the top of the island to the wetting layer
$E^{unstable}_{t\to WL}$	0.21	- hopping from unstable layer of the top of the island to the wetting layer
$E_{7\to6}$	0.2	- falling from the 7^{th} layer to the 6^{th} layer
$E_{WL\to t}$	0.25	- "climbing" up from WL to the top
E_{bond}	0.1	- periphery diffusion - energy per bond
i_b, i_c	8, 8	- critical size in the ring (i_b) and in the center (i_c)
$\overline{n}_p$	5	- the rate at which the deponed atoms from WL reach the island base
T	180K	- temperature
R	30	- radius of the island in the number of atoms

Table 4.1: The barriers and parameters used in the MC simulation

From the experiment it seems that the border diffusion of Pb along the clusters Pb/Pb is slow. It is quite an interesting result because the single atom diffusion is surprisingly quick and for other metal fcc(111)is the border diffusion usually quick [58]
The border diffusion is also included in the kinetic model using a simple bond counting model in which the barrier for diffusion on the border ($_b$) or terrace ($_t$) is given as $E'_{t(b)} = E_{t(b)} + nE_{bond}$, where $E_{t(b)}$ is a barrier on a free surface (superscript t) or on the border

(subscript b) respectively, n is the number of bonds of atom to the cluster and E_{bond} is the free parameter of MC which represents the energy per bond. In our MC we set $E_{bond} = 0.1eV$. The barrier for falling from the top of the island to the wetting layer was calculated by ab-initio [59] and this obtained a lower barrier for falling from an unstable rather than a stable layer. This difference is also included in our model.
In the implementation of this model we suppose or introduce the following:

1. In the experiment 0.5ML Pb was deposited randomly on the surface, which means that some of the atoms fall directly on the top of the island. In MC we suppose that the number of these atoms is small and can be ignored and that all atoms jump from the wetting-layer. Nevertheless in the next part will be shown that the small amount of atoms on the top can cause nucleation in the condition where nucleation of atoms which only diffuse from WL is impossible.

2. The terrace diffusion are marked steps in which all neighboring sites in lower layers are filled.

3. The periphery diffusion in this Monte Carlo means that there are jumps from a position in which an atom touches a cluster which is bigger than the critical size (CS) to a position which is also on the border of the cluster (but not necessarily the same position).

4. If the number of the nearest neighboring atoms in the bottom layer is smaller than three (i.e. due to periphery diffusion in the lower layer) then the atom will fall down on a free site without a barrier.

All other jumps are disabled (i.e. a jump from the 6th to the 7th layer, detachment from the cluster bigger than the CS, a jump from a position with 3 atoms in the upper layer to a position with only 2 atoms in the upper layer). The regular jump to a lower layer (7th to the 6th, 8th to the 7th and from the ring on the perimeter to the wetting layer) is possible only if the atom in the initial position does not touch a cluster bigger than the CS. The atom must have 3 neighboring atoms in the upper layer and between neighboring places in the same there layer must also be a place with less than 3 atoms in the lower layer.
The approximation in which all new atoms on the top jump from the WL is necessary because we do not know the frequency factor for "a jump" from the WL to the top of the island γ. In our simulation we use the time units $1t.u. = \gamma$ and then we have $\gamma = 1(t.u.^{-1})$. A frequency factor is usually in odder $10^8 s^{-1} - 10^{11} s^{-1}$ and represents the number of attempts of jumps per time unit, but if we want to use the SI units we must know the precise value of γ. If we want to add the deposition on the top of the island into the model, we need to know the size of the time unit (or prefactor γ) or set γ as a free parameter. Nevertheless for a small deposition rate, we can ignore the small current of atoms on the top of the island.

4.1.1 Nucleation in different layers

In the experiment was observed the start of nucleation on the border of the 6th and 7th layer, but new atoms from the WL do not nucleate in the 8th layer (see Fig(4.2)). Diffusion on both the 6th and 8th is described by the same set of barriers, but they have a different geometry. The 5th layer is completed and the atoms from the 6th layer can not jump to the 5th layer. On the other hand the 7th layer is ring-shaped and the atoms on it's top can escape the 8th layer and fall on the 7th or 6th. Consequently in our explanation the

quasi-equilibrium density ρ_b of atoms in the ring on the periphery in the 8th layer is smaller than some critical density $\rho_{cs}(i_b)$ at which the nucleation can start (see Fig(4.5)). i_b here is the critical size (CS) for nucleation on the border (see Tab(4.1))

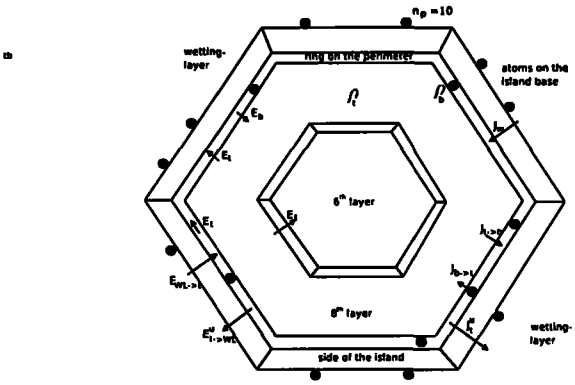

Figure 4.5: The schematic picture of the Pb island from the top. The current from the WL on the top is marked as J_w and from the ring on the perimeter into the center as $J_{b\to t}$. n_p is the actual number of atoms at the base of the island over a unit of time ($\overline{n}_p$ is the average value of n_p), ρ_b is the density of atoms in the ring.

This critical density depend on the critical size (CS) of the island on the border (i_b). The quasi-equilibrium density of atoms in the hole on the perimeter ρ_b is given by the balance of current J_b of atoms leaving this ring on the perimeter and by the current J_w of new atoms from the WL. If the equilibrium density (when $J_t^u \simeq J_w$) ρ_b^{eq} is smaller than some constant value ρ_{CS} it means that the nucleation never start. The condition that $\rho_b > \rho_{CS}$ determine the condition on barriers $E_{WL\to t} \simeq E_{t\to WL}^{s(u)}$. The effective current J_b consists of the current from the ring on an upper layer (stable or unstable) to the wetting-layer $J_t^{s(u)}$, a second component is the current from the ring to the terrace $J_{b\to t}$ and the last is a backward current from the terrace to the border $J_{t\to b}$. For these currents we can write

$$J_b = J_t^{s(u)} + J_{b\to t} - J_{t\to b} \tag{4.1}$$

where:

$$J_t^{s(u)} = 6R\frac{1}{3}\rho_b \exp(-E_{t\to WL}^{s(u)}/k_BT) \tag{4.2}$$

$$J_{b\to t} = 6R\frac{1}{3}\rho_b \exp(-E_h/k_BT) \tag{4.3}$$

$$J_{t\to b} = 6R\frac{1}{3}\rho_t \exp(-E_t/k_BT) \tag{4.4}$$

$$J_w = 6R\overline{n}_p \exp(-E_{WL\to t}/k_BT) \tag{4.5}$$

$\rho_{t(b)}$ is the quasi-equilibrium density on the border or terrace respectively, R is the radius of the island and $\overline{n}_p$ is the average number of atoms per unit length, on the base of the island, which are ready to jump on the top of the island from the wetting-layer.
The condition of the momentary equilibrium can be written as

$$J_w + J_{t\to b} = J_t^{s(u)} + J_{b\to t} \tag{4.6}$$

The terms $J_t^{s(u)}$ and $J_{t\to b}$ are different for each layer. In $J_t^{s(u)}$ because the barrier for falling from the top of the island to the wetting-layer is different for stable and unstable layers. The

second term is accordingly (4.5) proportional to the density of atoms on the center of the island $J_{t\to b} \simeq \rho_t$ and this density is a function of geometry and barriers on different layers. On 8th the layer the probability of falling to the central vacancy height is ($E_{8\to 7} = 0$) and $\rho_t^8 \simeq 0$. On yhe 7th layer the barrier for falling on the 6th layer is quite large ($E_{7\to 6} = 4E_t$) and on the 6th layer falling to the 5th layer is impossible because this layer is completely filled. We can consider $\rho_t^6 > \rho_t^7 > 0$ so that the increase of atoms, which is described by the left side of the equation (4.6), is higher in the 6th and 7th layer than in the 8th layer.
In the 6th layer practically all the atoms which leave the ring quickly fall back, but in the 7th and 8th layer they can fall down. In a stable 7th layer this probability is quite low. Thus if an atom in the 6th or 7th layer leaves the ring on the perimeter, there is quite a high probability that this atom will fall back into the ring on the perimetr after some time. Nucleation in the 8th layer can start after the 7th layer is already completed.
The dependency of the probability of nucleation in the 8th layer on $E_{WL\to t}$ can be estimated from a simple theory of nucleation rate as:

$$J_n = \exp(-E_t/k_BT)\rho_{b(t)}^{i_{b(t)}} \tag{4.7}$$

where $\rho_{b(t)}$ is the density of atoms on the bordering or on the terrace respectively. Other values are described in Tab(4.1). Quasi-equilibrium density $\rho_{b(t)}$ can be expressed from the balance equation (4.6), from (4.5), and from the assumption that $\rho_t = 0$:

$$\overline{n}_p 6R\exp(-\frac{E_{WL\to t}}{k_BT}) = \frac{1}{3}6R\rho_t(\exp(-\frac{E_b}{k_BT}) + \exp(-\frac{E^u_{t\to WL}}{k_BT})) \tag{4.8}$$

thus

$$\rho_b = \frac{3\overline{n}_p \exp(-\frac{E_{WL\to t}}{k_BT})}{\exp(-\frac{E_b}{k_BT}) + \exp(-\frac{E^u_{t\to WL}}{k_BT})} \tag{4.9}$$

We want to know if, for a given set of barriers, nucleation is possible or not. The scale for this can be the ratio of probabilities that an atom which is on the perimeter leaves the ring in a time unit divided by the probabilities that this atom will nucleate in the ring. The probability of nucleation is proportional to nucleation rate (J_n) and the probability of leaving is proportional to current J_b (see Fig(4.5)). For this ratio of probabilities we obtain:

$$\frac{J_n}{J_p} = \frac{(3\overline{n}_p)^{(i_b-1)}\exp(-\frac{E_t+(i_b-1)E_{WL\to t}}{k_BT})}{2R(exp(-\frac{E^u_{t\to WL}}{k_BT}) + exp(-\frac{E_b}{k_BT}))^{i_b}} \tag{4.10}$$

This means that the probability of escaping the ring exponentially decreases with an increasing barrier $E_{WL\to t}$ (which implies smaller current $WL \to t$). By increasing $E_{WL\to t}$ by 0.02eV and $i_b = 8$ we obtain a reduction of the ratio of probability for nucleation in the ring and the probability of escape by the coefficient 10^{-4}. If we decrease the barrier $E_{WL\to t}$ (and increase the current from the WL) the probability of nucleation on the 8th layer increases exponentially. The influence of the barriers $E_{t\to WL}$ and E_b which are in the denominator of equation (4.10) is the opposite - if one of these barriers increases the probability of nucleation in the 8th layer also increases.
Thus for barrier $E_{WL\to t} = 0.27eV$ the probability of nucleation is smaller than the probability of escaping the ring. The term for the probability of the nucleation is approximate, but if we run the MC simulation with the barriers from table 4.1 where $E_{WL\to t} = 0.25eV$, we obtain nucleation in the 8th layer for "quicker growth" (a smaller barrier) but for $E_{WL\to t} = 0.26eV$ the average number of atoms in the ring is 5 and nucleation does not start in the 8th layer. The difference between both barriers is 7% which is quite small. The same results were

obtained without diffusion anisotropy in the 8th layer and with the current from $WL \rightarrow t$ independent of the height of the island. The amenity of this approximation is that we can decrease the barrier $E_{WL \rightarrow t}$ to a value which still allow up to find the ordination of the top of the island which corresponds to the simulation with a higher barrier. This trick allows the simulation to run in reasonable times.

4.2 Results of MC simulations

In this paragraph is the result of MC with barriers shown in Tab(3.5.3 is presented (reference model). The proposed set of barriers has some liberty for some barriers. To illuminate the influence of a different barrier, we also ran an MC simulation in which one of the parameters was changed in comparison with Tab(3.5.3).

4.2.1 Reference model

The specific attribute of the growth of a Pb island on a Si(111) surface is the double-layer growth which starts on the perimeter of the island. In double-layer growth the difference between stable and unstable islands heights is crucial. There are not any particles on the top of the island at the beginning of the simulation and new particles from WL diffuse to the free unstable layer on the top of the island (the island has a stable height). The barrier $E_{WL\to t}$ and $E^{u}_{t\to WL}$ are set so that the current from $WL \to top$ is slightly higher than the backward currents $top \to WL$. In experiment [50] after the addition of 0.5ML approximately 1/4 of all particles in a double-layer are on the top of the island, so the condition that the incoming current must be greater than the backward current is not so crucial. For nucleation to occur it is sufficient that the current from $WL \to top$ plus the deposition rate (in [50] 0.25ML/min) is slightly higher than the backward current determined by barrier $E_{t\to WL}$. In our MC we ignored the atoms which fall on the top of the island during the deposition. If we include the deposition in the model then the barrier for falling from the top to the wetting-layer can by smaller.

Nevertheless in our MC the difference between currents from the WL to the top of the

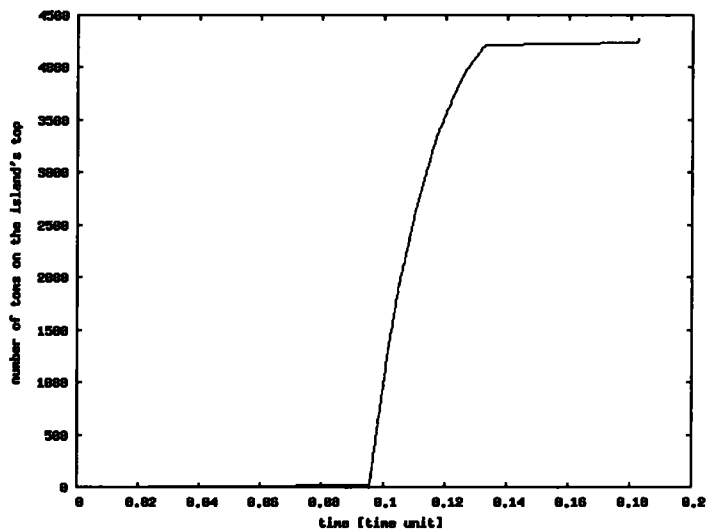

Figure 4.6: Dependency of the total number of particles on the top of the island on time. The time is in time unit where t=1/γ, and γ is a prefactor.

island and the backward current from the top to the WL is positive. The increase of the number of particles on the top of the island is really slow, the addition of the first 20 atoms on the surface needs 1/2 of the time for the whole simulation. After a cluster bigger than CS is formed, the probability of falling from the island from an unstable layer back to the WL quickly decrease and the growth is really quick (see Fig(4.7)). The barrier for falling from the top of the stable layer is higher than in an unstable layer so nucleation starts quickly in spite

of the fact that the part of the atoms fall into the central vacancy. But after the double layer ring is formed and new atoms from the WL jump on the unstable 8th layer the backward current increases again. Nucleation in the 8th layer does not start because the density of the atoms is smaller than on the 6th layer in the early phase of the simulation. The reason for this is the existence of the central vacancy in the 8th (and also 7th) layer.

The velocity of growth is caught in picture Fig(4.2.1). The low increase at the beginning

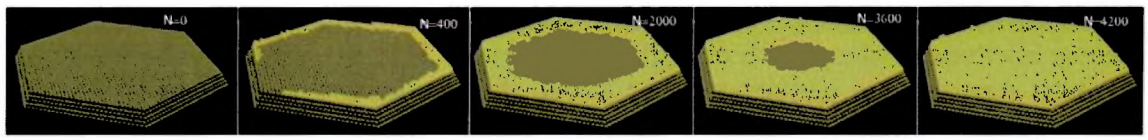

Figure 4.7: A set of pictures from the MC. We start the simulation with a free surface and stop it after the double layer is formed. The number of atoms on the top is written in the upper right corner of each picture.

corresponds to the beginning of the simulation before the nuclei formed. After this slow growth, the increment of atoms on the top decreases because of the backward current from the 8th layer to the WL. At the end of the simulation the island is completed and the growth waits for the creation of the nuclei in an unstable 8th layer again.
In the reference model the current from the WL was quite high. This corresponds to the experiment with a height deposition rate (0.5ML in 2 minutes). The situation at the moment when 1/2 of the top was filled is in Fig(4.8).

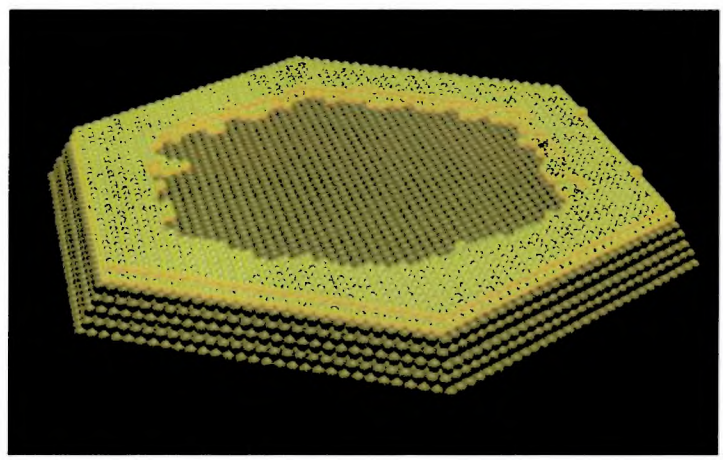

Figure 4.8: The reference case with barriers for MC steps described in Tab(3.5.3).

4.2.2 The barrier controls the current from the WL

The simulation was also realized with a low flux from the WL which is described by an effective barrier for a jump from the WL $E_{WL\to t} = 0.35eV$. With the current from the WL as low as this the simulation need a really long time for nuclei formation, so we start the simulation with 60 atoms on the surface. This number of atoms gives a coverage 0.023 at the top of the island with a radius of 30 atoms.
The low flux from the WL to the top of the island means that an atom in the 7th layer does not have enough time to fall either back on the WL or to the 6th layer, nucleation in

7th layer can not start until the central vacancy is filled and thus we obtained layer-by-layer growth in the simulation.
This can illuminate the STM observation at 180K [62] in which the mode of growth depends on the deposition rate. For a low flux the formation of the stable nuclei on the unstable 6th layer is crucial. This nuclei can be formed from an atom which falls on the top during the deposition as could be in experiment [50] and [62] or is moved from the WL by height voltage on the tip which could be significant mechanism in the experiment at RT with a constant coverage [61]. The pictures from the middle of the growth of the top of the island is in Fig(4.2.1).

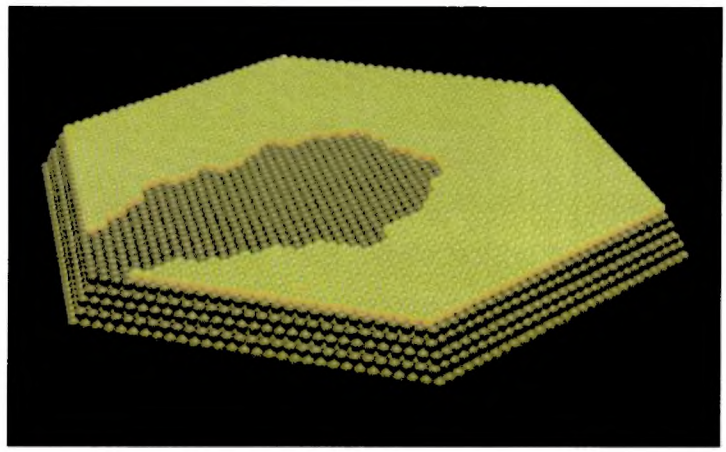

Figure 4.9: The modified MC which differs from 3.5.3 in the effective barrier for flux from the WL on the top of the island. In this case the barrier was changed to $E_{WL\to t} = 0.35eV$.

4.2.3 The non-homogeneity on the top of the island

In our model the double-layer ring observed in the experiment rises from the non-homogeneity of the the top of the island. We studied two types of the non-homogeneity. The first one is, as was mentioned above, the deep energy hole on the island perimeter. The second possibility is the different critical cluster size (CS) on the island's perimeter (i_b) and on the terrace (i_t). If the difference between both CS is high enough to eliminate a number of different sites on the perimeter and on the terrace, then the nucleation starts on the border.
Nevertheless after the nuclei is formed the growth continues in a classical way. The island in the new layer has a shape which tends to minimize surface energy on homogeneous surfaces (due to quite slow periphery diffusion, the shape is not fully ordered). This island is one layer thick, thus for the formation of the circle ring we need some other anisotropy on the surface.
In this case the influence of different backward currents for falling from the top of the island can be ignored. The dependency of the number of atoms on the top over time is linear (see Fig(4.2.3)). The reason is that the jump from the top of the island to the WL can only be realized by a free atom on the perimeter. In previous cases the position on the perimeter was preferred by free atoms, because of the energy hole which was there. Now the atoms have the same probability of occupancy of each site on the top of the islands, so the number of free atoms on the perimeter is low and the possible jump is infrequent in each layers.
Non-homogeneity in CS is not sufficient to reproduce the experiment. It seems that the hole

on the perimeter of the island is an important part of our microscopic model.

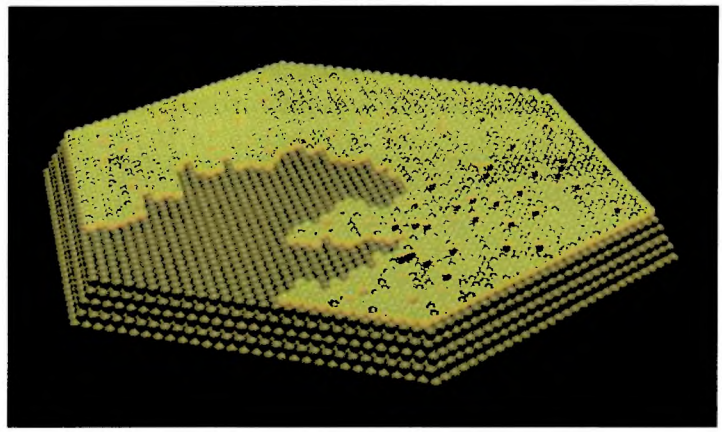

Figure 4.10: The case where anisotropy of the surface is not provided by an energy hole on the perimeter, but by a different critical cluster sizes (CS) on the perimeter $i_b = 2$ and on the terrace $i_t = 8$.

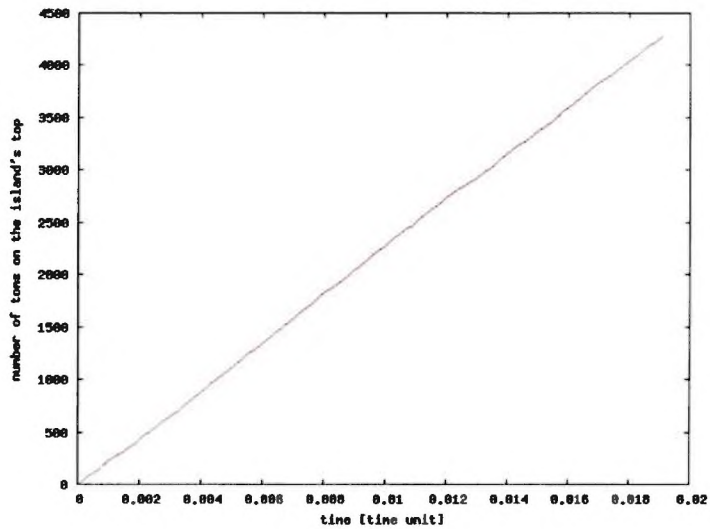

Figure 4.11: The dependency of the number of atoms on the top of the island in the case of different critical cluster sizes (CS) on the perimeter $i_b = 2$ and on the terrace $i_t = 8$.

4.2.4 The critical cluster size (CS)

For the double-layer growth the low probability of nucleation in the 8th layer is critical. This probability is given by the average number of atoms in the ring on the perimeter - nucleation can start if their number is higher than a critical number. From this it is clear that the critical cluster size on the border (i_b) influences the time in which the number of atoms slowly increases on the surface - for higher i_b the average number of atoms in the ring must also be higher and the time for the start of nucleation increases. For smaller i_b=4 and the

same barrier as in Tab(3.5.3) the density of atom in the ring in the 8th layer is bigger than the critical density $\rho_{cs}(i_b = 4)$, so nucleation starts and we can observe a multi-layer ring (see Fig(4.2.4)).

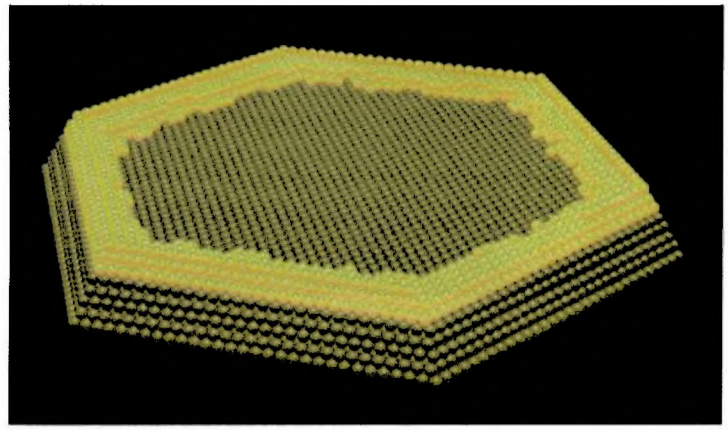

Figure 4.12: A picture from the middle (N=2200 atoms on the top) of the simulation with $i_b = i_t = 4$.

4.2.5 Slow diffusion on the surface

There should be another possibility to explain the ring on the perimeter with a homogeneous surface. This is slow diffusion on the top of the island. If the diffusion on the top is slower than the diffusion from the WL to the top thet the density of atoms and the probability of the nucleation on the border increases. If we used constant barriers for the flux from the WL and the diffusion on the layers we, obtained multilayer growth. In case of a slow deposition rate the current of particles from the WL decreases and we obtain layer-by-layer growth which agrees with the experiment.
The problem is how to explain double-layer growth within this model. Nucleation is joined with high flux and layer-by-layer with low flux from the WL, so for double-layer growth high flux on the 6th layer (or slow diffusion) and low flux on the top of the uncompleted 8th layer (or quick diffusion) is necessary. After the 7th layer is filled, a new double-layer is formed and now the high flux on the 8th layer is necessary. But from energetics calculations of QSE [52] it seems that there is no reason for such a huge difference between the unstable 6th and unstable 8th layers and also the difference in barriers for a jump to the top of the completed and uncompleted layer is disputable. For all these reasons we prefer a model with different barriers for the stable and unstable layers.

4.2.6 Periphery diffusion

It seems that periphery diffusion does not have a strong influence on the results of the simulation. The simulation was originally done for value E_b=0.1eV, then for E_b=0.05eV and E_b=0.15eV. There are small differences in the number of atoms in the second layer at the beginning of the simulation but in the middle of the filling of the double-layer there is no difference (see Fig(4.2.6))

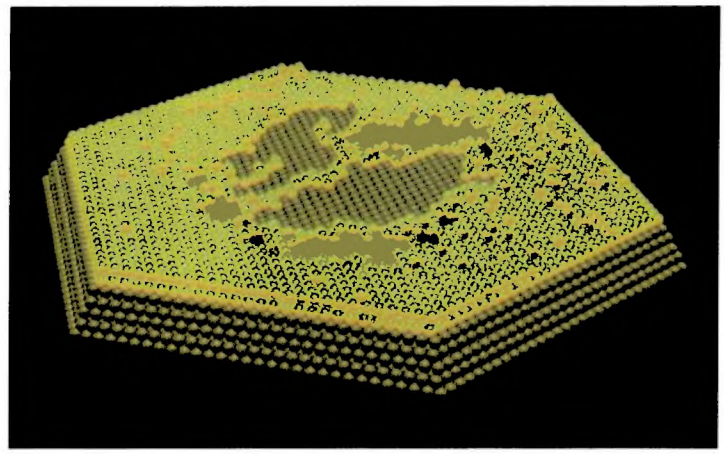

Figure 4.13: A picture from the middle (N=2200 atoms on the top) of the simulation with slow diffusion and without a hole on the border ($E_b = E_t = 0.17eV$).

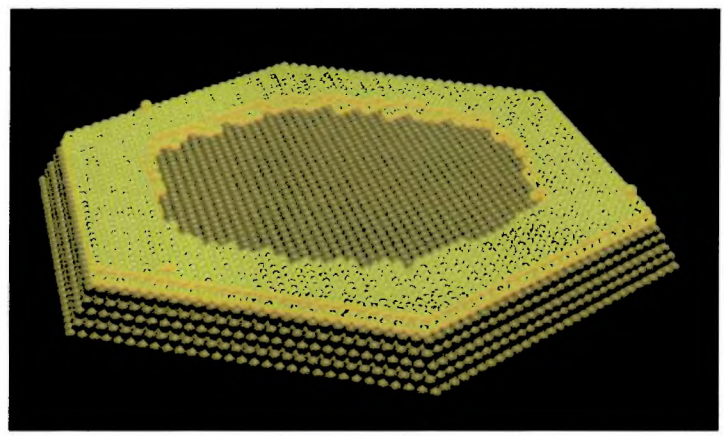

Figure 4.14: A picture from the middle (N=2200 atoms on the top) of the simulation with slow periphery diffusion ($E_b = 0.15eV$).

4.3 Conclusion

The fact that the MC simulation provides a nice agreement with the experiment is not a complete proof of our assumptions. But both MC and ab-initio [59] imply that the dependency on the height of the current from the WL to the top of the island is true. In the previous section was introduced the simple model of growth of Pb islands on Si(111) which try to reproduce the phase diagram measured in [54]. A constant current from $WL \rightarrow$ island's sides per unit length and the constant probability for a jump from the sides of the island to the top never gives way to the switching of modes of growth in height and in radius with an increasing coverage. This fact implies that there must be some dependency of the total current from $WL \rightarrow t$ (in the model described in caption 3 divided into two steps: a jump from $WL \rightarrow$ *side* and a jump *side* $\rightarrow$ *top*) on radius and on height. The dependency on radius can be caused by the deformation of the WL in the area surrounding the island's base (Pb and Si have different lattice constants and also the bulk structure). But the dependency on height (and probably also on radius) is probably evoked by the quantum size effect which

is described in ab-initio calculations for Pb/Si [52]. Nevertheless the more precise surface potential which we propose here needs the ab-initio calculations of the surface potential close to the perimeter of the island.
In our microscopic model the differences between islands with different height and radius are not important but the main characteristic is the difference between the stable and unstable heights together with the existence of the energy hole on the island's perimeter. The other parameters influence the result only if they change the probability of leaving the ring on the perimeter which changes the density of atoms there and also the probability of nucleation. The set of barriers which is used here is not final and only one possibility. It was shown that some changes did not influence the result (i.e. E_b) and some couples of parameters reciprocally interrupt the others influence (i.e. $E_{WL\to t}$ and $E_{t\to WL}$).
Nevertheless we suppose that this set of barriers roughly describes the energetic surface on the top of a Pb/Si(111) island.

Chapter 5

In conclusion

The MC simulation is a quite powerful method especially in combination with Molecular Dynamics or some other methods which can determine the surface potential "in run" and thus allow the use of a more precise microscopic model of processes on the mezoscopic scale. In our simulations we used a simple MC simulation in which the surface potential has to be known before the start of the simulation. This limits the number of processes which includes the microscopic model (the surface potential has a lot of free parameters) but on the other hand this simple method allows for the simulation of the time development of a huge nano-object for a sufficiently long time. In the case of Ag/Ag in this work it was shown that even barriers calculated by semi-empirical methods or by MD are not fully relevant and thus the question arises how much the simulation joins with the actual systems. The answer to this question is not unique, but our simulation still shows that there exist some limits for the use of thermodynamic approximation on small scales and for the description of the evolution of non-equilibrium systems. Besides, the question of how much certain methods can describe physical reality is not unique only for MC but practically for all methods in physics. Contrary to the analytical calculation in MC it is possible to set more precise and complicated models which can more precisely describe reality.

5.0.1 In addition

The work in the first two chapters is quite similar. The calculation of single atom diffusion was done only for comparison with the MC simulation [20] with the aim to show that the adsorption places considered by the group of Vladimir Chab agree with the experimental STM pictures. This goal was fulfilled.
In the case of simulation Ag/Ag(111) some characteristics different from the predictions of thermodynamics G-T approximation were obtained. But the completion of temperature dependencies, the determination of the Ehrlich-Schwëbel barriers and the ratio of prefactors proved to be impossible for such a large system. The simulation of the whole system was quite costly in time and the simulation of the central island was too sensitive to external parameters (see Appendix A).
In the case of the Pb islands we set up a model which could explain the experimental phase-diagram and then we stopped with this work and focused, in our second model, on the formation of the new double-layer on the top of the Pb island. Nevertheless with a new experiment or ab-initio calculations we might return to our model to state it more precisely or replace it with another if the previous model proves to be unsuitable. At present there are no available ab-initio calculations or experiments which can validate or refute the assumptions of our model. Nevertheless the results, which are in perfect agreement with the experiment,

show that our model might be right.
There are still a lot of open questions about the system of Pb/Si at height coverages. For us it is crucial that the potential is at least roughly correct. The answer to this question can only be given by the ab-initio calculation which is impossible with regards to the size of the system. But there also exist lots of questions about the kinetic model: is the layer-by-layer, double-layer or multi-layer growth driven by the flux of atoms from WL or by the temperature or by the size of the cluster or does something else play a role? How much does the stability of the last layer of the island depend on its height and how can this be included in the model. In the future we plan to make our model more precise in order to also simulate experiments with a low flux and a large size of simulated islands.
The experiment at RT is really interesting in a lot of aspects. First after the ring along the perimeter is formed, the flux of the atoms into the central "vacancy" is so slow that the layer on the top of the ring is formed before the central vacancy is filled. It is not clear if the reason is the huge size of the island (the atom needs a lot of time to reach the border of the vacancy) or some changes in surface potential. The simulation with r=1000atoms is very expensive in computer time thus it is difficult to verify it by MC.

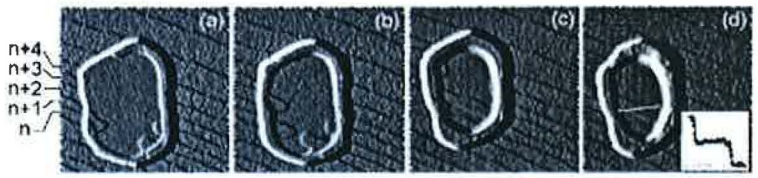

FIG. 3. Sequentially recorded STM images (8000 Å × 8000 Å) showing a sequential strip-flow growth on alternating strips on the plateau inside the ring. The inset shows the step height profile along the white line in (d).

Figure 5.1: The referenced picture from [60]. The interest here is the filling of the central vacancy in bands which corresponds with the position of the stairs on the substrate.

Fig(5.1) adopted from [60] is important for our model. In this experiment the huge Pb island grows on a substrate with steps, so the thickness of the island was different in each part of the island. After the formation of a multilayer ring on the perimeter the filling of the central empty area of the island was observed. First a new layer was completed on the part of the island with the smallest "unstable" height, then the top of the next "unstable" part was filled. The reason for the creation of these bands could be the difference in surface diffusion at the top of the stable and unstable layer. If the diffusion on the stable layer is much quicker than the diffusion on the unstable layer, then the atoms from the stable part of the "band" can diffuse to the area with an unstable height where the diffusion is much slower. The difference between the diffusion of a free atoms at the tops of the stable and unstable layers was calculated in [59] as $E_t = 0.01eV$ for stable and $E_t = 0.05eV$ for unstable. Nevertheless in the previous consideration, we needed the difference in diffusion along the cluster which means different E_b for stable and unstable and only the MC simulation can show if this model can describe the experiment.
The inclusion of this unusual behavior during growth into the model could make our model more precise or, on the contrary, show the inaccuracy of our model. The continuation of our work can proceed in these directions.

Appendix A

The temperature dependency of the decay of Ag/Ag(111) islands

In Chapter 1 we discussed the decay of adatom and vacancy islands at RT. In the next step we will simulate the decay of the island at different temperatures. This part will be quite brief as we did not find a quick and certain method how to simulate the vacancy decay for the height effective Ehrlich-Schwöbel barrier E_s^{eff} thus this results are not unambiguous. The simulation of the decay of an adatom island at RT takes approximately 3 weeks of computer time, and from [10] it is known that vacancy decay is 18-times longer than the decay of an adatom island at RT. Thus to simulate vacancy decay by our method would be really expensive in computer time and to find the value of $E_s'^{eff}$ which gives the same ratio of decay times is practically impossible. At the end of this appendix a method to speed up the MC simulation will be suggested .

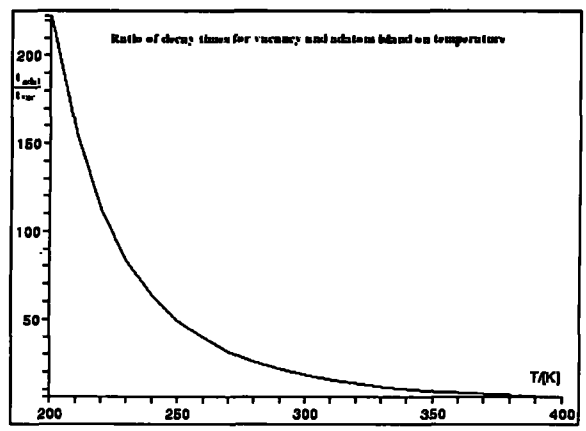

Figure A.1: The ratio of decay times $\frac{t_v}{t_a}$ for adatom and vacancy islands as a function of T - the curve is a solution of (1.1) with parameters from [10].

The aim of this part is to determine the ratio of prefactors $\frac{\nu_s}{\nu_t}$ and the Ehrlich-Schwëbel barrier. It is possible to separate only their temperature dependencies. The probability of a jump across the edge works only with the effective Ehrlich-Schwëbel barrier E_s^{eff} in our MC simulation. To determine a real Ehrlich-Schwöbel barrier we must first find an Ehrlich-Schwëbel barrier which provides the expected vacancy decay time $t_v^{exc}(E_s'^{eff})$ for each temperature and than to separate it from the Arrhenius plot by using the deffinition of

$E_s^{'eff}$:

$$exp(-\frac{E_s^{'eff}}{kT}) = \frac{\nu_s}{\nu_t} exp(-\frac{E_s}{kT}) \tag{A.1}$$

The expected ratio of decay times (t_v^{exc}) was measured in [10] but only the parameters of the curve which fit on this data were published. Using these parameters $\{E_e, E_s, \frac{\nu_s}{\nu_t}, \beta_o, \gamma\}$ published in [10], we solve equation (1.1) which was in [10] fit to the experimental data. The numerical solution of this equation is in Fig(A.1).
The values of the ratio of decay times $(\frac{t_v}{t_a})'$ at the mentioned temperatures are written in Tab(A.1). After correcting the sizes we obtained the ratio of decay times $\frac{t_v}{t_a}$ which is relevant in our MC simulations. We obtained the expected time of vacancy decay (t_v^{exc}) as the product of the corrected ratio of decay times and the decay time of the adatom island.
Now we can try to estimate variate the effective Ehrlich-Schwöbel barrier for which the

T[K]	ratio of decay times $(\frac{t_v}{t_a})'$ from [10]	ratio of decay times size correction $\frac{t_v}{t_a}$	t_a decay time of adatom island	t_v^{exc} - expected decay time of vacancy island
300K	18.5	15.42	$5.9\ 10^{10}$	$9.1\ 10^{11}$
340K	10.59	8.83	$6.9\ 10^{9}$	$5.8\ 10^{10}$
360K	8.4	7.05	$2.8\ 10^{9}$	$1.9\ 10^{10}$
380K	6.95	5.78	$1.15\ 10^{9}$	$6.6\ 10^{9}$

Table A.1: The temperature dependency of the ratio of decay times of the vacancy and adatom island. The ratio of decay times $(\frac{t_v}{t_a})'$ was derived from equation (1.1) with the parameters measured in [10] (first column) and the value $\frac{t_v}{t_a}$ is corrected to size effect (second column). In the next column are the decay times of adatom islands t_a taken from MC (see Fig(A.2)). The expected decay time of vacancy decay t_v^{exc} (fourth column).

decay time of vacancy island $t_v(T, E_s^{eff})$ will be equal to the expected decay time of vacancy island t_v^{exc}.
First we simulate the adatom decay with the same parameters as in RT Tab(1.1) but at temperatures 340K, 360K, 380K. The shape of all dependencies are similar, but the decay time t_a decreases with increases in temperature. The results are in picture Fig(A.2) and the decay times of adatom island t_a at different temperatures are written in the third column of Tab(A.1).
In the second step we run the set of the MC simulation with different $E_S^{eff} \in \{0.1, 0.23, 0.28, 0.32, 0.35\}eV$ at each temperature $T \in \{300, 340, 360, 380\}K$. The results of these simulations are in the set of figures Fig(A.3). MC at the same temperatures are classed in columns of Fig(A.3). We only ran also the simulation for RT and E_s^{eff}=0.35eV up to the end, for the other temperatures the highest effective barrier was E_S^{eff}=0.32eV. But this barrier is too hight, thus the computer time to complete the simulation is too long (for $E_s^{eff} = 0.35eV, T = 300K$, it was more than half a year). For this reason we stopped the simulation after some computer time (a month) and the decay time was determined by extrapolation, nevertheless this technique is bring in an error which could misrepresent the results, especially at lower temperatures.
The decay times $t_v^{MC}(T, E_s)$ for different temperatures and the E-S barrier are written in Tab(A.2). In this table are also the parameters of the exponential dependencies $N = (a+b.t)^q$ which were fitted to the data N(t) from MC. Now we can plot the dependency of the decay time of the vacancy island on the E_s^{eff} barrier for each temperature. By projecting the points in the chart of the power dependency and the Ehrlich-Schwöbel barrier, the relevant value

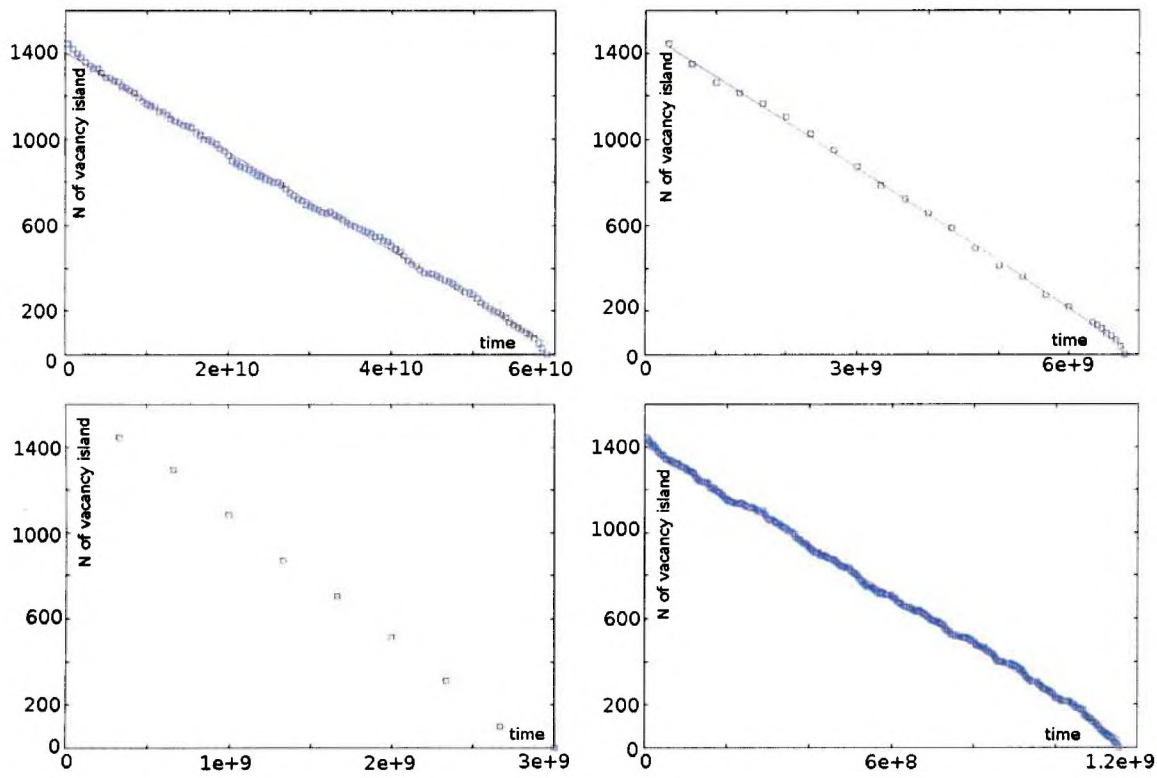

Figure A.2: The dependency of the number of atoms in the central adatom island over time at different temperatures $T \in \{300,340,360,380\}K$ (from left to right).

of t_v^{exc} is determined (see Fig(A.4)). The Arrhenius plot (the dependency of the effective Ehrlich-Schwöbel barrier $E_s^{eff}(T)$ over time) is in Fig(A.3). As a result of fitting the dependency $\exp(-\frac{E_s^{eff}(T)}{k_B T}) = \frac{\nu_s}{\nu_t}\exp(-\frac{E_s}{k_B T})$ we obtain the wanted Ehrlich-Schwöbel barrier for a jump across the edge and the value of the ratio of prefactors for a jump on the terrace and across the edge $\frac{\nu_s}{\nu_t}$. For the plot only higher temperatures were used. The points at a higher temperature are determined with a higher precesion because $E_s^{eff}(T)$ is decreasing for increases in temperature. The data for the Arrhenius plot are written in Tab(A.3)

E_S/eV	T/K	decay time	a	b	q
0.10	300	$7.17\ 10^{9}$	$1.89\ 10^{3} \pm 37.7$	$-2.67\ 10^{-7} \pm 9.08\ 10^{-9}$	$0.96 \pm 4.750\ 10^{-3}$
0.10	340	$6.63\ 10^{8}$	$1.07\ 10^{3} \pm 24.1$	$-1.64\ 10^{-6} \pm 6.26\ 10^{-8}$	$1.04 \pm 6.100\ 10^{-3}$
0.10	360	$2.50\ 10^{8}$	$8.63\ 10^{2} \pm 15.4$	$-3.45\ 10^{-6} \pm 1.17\ 10^{-7}$	$1.07 \pm 4.850\ 10^{-3}$
0.10	380	$1.16\ 10^{8}$	$6.42\ 10^{2} \pm 17.2$	$-5.54\ 10^{-6} \pm 2.83\ 10^{-7}$	$1.12 \pm 7.970\ 10^{-3}$
0.23	300	$9.38\ 10^{9}$	$2.72\ 10^{2} \pm 4.40$	$-2.84\ 10^{-8} \pm 1.06\ 10^{-9}$	$1.29 \pm 5.380\ 10^{-3}$
0.23	340	$9.94\ 10^{8}$	$2.48\ 10^{2} \pm 4.55$	$-2.49\ 10^{-7} \pm 1.10\ 10^{-8}$	$1.31 \pm 6.580\ 10^{-3}$
0.23	360	$3.76\ 10^{8}$	$3.71\ 10^{2} \pm 14.2$	$-1.01\ 10^{-6} \pm 8.91\ 10^{-8}$	$1.22 \pm 1.290\ 10^{-2}$
0.23	380	$1.57\ 10^{8}$	$4.40\ 10^{2} \pm 6.78$	$-2.83\ 10^{-6} \pm 9.52\ 10^{-8}$	$1.19 \pm 4.870\ 10^{-3}$
0.28	300	$2.5\ 10^{10}$	65.9 ± 7.84	$-2.64\ 10^{-9} \pm 1.07\ 10^{-10}$	$1.72 \pm 6.360\ 10^{-3}$
0.28	340	$\star\ 2.06\ 10^{9}$	$1.30\ 10^{2} \pm 0.175$	$-6.32\ 10^{-8} \pm 2.36\ 10^{-9}$	$1.48 \pm 5.700\ 10^{-3}$
0.28	360	$8.12\ 10^{8}$	$1.28\ 10^{2} \pm 4.29$	$-1.56\ 10^{-7} \pm 1.88\ 10^{-8}$	$1.49 \pm 1.390\ 10^{-2}$
0.28	380	$\star\ 2.80\ 10^{8}$	$4.93\ 10^{2} \pm 6.37$	$-1.76\ 10^{-6} \pm 7.03\ 10^{-8}$	$1.16 \pm 3.440\ 10^{-3}$
0.32	300	$\star\ 8.7\ 10^{10}$	30.7 ± 0.104	$-3.54\ 10^{-10} \pm 1.62\ 10^{-11}$	$2.10 \pm 2.260\ 10^{-3}$
0.32	340	$\star\ 4.92\ 10^{9}$	$1.67\ 10^{2} \pm 2.07$	$-3.40\ 10^{-8} \pm 2.29\ 10^{-9}$	$1.41 \pm 4.170\ 10^{-3}$
0.32	360	$\star\ 1.65\ 10^{9}$	$4.49\ 10^{2} \pm 5.0$	$-2.73\ 10^{-7} \pm 9.76\ 10^{-9}$	$1.18 \pm 2.97\ 10^{-3}$
0.32	380	$\star\ 9.91\ 10^{8}$	52.4 ± 0.47	$-5.29\ 10^{-8} \pm 1.89\ 10^{-9}$	$1.82 \pm 5.14\ 10^{-3}$
0.35	300	$5.4\ 10^{11}$	—	—	—

Table A.2: The decay times of the vacancy island and the parameters of dependencies $N = (a + bt)^q$ applied to the decay laws for temperatures 300K, 340K, 360K and 380K and barriers $E_s^{eff} \in \{0.1eV, 0.23eV, 0.28eV, 0.32eV, 0.35eV\}$. Symbol $\star$ mark values obtained by extrapolation to N=0.

T [K]	$E_s'^{eff}(T)$
300	0.36eV
340	0.455eV
360	0.45eV
380	0.38eV

Table A.3: The $E_s'^{eff}$ obtained from interpolations of the dependency of decay times on E_s^{eff} which provides a vacancy decay time in MC equal to the expected decay time t_v^{exc}.

From this table we can separate the E-S barrier and the ratio of prefactors. The $E_s'^{eff}$ is defined as

$$\exp(\frac{-E_s'^{eff}(T)}{k_B T}) = \frac{\nu_t}{\nu_s}\exp(\frac{-E_s}{k_B T}) \tag{A.2}$$

From this equation we can derive:

$$E_s'^{eff} = -k_B \log(\frac{\nu_t}{\nu_s})T + E_s \tag{A.3}$$

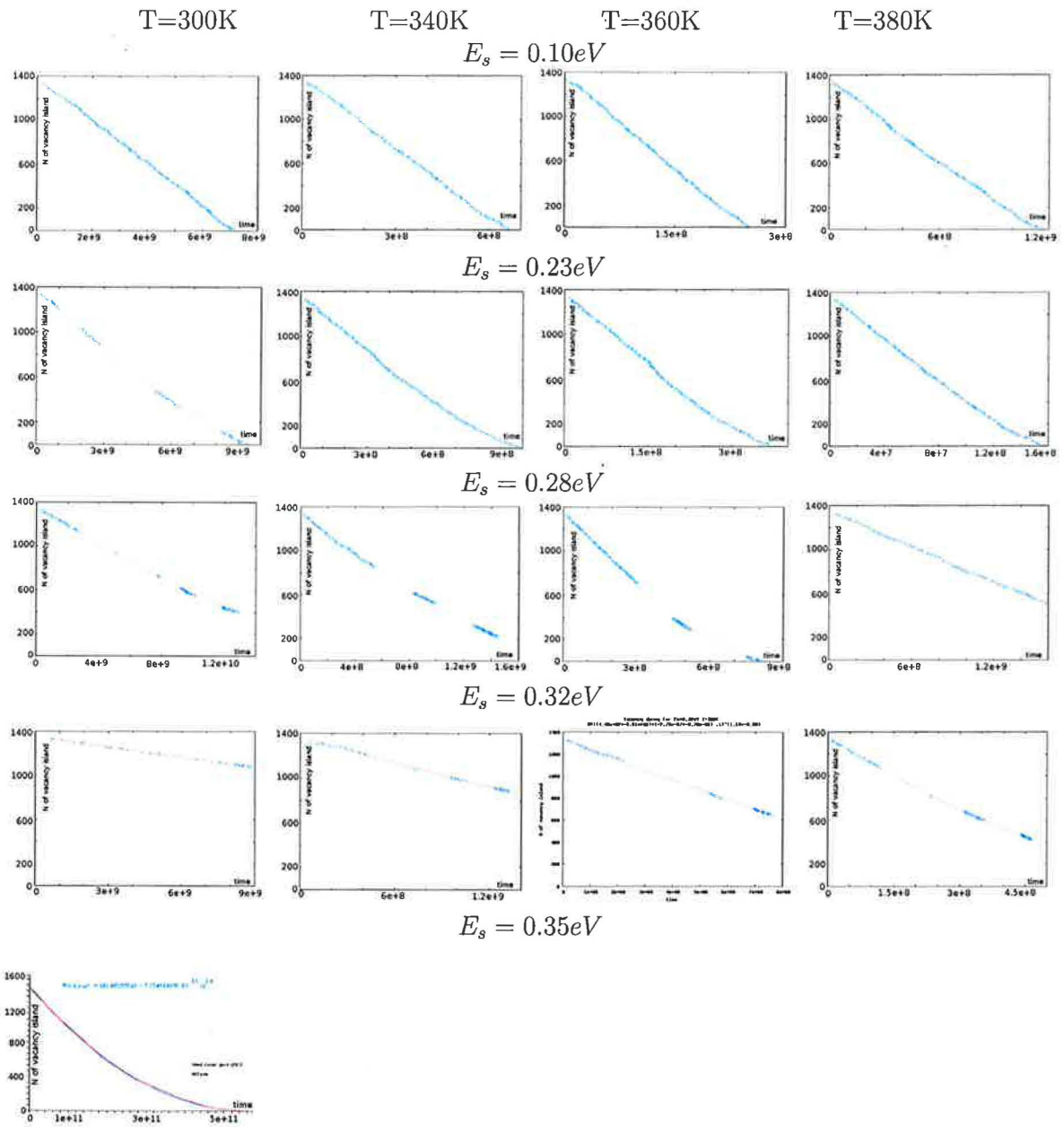

Figure A.3: Decay laws for different temperatures (constant temperatures in columns) and effective E-S barrier E_s^{eff} (constant values of E_s^{eff} are in the same rows). The parameters of the fitted curves are in Tab(A.2).

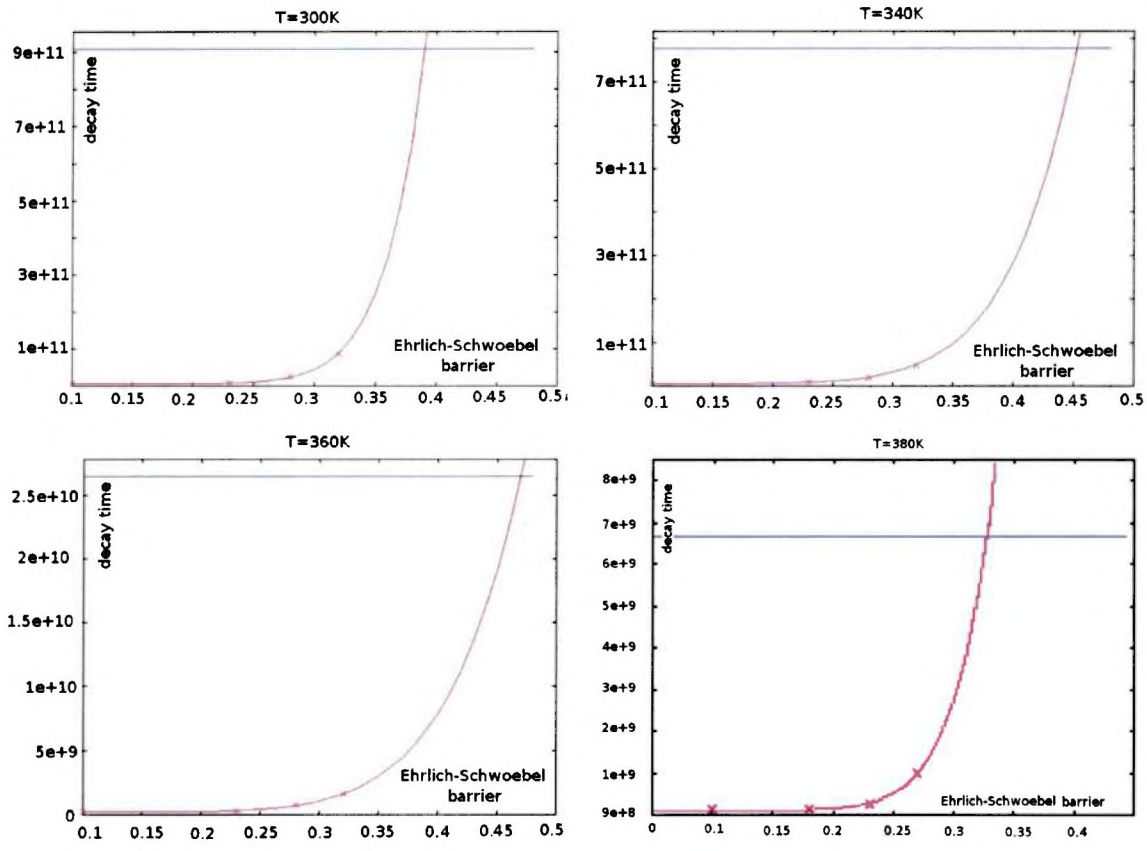

Figure A.4: The interpolation of decay laws by the dependencies $N = (a + bt)^q$. The vertical line is $t = t_v^{exc}$. The right value of $E_s^{'eff}$ which provides the expected decay time t_v^{exc} is estimated as the cross points of the interpolated dependency and the line $t = t_v^{exc}$.

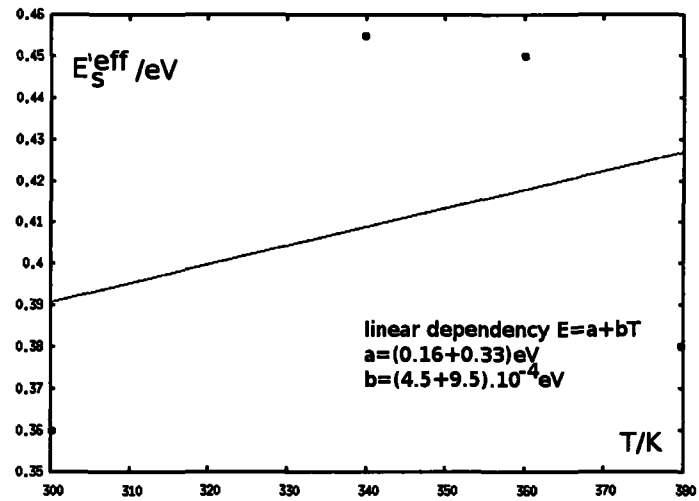

Figure A.5: The Arrhenius plot: plotted data is $E_s^{'eff}$ which provide a vacancy decay time in MC equal to the expected decay time t_v^{exc} at the given temperature. At this point is applied the dependency $E_s^{'eff} = -aT + b$, where b is the Ehrlich-Schwöbel barrier and $a = k_B \log(\frac{\nu_t}{\nu_s})$.

In Fig(A.5) are plotted the data from table Tab(A.3) and through this point is fitted the dependency in shape $y = -a.T + b$ (A.3) with the parameters:

$$a = (-4.5 \pm 9.5)10^{-4}eV \qquad b = (0. \pm 0.82)eV \tag{A.4}$$

The second parameter is identical with Ehrlich-Schwöbel barrier E_s and the ratio of the prefactor can be derived from (A.3). The result is handicapped by a large margin of:

$$\frac{\nu_t}{\nu_s} = (0.005 \pm 0.06) \tag{A.5}$$

$$E_s = (0.25 \pm 0.33)eV \tag{A.6}$$

which can be rewritten in form:

$$\frac{\nu_t}{\nu_s} << 1 \tag{A.7}$$

$$E_s < 0.58eV \tag{A.8}$$

Nevertheless the error is so great that these results do not say anything about the right values. The calculation of these four points in the Arrhenius plot take approximately a year of computer time and a large part of the calculations has still not been completed. E_s^{eff} is still too small to give the expected decay time T_v^{exc} and the right value was determined by the next extrapolation. The completion of the simulation with the presented algorithm and with E_s^{eff}, close to expected value of Ehrlich-Schwöbel barrier, is practically impossible with todays computers. And the double extrapolation adds a huge margin of error to our results. In the next paragraph we introduce the quicker model.

A.0.2 A quicker algorithm for the MC simulation of vacancy decay

In the original model we had practically constant computer time for the movement of the atoms, but the majority of these movements are on the edge of the big vacancy island. There are many different types of atoms with different probabilities to jump, but still there are

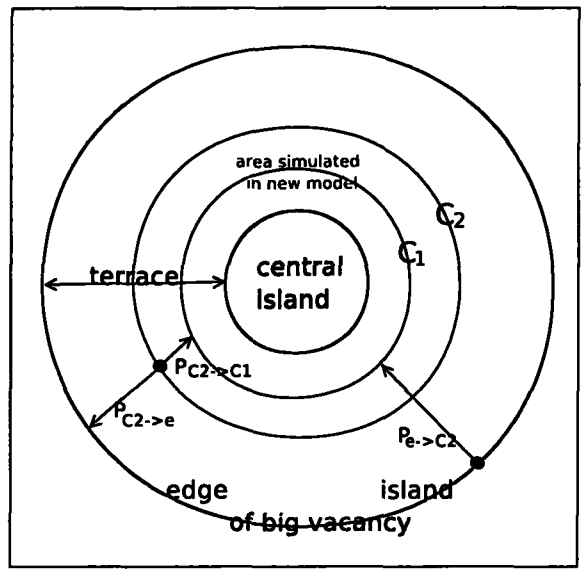

Figure A.6: The simulated area in the quicker MC simulation is inside circle C_2. In the previous simulation the majority of movement was done on the edge of the big vacancy island. The Ag atoms detaches from the edge of big vacancy island are added on the circle C_1.

35*6 atoms on the edge of the big vacancy and maximally 6*15 atoms on the edge of the central island (at the end of the simulation there are much less).
This means that for $R/(R+r) \simeq 70\%$ of the computer time, we simulate only the periphery diffusion on the big vacancy island. In the new version algorithm we simulate only the central area of the big vacancy island where the central island is located. This is the area inside circle C_2 in Fig(A.6) and includes part of the terrace and the central adatom/vacancy island. The advantage of this method is that we simulate only the central island and sometimes atoms which diffuse on the terrace inside circle C_2. The flux of particles from the edge toward central island is in this model realized by adding of atoms to circle C_1. The frequency of adding of atoms on C_1 is equal to frequency whit which atoms detaches from border of big vacancy island and reach circle C_1. This frequency we obtain from taken from the previous full MC simulation (it is described by the probability $P_{e\to e}$). Circle C_1 is smaller than C_2 and both circles has identical centers. In our MC we used $r(C_1) = 1.5r, r(C_2) = 1.5r + 5$ where r is the radius of central island. After the adding of the atom on C_1 we simulate its diffusion and if it crosses circle C_2 than it either leaves the simulated area (with the probability $P_{C_2\to e}$ also taken from MC) or it is added to C_1 (with the probability $P_{C_2\to C_1}$). The atoms on the edge of the central vacancy can still diffuse and their motion is simulated.
The exchange of the particle between the edges of the big vacancy island and the central vacancy island is the only parameter in this model which is determined from the full MC simulation of the system. The exchange is described by the probabilities that:

- some atom which detaches from the edge of big vacancy island crosses the circle C_1 ($P_{e\to C_1}$ in Fig(A.6))
- an atom which crosses circle C_2 diffuses back on circle C_1 ($P_{C_2\to C_1}$)
- an atom crossing C_2 falls back on the edge of the big vacancy island ($P_{C_2\to e}$)

The first probability represent the probability of this events per time unit and is obtained from the full MC simulation of the decay of the adatom island. In the last two it is only the probability that one of these events will be realized. In practice these probabilities would also be the probability of these events per time unit, but we suppose that the jump back on the circle C_1 is quick and, in the second case, the time which the atom needs to join the edge of the big vacancy island does not play a role, because it is out of the simulated area. Thus if we ignore the time which the atom needs for diffusion from C_2 on C_1 then we can write: $P_{C_2 \to e} + P_{C_2 \to C_1} = 1$. Then the exchange between the edge of the big vacancy island and the simulated area can be described by only two parameters.
The determination of these mentioned parameters is the main problem of this method. The parameters are calculated in the full MC simulation. The first four parameters are (at a low density on the terrace) determined only by geometry in fact. The main problem in this model is that none of these parameters are constant over time. The probability depends sensitively on the density of the atom close to the edge or on the terrace, which depends on the shape of the big vacancy island. But one of the results was the dependency of the shape of the big vacancy island on the density of atoms on the terrace (see Fig(1.16).b). Thus we can expect that the parameters can depend on the size of the central island and the MC verifies this (see Fig(A.7)).

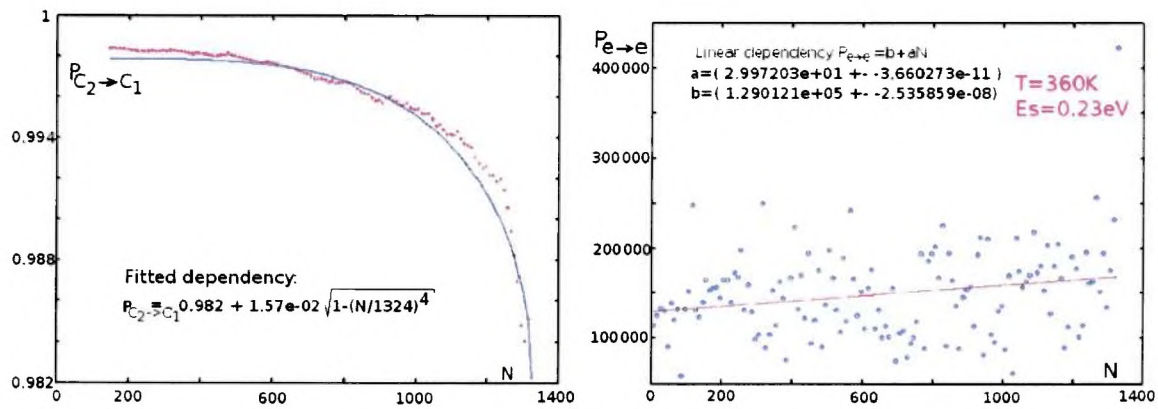

Figure A.7: The probabilities $P_{e \to C_1}$, $P_{C_2 \to C_1}$ as functions of the number of atoms in the central island. In the MC the fitted curves are substituted. The shape of the applied dependencies is shown in the chart. The points are taken from the full MC simulation of vacancy decay with $E_s^{eff} = 0.23eV$

The main problem is determining the dependencies $P_{e \to C_1}$, $P_{C_2 \to C_1}$ over time during the simulation. But the decay time, which is crucial in our work, sensitively depends on the probabilities described in Fig(A.6). In addition, these probabilities change with time and this time dependency is different for each value of E_s^{eff}. We tried to substitute the probabilities $P_{e \to C_1}$, $P_{C_2 \to C_1}$ as functions of the number of atoms in the central island (see Fig(A.7)) to correct this time dependency. Nevertheless these dependencies are really inaccurate because the dependencies obtained from the MC simulations have a wide diversion.
For this reason we were probably not able to obtain the same decay times with the full model and with this quicker (but less precise) algorithm. The results differ by 20% and it seems that it depends very sensitively on the parameter $P_{C_2 \to C_1}$ especially. The second problem is that these dependencies are different for each combination of E_s^{eff} and temperature T. And this is the second problem with parameter $P_{C_2 \to C_1}$ because it mainly changes at the end of the simulation, so the determination of this parameter represents the realization of the whole

simulation. And if we only use a constant value, we do not obtain the same exponent q of the decay law as in the full MC simulation.

A.1 Conclusion

Because of the sensitivity of the parameters for the quick MC simulation, this simulation provides different results than the simulation of the whole area. For this reason we did not use this algorithm to obtain the Arrhenius plot. Nevertheless the sensitivity of decay time on these parameters which depends sensitively on the shape of the central vacancy islands could also be an indication that the simple semi-classical model, which only include the curvature of the edges (dependency on $1/r$) is not satisfactory.
Nevertheless we are not able to to determine the Ehrlich-Schwöbel barrier and the ratio of prefactors. The computer times for the full simulations are too slow to even complete the calculations for only four points. The quick algorithm where the parameters are substituted by sortable functions provides incorrect results and the shape of these functions is too complicated to be forecast from a partial run of the full MC simulation.
This means that the decay of simulated system is too complex and the decay law depends quite sensitively on conditions which drive the shaping of the big vacancy island.

Bibliography

[1] Surface Diffusion: Atomistic and Collective Processes, Ed. M.C.Tringides (Plenum New York 1997)

[2] C.T. Campbell, S.C.Parker, D.E. Starr; Science 298(2002)811.

[3] D.S. Sholl and R.T. Skodje; Phys.Rev.B 75(1995)3158

[4] P. Wynblatt and N.A. Gjostein in J.O. McCaldin and G. Samorjai (edts) Prog. in Sol.Sta.Chem. 9(1975)21

[5] K. Bromann, H. Brune, H. Röder, K. Kern; Phys.Rev.Lett. 75(1995)677

[6] J. Tersoff, A.W.Denier van der Gon and R.M.Tromp; Phys.Rev.Lett. 72(1994)266

[7] K.R. Roos, M.C. Tringides; Surface Review and Letters 5(1998) 833

[8] J. Vrijmoeth, H. A. van der Vegt, J. A. Meyer, E. Vlieg, and R. J. Behm; Phys.Rev.Lett. 72(1994)3843

[9] K. R. Roos, M.C. Tringides; Phys.Rev.Lett. 85(2000)1480

[10] K. Morgenstern, G. Rosenfeld, E. Laegsgaard, F. Besenbacher, G. Comsa; Phys.Rev.Lett. 80(1998)556

[11] J.G. McLean,*B. Krishnamachari, D.R. Peale, E. Chason, J.P. Sethna and B.H. Cooper; Phys.Rev.B 55(1997)1811

[12] Z. Chvoj, M.C. Tringides, T. Rahman; Phys.Rev.B 66(2003)035419

[13] A.B. Bortz, M.H. Kalos, J.L. Lebowitz; J.of Comp.Phys. 17(1975)10

[14] Z. Chvoj, C. Ghosh, T.S. Rahman and M.C. Tringides; J.of Phys.- Condensed Matter 15(2003)5223

[15] J. Jacobsen, B.H. Cooper and J.P. Sethna; Phys.Rev.B 58(1998)15847

[16] S.M. Foiles, M.I. Baskes, M.S. Dew; Phys.Rev.B 33(1986)7983

[17] M. Giesen, C. Steimer, H. Ibach; Surf.Sci. 471(2001)80

[18] Personal Comunication with Karina Morgernsein

[19] P. Sonnet, L. Stauffer, C. Minot; Surf.Sci. 407(1998)121

[20] P. Jelinek, M. Onderejcek, J. Slezak, V. Chab; Surf.Sci. 554(2003) 339

[21] J.M. Gomez-Rodrigez, J.J. Saenz, A.M. Baro; Phys.Rev.Lett. 76(1996)799

[22] J. Slezak, V. Chab, Z. Chvoj, P. Mutombo; J. Vac.Sci.Technol.B 18(2000)1151

[23] J.M. Gomez-Rodrigez, J.-Y. Veuillen, R.C. Ciniti; Surf.Rev.Lett. 4(1997)335

[24] O. Custance, S. Brochard, I. Brihuega, E. Artacho, J.M.Soler, A.M. Baro, J.M. Gomez-Rodrguez; Phys.Rev.B 67(2003)235410

[25] X.P. Li, G. Chen, P.B. Allen, J.Q. Broughton; Phys.Rev.B 38(1988)3331

[26] W. Daum, H. Ibach, J.E. Muller; Phys.Rev.Lett. 59(1987)1593

[27] L.K. Runnels, in: C. Domb, M.S. Green (Eds.), PhaseTransitions and Critical Phenomena, vol. 2, Academic Press,London, New York, 1972, p. 305

[28] R. Olesinki, G. Abbaschian; Bull. Aloy Phase Diagrams 5(1984)271

[29] G. L. Lay, J. Peretti, M. Hambucken, W. Yang; Surf.Sci. 204(1988)57

[30] G. L. Lay, M. Abraham, A. Kahn, K. Hricovini, J. Bonnet; Phys.Scr.T 35(1991)261

[31] J. Gomez-Rodriguez, J.-Y. Veaillen, R. Cinti; Surf.Sci 377-379(1997)45

[32] E. Ganz, I.-S. Hwang, F. Xiong, K. S. Theiss, J. Golovchenko; Surf.Sci. 257(1991)259

[33] T. L. Chan, C. Wang, M. Hupalo, M. Tringides, Z.-Y. Lu, K. Ho; Phys.Rev.B 68(2003)045410

[34] J. Slezak, P. Mutombo, V. Chab; Phys.Rev.B 60(1999)13328

[35] K. Horikoshi, X. Tong, T. Nagao, S. Hasegawa; Phys.Rev. B 60(1999)13287

[36] O. Custance, J. Gómez-Rodríguez, A. Baro, L. Jure, P. Mallet, J.-Y. Veuillen; Surf.Sci. 482-485(2001)1399

[37] I. Brihuega, O. Custance, R. Pérez, J. M. Gómez-Rodríguez; Phys.Rev.Lett 94(2005)046101

[38] J. Carpinelly, H. Weitering, E. Plummer, R. Stumpf; Nature 381(1996)398

[39] A. Melechko, J. Braun, H. Weitering, E. Plummer; Phys.Rev.Lett. 83(1999)399

[40] J. Shi, B. Wu, X. Xie, E. Plummer, Z. Zhang; Phys.Rev.Lett. 91(2003)076103

[41] I. Brihuega, O. Custance, R. Perez, J. Gomez-Rodriguez; Phys.Rev.Lett. 94(2005)046101

[42] A. Petkova, J. Wollschlager, H.-L. Gunter, M. Henzel; Surf.Sci. 471(2001)11

[43] L. Seehofer, G. Falkenberg, D. Daboul, R. Johnson; Phys.Rev.B 51(1995)13503

[44] V. Yeh, M. Yakes, M. Hupalo, M. Tringides; Surf.Sci. 562(2004)L238

[45] M. Hupalo, J. Schmalian, M.C. Tringides; Phys.Rew.Lett. 90(2003)216106

[46] C.A. Jeffrey, E.H. Conrad, R. Feng, M. Hupalo, C. Kim, P.J. Ryan, P.F. Miceli, and M.C. Tringides; Phys.Rev.Lett. 96(2006)106105

[47] R. Otero, A.L. Vazquez de Parga, and R. Miranda; Phys.Rev.B 66(2002)115401

[48] I.B. Altfeder, K.A. Matveev, and D.M. Chen; Phys.Rev.Lett78(1997)2815

[49] S.H. Chang, W.B. Su, W.B. Jian, C.S. Chang, L.J. Chen, and T.T. Tsong; Phys.Rev.B 65(2002)245401

[50] A. Menzel, M. Kammler, E. H. Conrad, V. Yeh, M. Hupalo, and M. C. Tringides; Phys.Rev.B 67(2003)165314

[51] T.Nishio, M. Ono, and T. Eguchi; Appl.Phys.Lett. 88(2006)113115

[52] C. M. Weil and M. Y. Chou; Phys.Rev.B 66(2002)233408

[53] P. Czoschke, H. Hong, L. Basile, and T.C. Chiang Phys.Rev.B 72(2003)075402

[54] M. Hupalo, S. Kremmer, V. Yeh, L. Berbil-Bautista, E. Abraham, M.C. Tringides Surf.Sci. 493(2001)526

[55] H. M. Koduvely and A. Zangwill; Phys.Rev.B 60(1999)2204

[56] Ch.Heyn; Phys.Rev.B 64(2001)165306

[57] M. Hupalo, M.C. Tringies; Phys.Rev.B 65(2002)115406

[58] M. Giesem Progress in Serf.Sci 68(2001)1

[59] T.L. Chan, C.Z. Wang, M. Hupalo, M.C. Tringides, and K.M. Ho Phys.Rev.Lett 96(2006)226102

[60] H. Okamoto, D. Chen and T. Yamada Phys.Rev.Lett. 89(2002)256101

[61] C.S. Jiang, S.C. Li, H.B. Yu, D. Eom, X.D. Wang, Ph. Ebert, J.F. Jia, Q.K. Xue, and C.K. Shih Phys.Rev.Lett. 92(2004)106104

[62] Z. Kuntova, Z. Chvoj, M.C. Tringides, Surf.Sci. (accepted 2006)